이 학 박 사 학 위 논 문

Rad51 에 의한 DNA 이중가닥 절단 수선과 유전자 재조합 기전 연구

Regulation of Rad51-mediated DNA double-strand break repair and genetic recombination

2015년 2월

서울대학교 대학원

생명과학부

윤 상 욱

이 학 박 사 학 위 논 문

Rad51 에 의한 DNA 이중가닥 절단 수선과 유전자 재조합 기전 연구

Regulation of Rad51-mediated DNA double-strand break repair and genetic recombination

2015년 2월

서 울 대 학 교 대 학 원

생명과학부

윤 상 욱

Rad51 에 의한 DNA 이중가닥 절단 수선과 유전자 재조합 기전 연구

Regulation of Rad51-mediated DNA double-strand break repair and genetic recombination

指導敎授 黃 德 秀

이 論文을 理學博士 學位 論文으로 提出함

2014년 12월

서울대학교 대학원 생명과학부

尹 相 旭

尹相旭의 理學博士 學位論文을 認准함

2014년 12월

委 員 長 _____

副委員長 _____

委 員 _____

委 員 _____

委 員 _____

Regulation of Rad51-mediated DNA double-strand break repair and genetic recombination

A dissertation submitted in partial fulfillment
of the requirements for the degree of
DOCTOR OF PHILOSOPHY

to the Faculty of the School of Biological Sciences

at
SEOUL NATIONAL UNIVERSITY

by
Sang Wook Yoon

Date Approved

_____ _____

_____

_____

_____

_____

ABSTRACT

Regulation of Rad51-mediated DNA double-strand break repair and genetic recombination

Sang Wook Yoon

Embryonic stem cells (ESCs) are pluripotent and self-renewing cells that originate from inner cell mass of blastocyst. ESCs should have ability to divide and grow indefinitely while sustaining their pluripotency. To preserve their self-renewal ability and faithful DNA replication responsible for genomic stability, ESCs have developed powerful machineries to preserve genomic integrity distinguished from differentiated cells, but they are not fully elucidated yet. Therefore, the suppression of mutations against DNA damage in ESCs is essential for the maintenance of genomic integrity as well as cell proliferation and inheritance of genetic trait.

Homologous recombination (HR) is one of the key processes to maintain genomic integrity against DNA replication stress. Rad51 is an important protein of HR in all eukaryotes and its functions are homology search and strand invasion. Here, I investigated that Rad51 preserves G2/M transition to regulate cell cycle progression and the level of Rad51 is a reflective of high

percentage of S phase in ESCs.

ESCs exhibit prominent populations of S-phase cells compared with differentiated somatic cells. Different from many somatic cells that express Rad51 protein in cell cycle-dependent manner, Rad51 in ESCs is constitutively expressed independent of each cell cycle phases and its level is extremely higher than somatic cells. Unlike its continuously elevated protein level, the formation of Rad51 foci increased as cells enter S-phase, and decreased as cells prepare their division. The foci formation tendency is consistent with γH2AX, the marker of DNA double-strand breaks (DSBs). Also, Rad51 is entirely dissociated from chromosome during mitosis. Rad51 knockdown induces the phosphorylation of Chk1, the sign for DNA damage checkpoint activation. The FACS analysis showed that the populations of G2/M phases are accumulated and BrdU incorporation is reduced in Rad51-knockdown cells. In conclusion, HR activity of Rad51 is essential to repair spontaneously occurred DSBs, which are caused by rapid and frequent DNA replication events.

Meiosis includes a complex progression of chromosomal events which results in the physical connection of homologous chromosomes. During meiosis, cohesin complexes physically hold sister chromatids together, they are required for DSB repair and faithful chromosome segregation. Rec8 is a key component of the meiotic cohesin complex, which regulates sister chromatid cohesion and recombination between homologous chromosomes. DNA physical analysis of

recombination in yeast mutant strains that Rec8 phosphorylation sites were mutated to alanines reveals a general principle: Rec8 phosphorylation is required for the timely and efficient progression of recombination at DSB-to-double Holliday Junction (dHJ) transition in the stage of homologous partner choice with the first DSB end releasing. I demonstrate that Rec8 phosphorylation does not affect for the homologous partner choice but is required for latter stages of crossover (CO)-designated meiotic recombination. Further, elimination of Mek1 kinase, which impedes checkpoint activation, relieves the meiotic progress delay caused by Rec8 deletion or Rec8 phosphorylation-defective alleles. The obtained results point to a general logic for the relationship between Rec8 and Mek1 kinase that involve in recombination progression and regulatory surveillance during meiosis.

Key words: embryonic stem cell, homologous recombination, Rad51, cell cycle, DNA replication, genomic integrity, meiotic recombination, Rec8, Mek1, Cdc6, phosphorylation, crossover

Student ID : 2007-22846

TABLE OF CONTENTS

LIST OF FIGURES

LIST OF TABLES

LIST OF ABBREVIATIONS

BrdU	5-bromo-2’-deoxyuridine
CBB	Coomassie brilliant blue
Cdc5	Cell division cycle 5
Cdc6	Cell division cycle 6
Cdc7	Cell division cycle 7
CDT1	Chromatin licensing and DNA replication factor 1
Chk1	Checkpoint kinase 1
Chk1 (Ser317)	Phosphorylation on Ser317 residue of Chk1
CO	Crossover
DAPI	4’,6’-diamidino-2-phenylindole
DDK	Dbf4-dependent kinase
dHJ	Double Holliday junction
DMEM	Dulbecco’s modified eagle’s medium
Dmc1	Disrupted meiotic cDNA protein 1
DPI	Diphenyleneiodonium
DSB	Double-strand break
dsDNA	Double-stranded DNA
FACS	Fluorescence-activated cell sorting

FITC	Fluorescein 5-isothiocyanate
γH2AX	Phosphorylation on Ser139 residue of histone H2AX
HEPES	4-(2-hydroxyethyl)-1-piperazineethanesulfonic acid
HR	Homologous recombination
Hrr25	Casein kinase 1 homolog Hrr25
IH-CO	Interhomolog-crossover
IH-dHJ	Interhomolog-double Holliday junction
IH-NCO	Interhomolog-non-crossover
IS-CO	Intersister-crossover
IS-dHJ	Intersister-double Holliday junction
JM	Joint molecule
LIF	Leukemia inhibitory factor
MEF	Mouse embryonic fibroblast
Mek1	Meiotic kinase 1
mek1-as	ATP analog-sensitive allele of Mek1
MEM-NEAA	Minimal essential medium-nonessential amino acids
Mer3	ATP-dependent DNA helicase Mer3
mESC	Mouse embryonic stem cell
MRN	Mre11-Rad50-Nbs1
Msh4/5	MutS homolog 4/5
NCO	Non-crossover

NHEJ	Non-homologous end joining
ORC2	Origin recognition complex subunit 2
Pds5	Sisters chromaid cohesion protein 5
pHH3 (Ser10)	Phosphorylation on Ser10 residue of histone H3
PMSF	Phenylmethylsulfonyl fluoride
PP2A	Protein phosphatase protein 2A
Pre-RC	Pre-replicative complex
Rad51	DNA repair protein Rad51
Rec8	Meiotic recombination protein Rec8
RMH	Red1-Mek1-Hop1
RNAi	RNA interference
RPA	Replication protein A
SC	Synaptonemal complex
SDSA	Synthesis-dependent strand annealing
SEI	Single-end invasion
Sgo1	Shugosin 1
siNS	Non-specific small interfering RNA
siRad51	Rad51 small interfering RNA
siRNA	Small interfering RNA
SPM	Sporulation medium
Spo11	Meiosis-specific sporulation protein 11

SPS	Supplemented pre-sporulation medium
ssDNA	Single-stranded DNA
TopBP1	Topoisomerase IIβ binding protein
UV	Ultraviolet light
YPD	Yeast extract-peptone-dextrose
YPG	Yeast extract-peptone-glycerol
Zip1	Synaptonemal complex zipper protein 1
Zip1-PC	Zip1 polycomplex
Zip3	Synaptonemal complex zipper protein 3
ZMM	Zip1/2/3/4, Msh4/5, Mer3
1D gel	One-dimensional gel
1-NA-PP1	1-(1,1-dimethylethyl)-3-(1-naphthalenyl)-1H-pyrazolo(3, 4-d)pyrimidin-4-amine
2D gel	Two-dimensional gel

CHAPTER 1

Rad51 preserves G2/M transition in mouse embryonic stem cells to regulate cell cycle progression

Abstract

Homologous recombination (HR) maintains genomic integrity against DNA replication stress and deleterious lesions such as double-strand breaks (DSBs). Rad51 recombinase is critical for HR events that mediate the exchange of genetic information between parental chromosomes in eukaryotes. Additionally, Rad51 and HR accessory factors may facilitate replication fork progression by preventing replication fork collapse and repair DSBs that spontaneously arise during the normal cell cycle. In this study, I demonstrated a novel role for Rad51 during the cell cycle in mouse embryonic stem cells (mESCs). In mESCs, Rad51 was constitutively expressed throughout the cell cycle, and the formation of Rad51 foci increased as the cells entered S phase. Suppression of Rad51 expression caused cells to accumulate at G2/M phase and activated the DNA damage checkpoint, but it did not affect the self-renewal or differentiation capacity of mESCs. Even though Rad51 suppression significantly inhibited the proliferation rate of mESCs, Rad51 suppression did not affect the replication fork progression and speed, indicating that Rad51 repaired DNA damage and promoted DNA replication in S phase through an independent mechanism. In conclusion, Rad51 may contribute to G2/M transition in mESCs, while preserving genomic integrity in global organization

of DNA replication fork.

Introduction

Embryonic stem cells (ESCs) are derived from the inner cell mass of the early stage embryo (Rossant, 2001). They can remain in a pluripotent state indefinitely under optimal culture conditions (Andrews et al., 2002). During the process of asymmetric cell division and self-renewal to establish a cellular continuum, stem cells undergo chronological aging caused by the accumulation of damaged or aberrant molecules. Aberrant chromosomes are observed in up to 50% of human ESCs in long-term culture (Maitra et al., 2005; Baker et al., 2007). Aging and the accumulation of mutations in stem cells can change the fate or cellular function of stem cell progeny. To avoid the accumulation of mutations and to prevent their transmission to subsequent generations, ESCs have developed robust systems to maintain genomic stability, including DNA repair machineries. In addition to active DNA damage repair mechanisms, faithful DNA replication is essential for maintaining genomic integrity in the normal cell cycle. In asynchronous, exponentially growing cells, up to 60% of mouse ESCs (mESCs) were in S phase, compared with 20% of mouse embryonic fibroblasts (MEFs) (Savatier et al., 2002; Serrano et al., 2011; Tichy, 2011; Tichy et al., 2012). Obstacles on the DNA template, caused by exogenous or endogenous factors such as

ultraviolet light (UV), reactive oxygen species (ROS), nutrient deficiency, and de-regulation of replication activity frequently impede replication fork progression, which can result in fork collapse and the formation of replication-dependent DNA double-strand breaks (DSBs) (Burhans and Weinberger, 2007; Branzie and Foiani, 2010). Many redundant pathways preserve the integrity of the replication fork and thereby prevent the lethal effects caused by complete dissociation of the replication machinery on stalled or collapsed replication forks.

Homologous recombination (HR) is the predominant mechanism for the repair of DSBs and recovery of stalled DNA replication. HR is a high-fidelity form of repair because the mechanism uses a sister chromatid template containing homologous sequences to repair lesions (Paques and Haber, 1999). HR predominantly occurs in the late S and G2 phases of the cell cycle, when sister chromatids are more readily available as repair templates. Competition between HR and non-homologous end joining (NHEJ) in DSB repair or at a stalled replication fork is specifically caused by template usage in S/G2 phase (Filippo et al., 2008). Failed DSB repair or inaccurate DNA repair causes chromosomal rearrangement, chromosome loss, or carcinogenesis (Sieber et al., 2003; Blow and Gillespie, 2008). In mESCs, DSBs are predominantly repaired through the high-fidelity HR pathway, which occurs throughout the

cell cycle (Adams et al., 2010; Serrano et al., 2011). The essential role of HR in mESCs is supported by the fact that basal levels of proteins involved in HR are higher in mESCs than in fibroblasts. The protein levels correlate with HR repair activity, which is two- to four fold higher in mESCs than in MEFs (Tichy et al., 2010). In addition, knockout of genes involved in HR leads to early embryonic lethality in mice (Lim and Hasty, 1996; Tsuzuki et al., 1996).

Rad51, the eukaryotic ortholog of RecA in *Escherichia coli*, is a key player in the HR pathway. Rad51 has an essential role in homology recognition and strand exchange between two homologous templates during mitotic DSB repair and meiotic recombination (West, 2003). The Mre11-Rad50-Nbs1 (MRN) complex resects initial DSBs to generate 3′ single-stranded DNA (ssDNA) tails that invade the duplex template DNA. Replication protein A (RPA) initially binds to 3′ ssDNA overhangs to produce stable RPA-coated ssDNA (Filippo et al., 2008; Krejci et al., 2012); Rad51 cofactors then dissociate the RPA-ssDNA filaments. A loading factor, BRCA2, helps Rad51 bind efficiently to ssDNA (Liu et al., 2010; Holloman, 2011). Rad51 plays a role in replication fork progression, which is critical for maintaining the structural integrity of chromosomes and ensuring cell proliferation in vertebrates (Tsuzuki et al., 1996; Sonoda et al., 1998; Carr et al., 2011). Rad51 mediates two distinct pathways that suppress replication fork disruption. One

pathway promotes replication restart when a replication fork encounters DNA damage or reduced nucleotide pools (Petermann et al., 2010). The other pathway uses HR to repair DSBs that occur after exposure to some genotoxins or at broken replication forks. To promote HR, Rad51 forms a filament on the 3′ ssDNA, which then invades and anneals to a homologous template provided by replicating sister chromatids or homologous chromatids (Filippo et al., 2008). ATPase activity of Rad51 is critical for stabilizing the catalytically active nucleoprotein filament (Chi et al., 2006). Rad51 mutants defective for either ATP binding or ATP hydrolysis are unable to restart stalled replication forks and repair DSBs in human ESCs (Kim et al., 2012). Recently, it was reported that Rad51 plays a direct role in replication fork progression by preventing the accumulation of ssDNA gaps at replication forks, which occurs independent of HR activity (Hashimoto et al., 2010).

In this study, I reveal a novel function of Rad51 in the cell cycle progression of mESCs. Unlike differentiated cells, mESCs constitutively expressed Rad51 protein throughout the cell cycle. Suppression of Rad51 led to the activation of the DNA damage checkpoint and the accumulation of cells at G2/M phase. Rad51 siRNA did not slow the replication fork progression time and speed, even though it significantly inhibited cell proliferation. Based on these results, I conclude that that Rad51 regulates HR in mESCs to overcome single-strand

breaks, possibly caused by the rapid replication of mESCs, after the completion of DNA replication at S phase.

Materials and Methods

Cell culture

The murine embryonic stem cell line J1 (Cat # SCR-1010) derived from a male agouti 129S4/SvJae embryo was obtained from ATCC. J1 mESCs were grown in Dulbecco's modified Eagle's medium (DMEM) plus GlutaMax1 (Cat # 10569; Gibco) supplemented with 10% horse serum (Cat # 16050-122; Gibco), 2 mM L-glutamine (Gibco), 10 mM HEPES (Gibco), 0.1 mM minimal essential medium-nonessential amino acids (MEM-NEAA; Gibco), 0.1 mM β-mercaptoethanol (Gibco), 100 units/mL penicillin, 100 μg/mL streptomycin (penicillin/streptomycin, Cat # 15140; Gibco), and 1,000 units/mL mouse ESGRO leukemia inhibitory factor (LIF; Cat # ESG 1107; Millipore) at 37 ℃ in a 5% CO_2 atmosphere. Before each experiment, mESCs were plated on culture plates briefly coated with 0.1% gelatin and without a feeder layer. MEFs generated from the blastocyst embryo of a CF1 pregnant female mouse on embryonic day 12.5 were used between passages 3 and 5 in all experiments. MEFs were cultured in DMEM (Cat # 11995; Gibco) supplemented with 10% fetal bovine serum (Cat # 16000-044; Gibco) and penicillin/streptomycin (Cat # 15140; Gibco). To maintain the mESCs in low-serum environment, cells growing in 10% serum were transferred and serially adapted to serum

concentrations of 5%, 2.5%, and 1% for 4 days.

Cell cycle synchronization and FACS analysis

For early G1/S phase synchronization, cells were treated with thymidine (Sigma) at a final concentration of 2 mM for 16 hr, washed twice with pre-warmed phosphate-buffered saline (PBS), and then grown in fresh medium. After a 6-hr release, thymidine was added again. Cells were incubated with thymidine for another 16 hr, washed, and released from the thymidine block with the addition of fresh medium. For synchronous release from G2-phase arrest, cells were treated with 5 μM diphenyleneiodonium chloride (DPI; Sigma) for 16 hr, washed, and released with the addition of fresh medium. Cells were collected at the indicated times for FACS, western blotting, and immunofluorescence analyses. For FACS analysis, the collected cells were immediately fixed in 70% ethanol after harvesting the cells and stained with propidium iodide (PI; Sigma) plus RNase A (Sigma) for 30 min at room temperature in the dark. The distribution of cell cycle phases was analyzed FACSCalibur flow cytometer (Becton Dickinson) and quantified with flow cytometry analysis software (FlowJo; Tree Star, Inc.).

BrdU FACS analysis

Cells were pulsed with BrdU (Sigma) to a final concentration of 10 μM for 20 min before harvesting. The harvested cells were washed with PBS and then fixed in 70% ethanol at 4 ℃ for 2 hr. The fixed cells were incubated with denaturation buffer (2N HCl, 0.5% Triton X-100) for 30 min. After washes with PBS, cells were recovered with neutralization buffer (0.1 M $Na_2B_4O_7 \cdot 10H_2O$, pH 8.5) for 30 min and incubated with BrdU antibody in PBS containing 1% bovine serum albumin (BSA) and 0.5% Tween-20 for 1 hr. Fluorescein 5-isothiocyanate (FITC)-conjugated secondary antibody was added to BrdU-treated samples. After 1 hr, cells were washed with PBS, stained with PI (including RNase A), and then analyzed using a FACSCalibur flow cytometer (Becton Dickinson).

RNA interference

For small interfering RNA (siRNA) knockdown of mouse Rad51 (siRad51), an siGENOME SMARTpool was used (Cat # M-062730-01-0005; Dharmacon). The siRNA pool contained a mixture of four targeting nucleotides with the following sequences: 5′-CAUCAUCGCUCAUGCGUCA-3′, 5′-UGUCAUACGUUGGCUGUUA-3′, 5′-GGUAAUCACCAACCAGGUA-3′, and 5′-GAGAUCAUACAGAUAACUA-3′. siRNA was purchased from

Dharmacon, and cells were transfected using DharmaFECT 1 (Dharmacon) and Lipofectamine 2000 (Invitrogen) according to the manufacturers' instructions. A non-specific siRNA (siNS) was used as a negative control (ON-TARGET plus Non-targeting pool; Dharmacon). Cells were incubated for 48 hr and collected for the experiments (cell cycle analysis, immunoblotting, and immunofluorescence).

Immnofluorescence

Cells attached to poly-L-lysine coated coverslips were fixed in 1% paraformaldehyde (PFA) for 15 min after and then permeabilized with 0.1% Triton X-100 in PBS for 15 min. Samples were washed three times with PBS between each step. Cells were blocked with 3% BSA in PBST (PBS + 0.1% Tween-20) for 30 min and then immunostained with the following primary antibodies, diluted with 3% BSA in PBST for 1 hr: Rad51 (Cat # sc-8349), RPA (Cat # sc-28709), Ki67 (Cat # sc-7846), Cyclin B1 (Cat # sc-752) and Geminin (Cat # sc-53923) from Santa Cruz Biotechnology; Phospho-Chk1^{Ser317} (Cat # 2344) from Cell Signaling; Rad51 (Cat # ab63801) and γH2AX (Cat # ab22551) from Abcam; ORC2 (Cat # NA73) and Cdt1 (Cat # 07-1383) from Millipore. The cells were washed with PBST three times, incubated with fluorescence-conjugated secondary antibodies (Cy3, FITC, and

Alexa 488) for additional 40 min, and then mounted on glass slides with a DAPI-containing mounting solution. Samples were visualized with an Olympus BX51 fluorescence microscope equipped with a DAPI filter and fluorescent channels. Digital images were obtained with Image Pro-Express software. Images of Rad51 and ORC2 foci in Fig. 1-8A were acquired with a confocal microscope (Leica TCS SP5 II) and processed with Leica Application Suite Advanced Fluorescence (LAS AF) software (Leica Microsystems).

Extract preparation and immunoblotting analysis

Samples were harvested and washed twice with PBS and lysed in cell lysis buffer (Cat # 9803; Cell Signaling Technology) containing a protease inhibitor cocktail (Calbiochem) or 1 mM PMSF. Protein samples (20–50 μg) were resolved by 10% SDS-PAGE. Antibodies against the following proteins were used: Rad51 (Cat # sc-8349), Cyclin B1 (Cat # sc-752), Cyclin A (Cat # sc-751), CDK1 (Cat # sc-54), Chk1 (Cat # sc-8408), p53 (Cat # sc-6243) and β-actin (Cat # sc-47778) from Santa Cruz Biotechnology; Phospho-Histone $H3^{Ser10}$ (Cat # 06-570) from Millipore; Phospho-$Chk1^{Ser317}$ (Cat # 2344), and α-tubulin (Cat # 2144) from Cell Signaling; and Rad51 (Cat # ab63801) and γH2AX (Cat # ab22551) from Abcam (Cambridge, MA). Proteins were transferred to polyvinylidene difluoride (PVDF) membranes (Millipore) and

blocked for 1 hr with 5% skim milk in tris-buffered saline (TBS) containing 0.1% Tween-20. The membrane was incubated with primary antibodies overnight at 4 ℃, washed with TBS containing 0.1% Tween-20 three times for 10 min each, and then incubated with HRP-conjugated secondary antibodies for 1 hr at room temperature. Immunoreactivity was detected with a WEST-ZOL immunoblot detection system (Cat # 16024; iNtRON Biotechnology). The relative amount of each protein was quantified using Quantity One software (Bio-Rad).

Results

Rad51 protein is expressed constantly throughout the cell cycle in mESCs

Compared to differentiated somatic cells, mESCs express higher levels of Rad51 proteins (Serrano et al., 2011; Tichy et al., 2010; Tichy et al., 2012). Also, the level of Rad51 protein in differentiated cells increases during S to G2 phases, but it is relatively low in thymidine- and nocodazole-arrested cells, as well as in asynchronous cells (Badie et al., 2010; Yata et al., 2012). To understand the Rad51 expression pattern in mESCs, cells were arrested at G1/S phase with a double thymidine block and released synchronously into the cell cycle (Figs. 1-1A and 1-1C). Unlike differentiated cells, mESCs maintained a steady level of Rad51 protein during the cell cycle (Figs. 1-1A and 1-1B). Cell cycle marker protein expression and FACS profiles indicated that cells entered mitosis and then returned to an asynchronous state in 5 hr and 10 hr, respectively, after release from the double thymidine block (Figs. 1-1B and 1-1C). The constitutive expression of Rad51 in mESCs during the cell cycle was confirmed by cell cycle arrest and release with diphenyleneiodonium chloride (DPI), which blocks cell cycle progression at G2 phase by downregulating cyclin B1 (Scaife, 2004; Figs. 1-1D, 1-1E and 1-1F). Besides, when the serum concentration was decreased during cell growth,

Figure 1-1. Expression of Rad51 protein throughout the cell cycle in mESCs.

(A) mESCs were synchronized with a double thymidine and then released from G1/S phase. The cells were collected at 2.5-hr intervals, as indicated. Cyclin B1/A and phospho-histone $H3^{Ser10}$ were used as markers for cell cycle progression. α-tubulin was used as a loading control.

(B) The level of each protein was quantified using Quantity One software (Bio-Rad). Relative ratio of each protein band over the band of α–tubulin was described in each time point. The numerical value of each sample at indicated time point was normalized by the value of asynchronous cells (As).

(C) Cell cycle profile in (A) was assessed by FACS analysis. (1C, single chromosome; 2C, replicated chromosome)

A

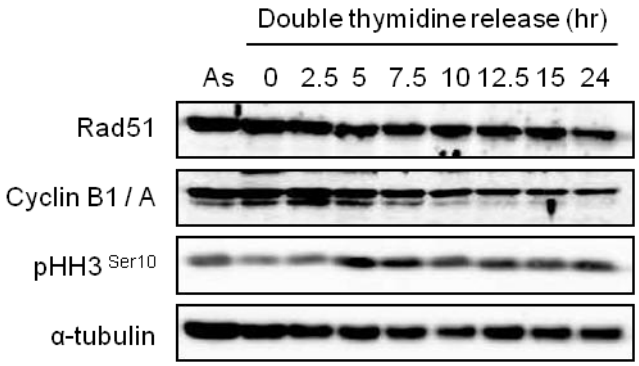
Double thymidine release (hr)
As 0 2.5 5 7.5 10 12.5 15 24
Rad51
Cyclin B1 / A
pHH3 Ser10
α-tubulin

B

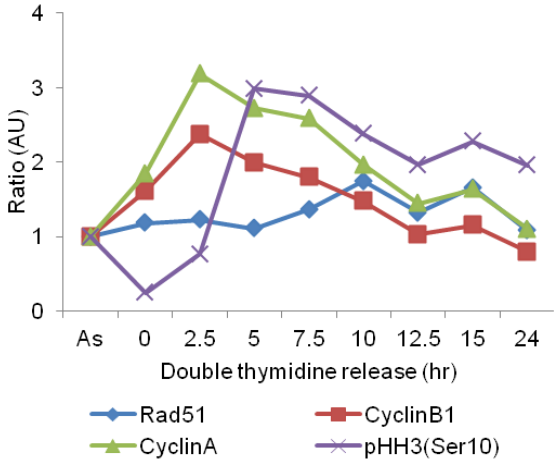
Ratio (AU)
0
1
2
3
4
As 0 2.5 5 7.5 10 12.5 15 24
Double thymidine release (hr)
Rad51
CyclinB1
CyclinA
pHH3(Ser10)

C

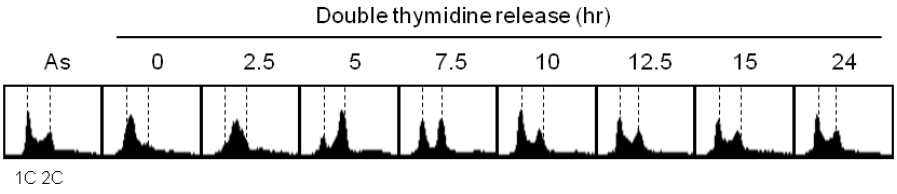
Double thymidine release (hr)
As 0 2.5 5 7.5 10 12.5 15 24
1C 2C

(D) DPI-treated mESCs were grown synchronously from G2 phase and released. Rad51 expression was confirmed by immunoblot analysis. α-tubulin was used as a loading control.

(E) The level of Rad51 protein to loading control (α-tubulin) was quantified using Quantity One software (Bio-Rad).

(F) The FACS profile indicated that cell populations containing 2C DNA progressed through the G2 phase of the cell cycle. (1C, single chromosome; 2C, replicated chromosome)

D

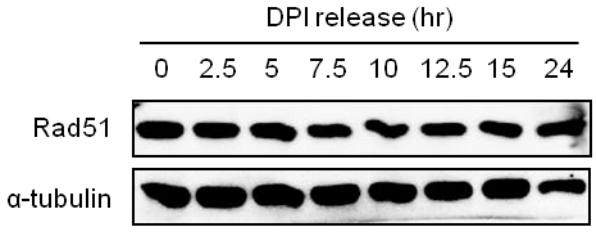
DPI release (hr)
0 2.5 5 7.5 10 12.5 15 24
Rad51
α-tubulin

E

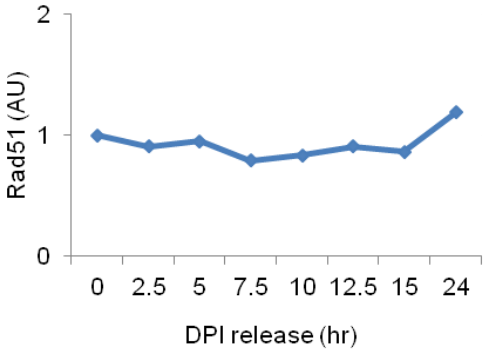
2
1
0
Rad51 (AU)
0 2.5 5 7.5 10 12.5 15 24
DPI release (hr)

F

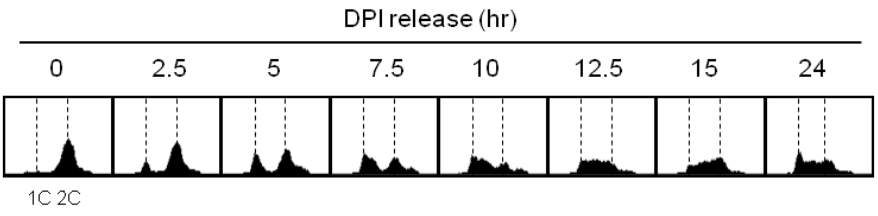
DPI release (hr)
0 2.5 5 7.5 10 12.5 15 24
1C 2C

Figure 1-2. The relationship of Rad51 protein with nutrient-insufficiency in mESCs.

(A) mESCs in exponential growth phase were transferred to and maintained in various serum concentrations as indicated. mESCs were harvested on day 4, and protein levels in mESCs and MEFs were compared. A MEF sample was used as a control for Rad51 protein expression in immunoblot analysis. The ratio of protein was normalized to the first lane using Quantity One software (Bio-Rad).

(B) A coomassie Brilliant Blue (CBB) staining was shown to ensure the equal loading of each lysates. Protein size marker was presented on the right.

(C) The number of mESCs growing in different concentrations of serum was counted every day using a hemocytometer.

A

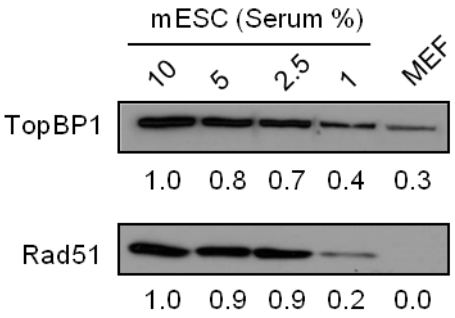
mESC (Serum %)
10
5
2.5
1
MEF
TopBP1
1.0 0.8 0.7 0.4 0.3
Rad51
1.0 0.9 0.9 0.2 0.0

B

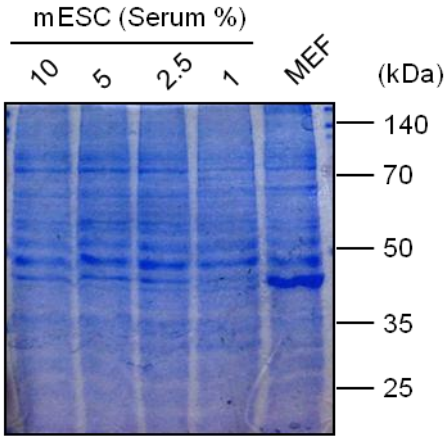
mESC (Serum %)
10
5
2.5
1
MEF
(kDa)
140
70
50
35
25

C

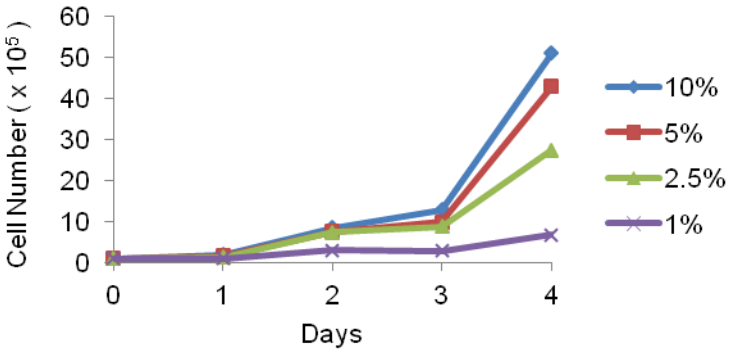
Cell Number (x 10⁵)
60
50
40
30
20
10
0
0
1
2
3
4
Days
10%
5%
2.5%
1%

the level of Rad51 protein (Figs. 1-2A and 1-2B) and the growth rate of mESCs (Fig. 1-2C) were decreased proportionally to serum concentration. This indicates that expression pattern of Rad51 protein is closely related to the proliferation of mESCs. Based on these results, I conclude that Rad51 protein is expressed at a high level throughout the cell cycle in mESCs.

Rad51 specifically localizes on S-phase chromosomes in mESCs

To understand the function of Rad51 of mESCs during cell cycle progression, I examined the stage-specific cellular localization of Rad51 by immunofluorescence. When cells were co-stained for Rad51 and RPA, which binds to ssDNA to prevent re-winding of the DNA double helix after unwinding by helicase (Wold, 1997), most RPA foci co-localized with Rad51 foci (Buisson et al., 2010; Fig. 1-3). This result indicates that Rad51 localizes to ssDNA in mESCs. Unchallenged mESCs and MEFs contain approximately five Rad51 chromosomal foci per nucleus (Sioftanos et al., 2010). In the analysis, I grouped Rad51 foci-positive cells into four categories, as shown in Fig. 1-4B. In the asynchronous state, approximately 5% of Rad51-positive cells of total mESCs contained more than 20 Rad51 foci (Fig. 1-4C). To further examine the pattern of Rad51 foci formation during cell cycle progression, mESCs were synchronized with a double thymidine block method

Figure 1-3. Co-localization of Rad51 and RPA foci in mESCs.

Co-localization of Rad51 and RPA foci in asynchronous mESCs. Mouse monoclonal anti-Rad51 antibody and rabbit polyclonal anti-RPA antibody were used to visualize endogenous Rad51 and RPA protein, respectively. The scale bar indicates 10 μm.

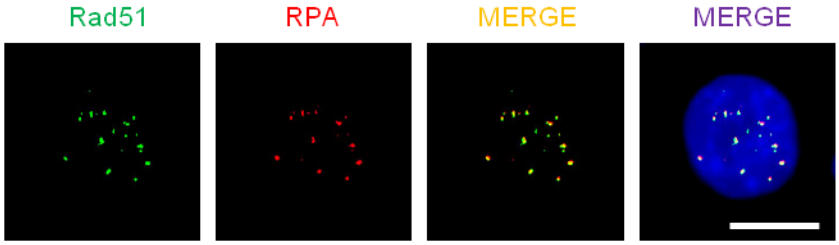
Rad51
RPA
MERGE
MERGE

Figure 1-4. Rad51 and γH2AX foci formation during the cell cycle in synchronized mESCs from G1/S phase. mESCs were synchronized with a double thymidine and then released from G1/S phase. Rad51 and γH2AX foci in mESCs were immunostained and visualized with fluorescence microscopy (×100).

(A) Representative images of cells forming Rad51 foci at the indicated time points. The same samples shown in Fig. 1-4B were co-stained for γH2AX. The cell cycle phases are indicated in the FACS profiles (right). The scale bar indicates 10 μm.

(B) Cells displaying fluorescent signals were categorized according to the number of foci per nucleus. The scale bar indicates 10 μm.

(C) The number of cells possessing Rad51 foci at each cell cycle phase was quantified. Three independent experiments were performed and at least, 200 cells were counted for each experiment.

(D) The number of cells possessing γH2AX foci at each cell cycle phase was quantified. Three independent experiments were performed and at least, 200 cells were counted for each experiment. Error bars indicate mean ± S.D (Standard deviation).

A

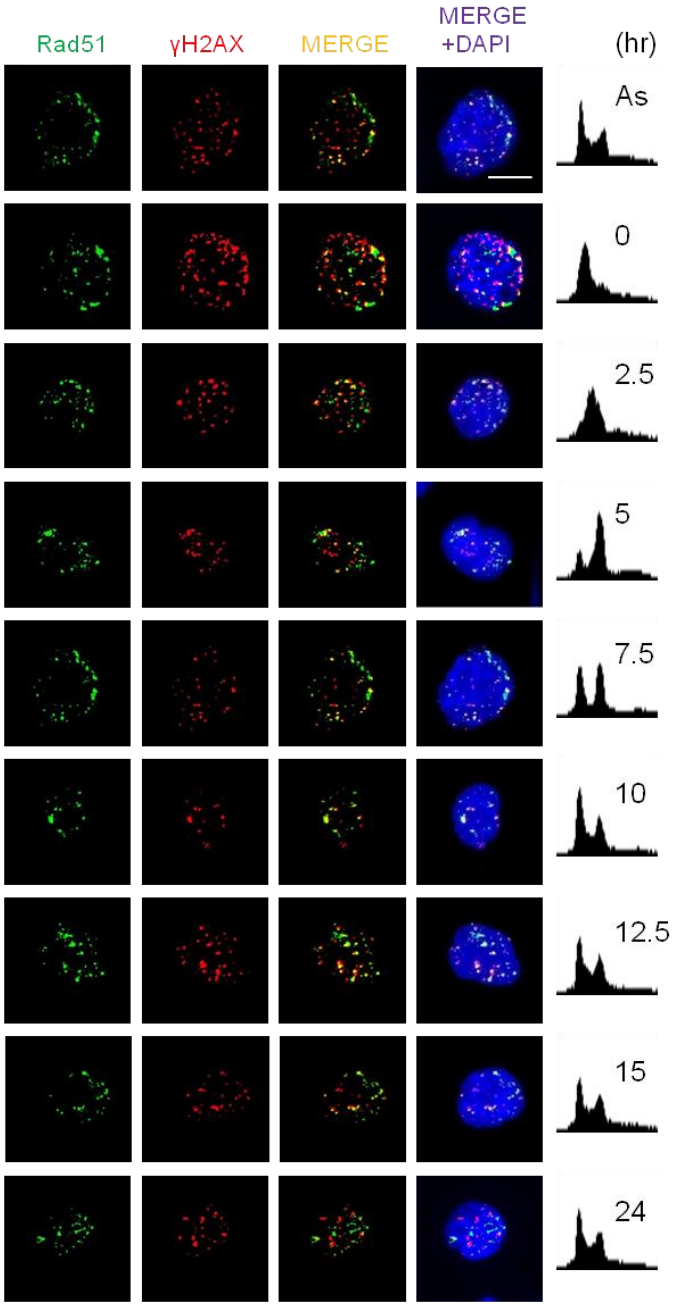

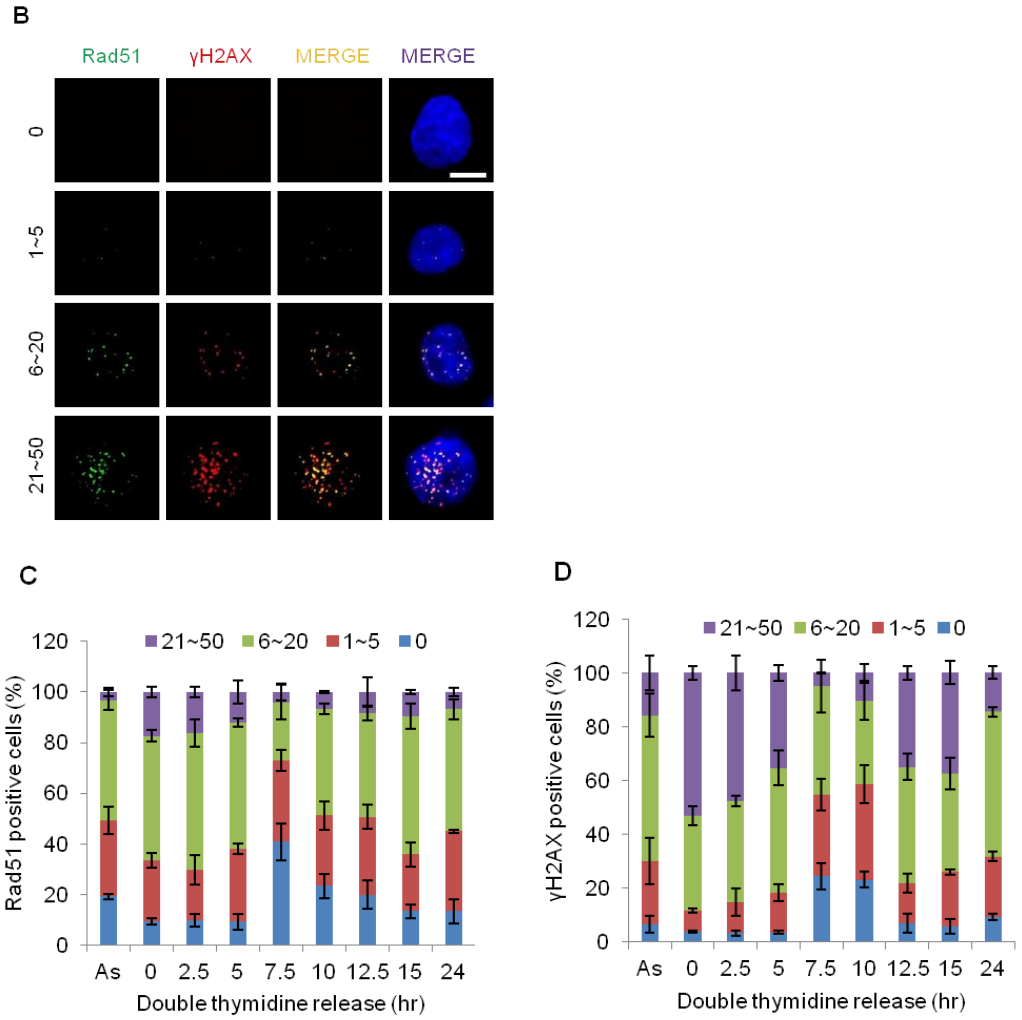
B
Rad51
γH2AX
MERGE
MERGE
0
1~5
6~20
21~50
C
21~50
6~20
1~5
0
Rad51 positive cells (%)
120
100
80
60
40
20
0
As
0
2.5
5
7.5
10
12.5
15
24
Double thymidine release (hr)
D
21~50
6~20
1~5
0
γH2AX positive cells (%)
120
100
80
60
40
20
0
As
0
2.5
5
7.5
10
12.5
15
24
Double thymidine release (hr)

Figure 1-5. Localization of Rad51 foci to DSB sites in mESCs.

The co-localization pattern for the number of Rad51 and γH2AX foci at the indicated time points after release from the double thymidine block. Error bars indicate mean ± S.D (Standard deviation).

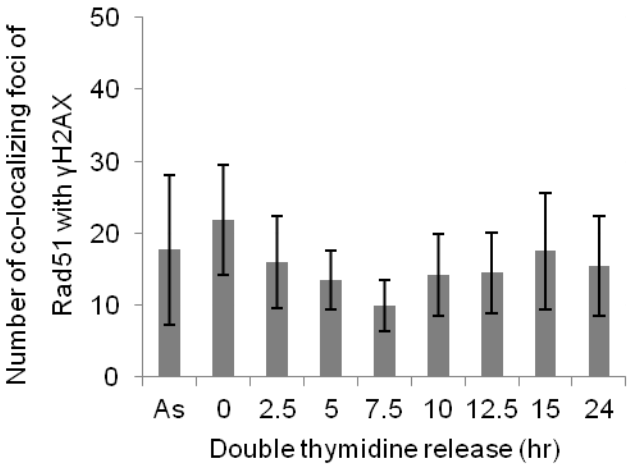
Number of co-localizing foci of Rad51 with γH2AX
50
40
30
20
10
0
As
0
2.5
5
7.5
10
12.5
15
24
Double thymidine release (hr)

Figure 1-6. Rad51 and γH2AX foci formation in MEFs.

(A) MEFs displaying fluorescent signals were categorized according to the number of foci per nucleus as in Fig. 1-4B. The scale bar indicates 10 μm.

(B) The number of cells possessing Rad51 and γH2AX foci was quantified. At least, 200 cells were counted for the experiment.

A

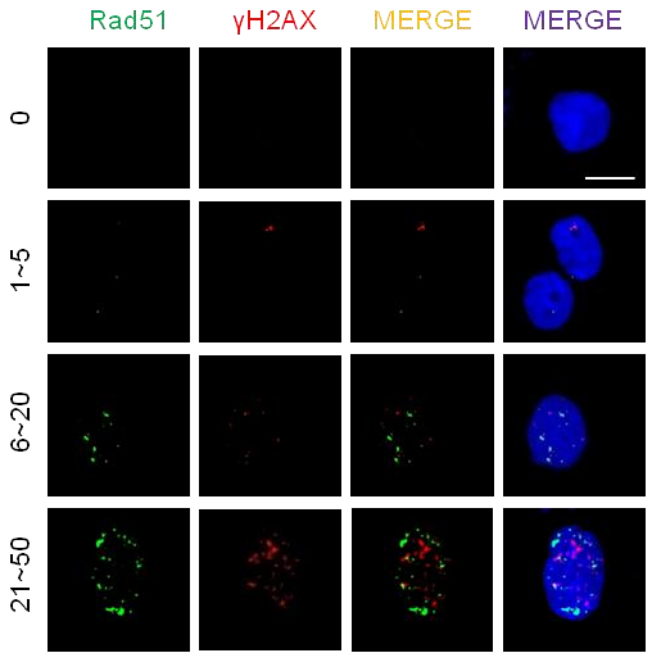
Rad51
γH2AX
MERGE
MERGE
0
1~5
6~20
21~50

B

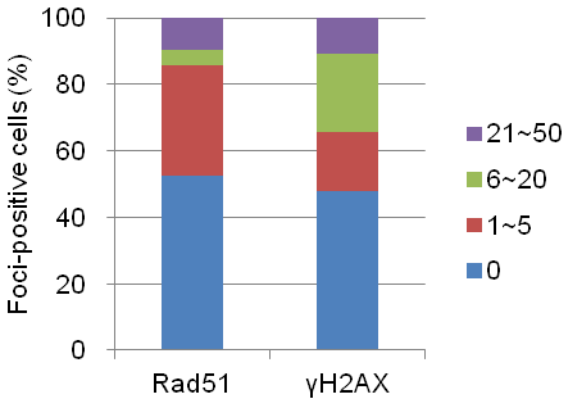
100
80
60
40
20
0
Foci-positive cells (%)
Rad51
γH2AX
21~50
6~20
1~5
0

and then released as in Fig. 1-1C. Interestingly, unlike Rad51 protein levels, Rad51 foci frequency oscillated during cell cycle in mESCs, and numerous foci formed at S phase. Approximately, more than 70% of Rad51 foci-positive cells in S phase had more than five Rad51 foci; among these cells, 20% contained more than twenty Rad51 foci (Figs. 1-4A and 1-4C).

The phosphorylated form of H2AX, denoted γH2AX, is commonly used to detect DNA DSB sites. To determine whether the frequency of Rad51 foci was related to the frequency of DSB sites, I analyzed the number of γH2AX foci in γH2AX foci-positive mESCs. Similar to our results with Rad51, approximately 90% of γH2AX-positive mESCs in S phase had more than five γH2AX foci, indicating that γH2AX foci accumulated from early S phase and decreased as the cell cycle progress to mitosis (Figs. 1-4A and 1-4D). The pattern of Rad51 and γH2AX foci co-localization resembled the pattern of Rad51 and γH2AX foci fluctuation during cell cycle progression in mESCs (Paull et al., 2000; Fig. 1-5). These results imply that functional Rad51 and γH2AX foci formed mainly during the DNA replication process in mESCs. In MEFs, by contrast, the percentage of Rad51-positive MEFs containing more than five Rad51 foci and the percentage of γH2AX-positive MEFs containing more than five γH2AX foci did not exceed 40% and 20%, respectively (Figs. 1-6A and 1-6B). Although the number of Rad51 foci was increased during S

Figure 1-7. Rad51 localization during mitosis in mESCs.

Mitotic cells were sub-classified into five stages according to chromosomal morphogenesis. Each mitotic phase was determined by DAPI staining. The samples were imaged from 5 to 7.5 hr after release from a double thymidine block.

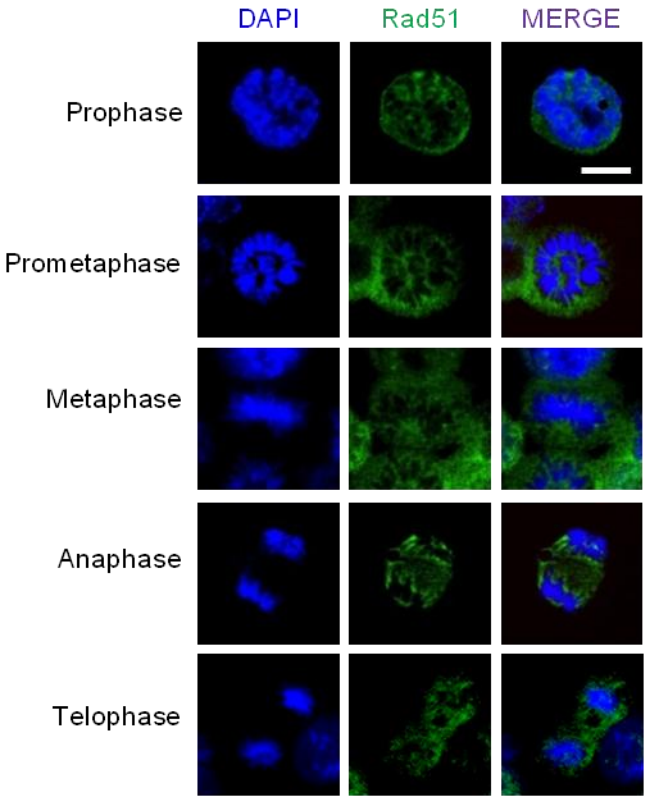
DAPI
Rad51
MERGE
Prophase
Prometaphase
Metaphase
Anaphase
Telophase

phase, Rad51 appeared to dissociate from chromosomes as diffuse during mitosis (Fig. 1-7).

Rad51 localizes inside the replication factory in mESCs

The increase in Rad51 foci during early S phase suggested that Rad51 might be recruited to replication fork area, including the origin of replication initiation. For DNA replication, a pre-replicative complex (pre-RC) composed of ORC (Origin Recognition Complex), CDC6 and CDT1 must assemble at the replication origin (Bell and Dutta, 2002). To uncover the relevancy of Rad51 localization with DNA replication, ORC2 as a key component of ORC was used as a marker of the replication origin. As shown in Figs. 1-8A and 1-8B, most Rad51 foci did not co-localize with ORC2 foci, implying that Rad51 is not particularly recruited to the replication fork area in undamaged mESCs. Approximately 80% of Rad51 and ORC2 existed as separate foci (entities) with some distance between them (Fig. 1-8B). In general, the components of the replication factory, including cell cycle regulators, are localized within an area 0.1-1 μm in diameter (Leonhardt et al.., 1992; Murti et al., 1996; Leonhardt et al., 2000). Thus, I next analyzed the distance between Rad51 and ORC2 foci (described in Fig. 1-9A). For most entities, the inter-foci distance between Rad51 and ORC2 was less than 600 nm (Fig. 1-9B). Rad51 foci were

Figure 1-8. Analysis of Rad51 foci in DNA replication sites.

(A) Representative images of confocal microscopy showing the formation of Rad51 and ORC2 (marker for DNA replication initiation) nuclear foci. The inter-foci distances between Rad51 and ORC2 in each cell were measured using LAS AF software. The scale bar indicates 10 μm. Foci inside the dotted square box were magnified (arrowhead: co-localization; arrow: side-by-side; full duplex arrow: entity). The scale bar in the magnified image is 1 μm.

(B) Based on the pattern of nuclear foci formation, cells were divided into three groups and quantified as in (A).

A

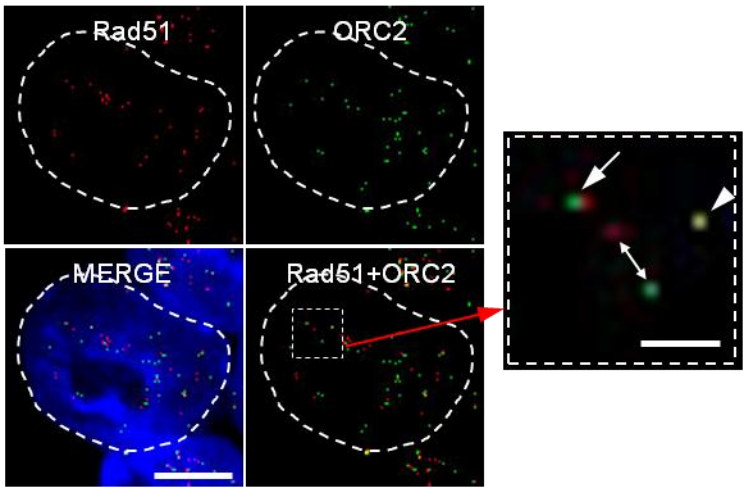
Rad51
QRC2
MERGE
Rad51+ORC2

B

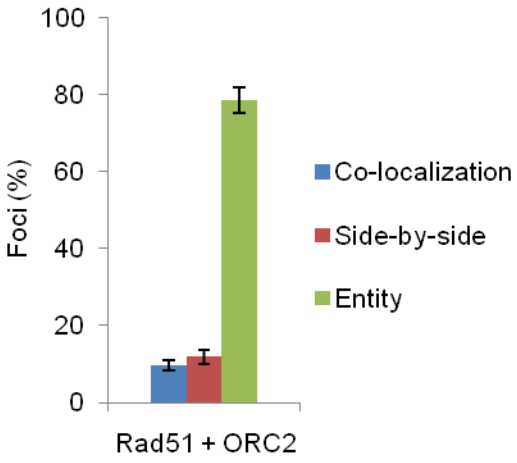
100
80
60
40
20
0
Foci (%)
Co-localization
Side-by-side
Entity
Rad51 + ORC2

Figure 1-9. Crosstalk between Rad51 foci and DNA replication.

(A) Scheme for the measurement of Rad51 and ORC2 nuclear foci distances in mESCs. The distance between Rad51 and ORC2 foci was measured using a single ORC2 entity as the center (red, Rad51; green, ORC2; yellow, co-localization).

(B) Cell populations existing as an independent entity were sub-divided into three groups based on the estimated replication factory size (Koberna et al., 2005).

(C) Rad51 foci inside the replication factory. The inter-foci distances of entity foci were categorized and quantified every 100 nm. Error bars indicate mean ± S.D.

A

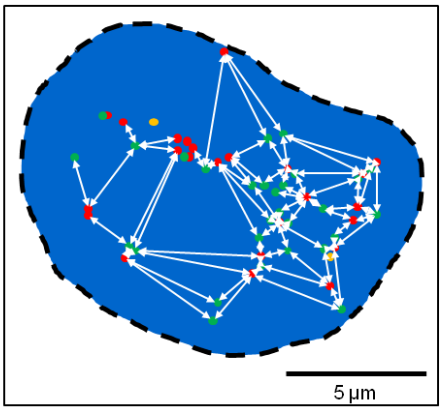
5 μm

B

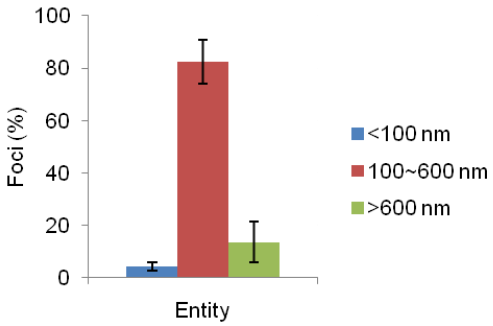
100
80
60
40
20
0
Foci (%)
Entity
<100 nm
100~600 nm
>600 nm

C

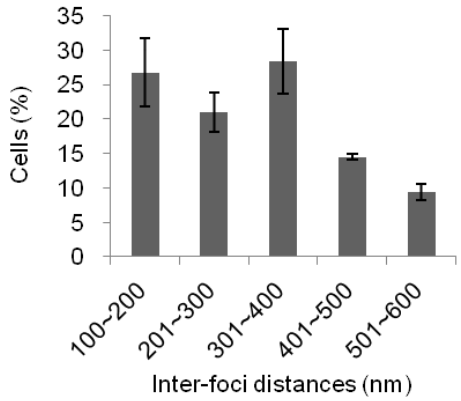
35
30
25
20
15
10
5
0
Cells (%)
100~200
201~300
301~400
401~500
501~600
Inter-foci distances (nm)

randomly distributed within 100-600 nm of ORC2 (Fig. 1-9C). These results suggest that the majority of Rad51 localizes near the replication origin, but not exactly at replication origin.

Rad51 depletion causes a proliferation defect in mESCs

To assess whether Rad51 regulates stem cell characteristics such as self-renewal, pluripotency and growth, I studied the effect of Rad51 depletion on mESCs using siRNA against Rad51 (siRad51) (Fig. 1-10A). The expression of self-renewal factors such as Oct3/4, Sox2, and pSTAT3 was not affected by Rad51 depletion (data not shown). However, the colony sizes of siRad51-treated mESCs were significantly smaller than those of control cells (data not shown). This observation raised the possibility that depletion of Rad51 affected the proliferation rate of mESCs. Consistently, cell-counting analysis revealed that Rad51 depletion significantly delayed the proliferation of mESCs (Fig. 1-10B). I confirmed that the lower cell number and smaller colony size after Rad51 depletion were not caused by apoptosis (data not shown). In addition, to check the relationship between cell proliferation and cellular senescence, I measured the level of Ki67 protein, a marker for senescence. Ki-67 protein is highly expressed in actively dividing cells, but is absent from resting cells (Scholzen and Gerdes, 2000). Ki-67 staining analysis revealed

Figure 1-10. Effect of Rad51 depletion to the proliferation rate of mESCs.

(A) The level of Rad51 protein in mESCs transfected with siNS or siRad51 was detected by immunoblot analysis. β-actin was used as a loading control.

(B) Effect of Rad51 on proliferation of mESCs. mESCs were transfected with siNS or siRad51, and the viable cells were counted at the indicated times.

A

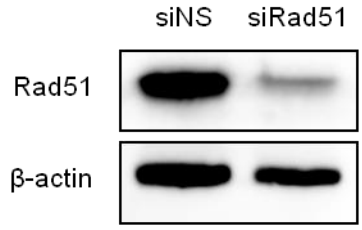
siNS
siRad51
Rad51
β-actin

B

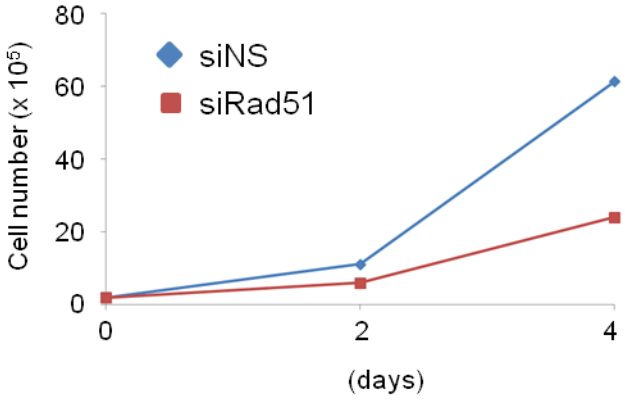
80
60
40
20
0
Cell number (x 10⁵)
siNS
siRad51
0
2
4
(days)

Figure 1-11. Insensitiveness of Rad51 depletion to cellular senescence.

(A) Cells were immuno-stained with anti-Ki67 antibody after siRNA transfection for 48 hr.

(B) The level of Rad51 and the relative proportion of Ki67-positive cells in (A) are shown. Error bars indicate mean ± S.D.

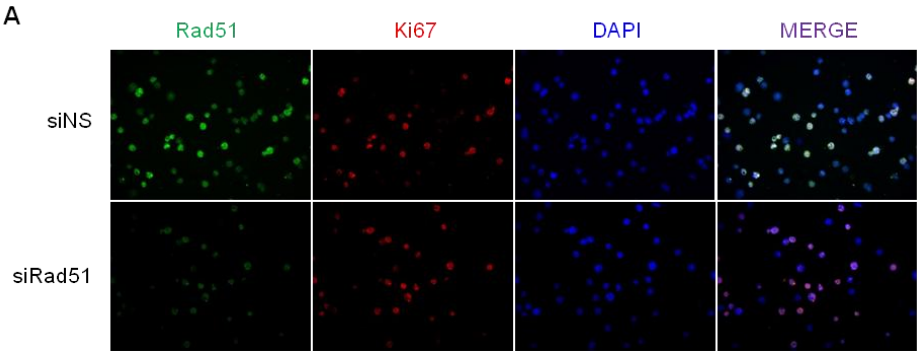
A
Rad51
Ki67
DAPI
MERGE
siNS
siRad51

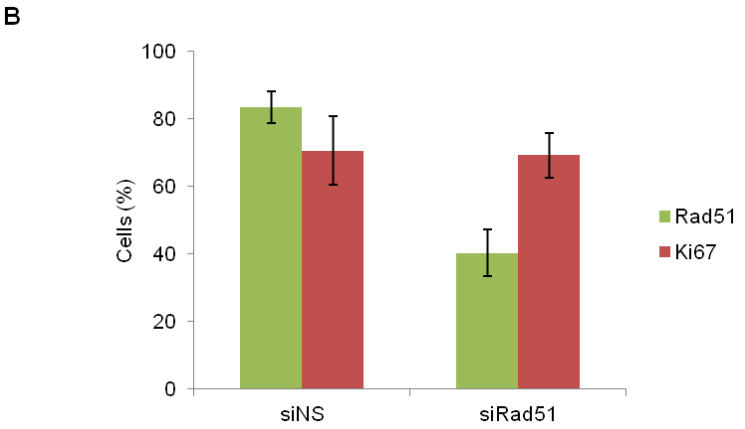
B
100
80
60
40
20
0
Cells (%)
siNS
siRad51
Rad51
Ki67

that the proliferation defect caused by Rad51 suppression was not attributable to cellular senescence of mESCs (Figs. 1-11A and 1-11B).

Proliferation delay in Rad51-depleted mESCs in due to the activation of the DNA damage checkpoint

To investigate the mechanism underlying the effects of Rad51 activity on cell proliferation in mESCs, Rad51 was depleted using siRNA knockdown method. Then, cell cycle progression and checkpoint activation were analyzed. When cells were transfected with siRad51, the number of mESCs, but not of MEFs, in G2/M phase was increased by approximately 10% (Figs. 1-12A, 1-12B and 1-12C). Immunofluorescence assay also showed that the level of cell cycle markers reflects the cell cycle profiles analyzed by FACS on Rad51 knockdown-mESCs (Fig. 1-13). I hypothesized that these G2/M phase-accumulated mESCs from siRad51 would not be externally influenced by G1/S phase synchronization. A double thymidine block method would not affect the cells that accumulated at G2/M phase. When the cell cycle of mESCs was experimentally induced at G1/S phase using thymidine, the number of cells in G2/M phase was determined. As I predicted, the increased populations of Rad51-depleted mESCs in G2/M phase were still remained at G2/M phase even in the presence of thymidine (Figs. 1-12D, 1-12E and 1-12F).

Figure 1-12. Accumulation of Rad51-depleted mESCs in G2/M phase.

(A) Analysis of cell cycle profiles after Rad51 knockdown in mESCs and MEFs. After siRNA transfection for 48 hr, cells were harvested and stained with PI for FACS analysis as described in Materials and Methods (As; asynchronous cells).

(B) FACS data in (A) were quantified using FlowJo software.

(C) The level of Rad51 protein in mESCs and MEFs transfected with siNS or siRad51 were detected by immunoblot analysis. β-actin was used as a loading control.

(D) mESCs transfected with siNS or siRad51 were attempted to synchronize at G1/S phase using double thymidine. The cell cycle profiles of the cells were then analyzed using FACSCalibur.

(E) The population of each cell cycle phase in (D) was quantified with FlowJo software.

(F) The level of Rad51 was determined by immunoblot analysis. –actin was used as a loading control.

A

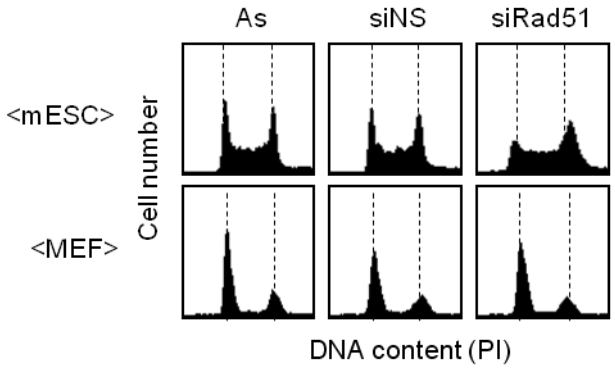
As
siNS
siRad51
<mESC>
<MEF>
Cell number
DNA content (PI)

B

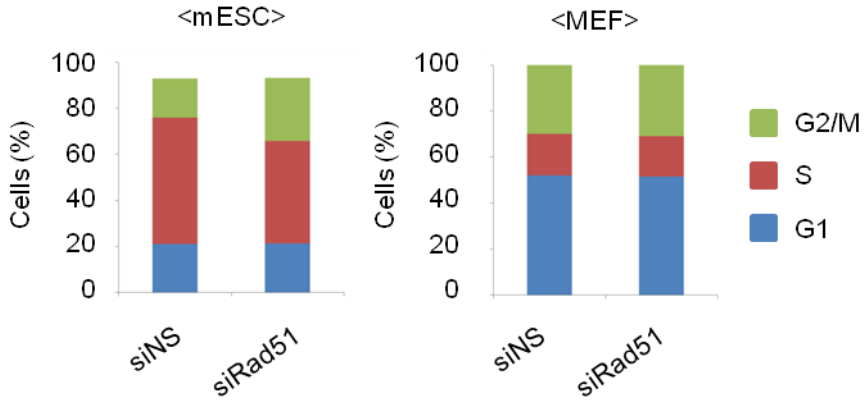
<mESC>
<MEF>
Cells (%)
100
80
60
40
20
0
siNS
siRad51
G2/M
S
G1

C

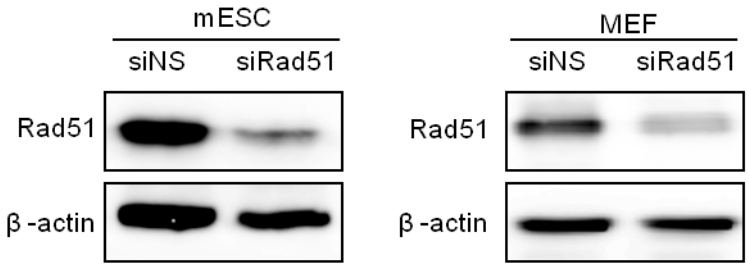
mESC
MEF
siNS
siRad51
Rad51
β-actin

D

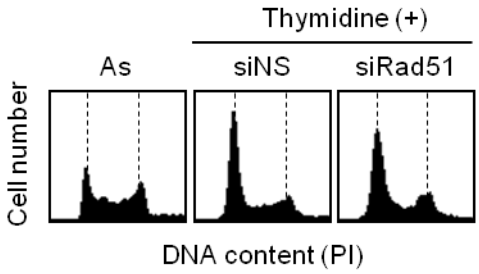
Thymidine (+)
As
siNS
siRad51
Cell number
DNA content (PI)

E

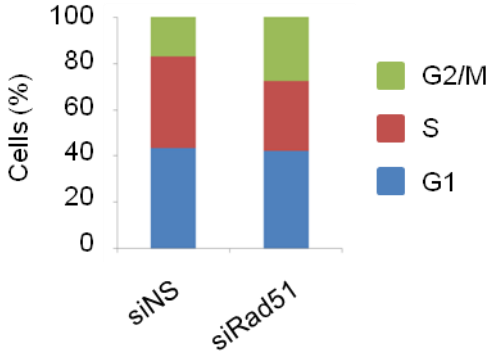
100
80
60
40
20
0
Cells (%)
G2/M
S
G1
siNS
siRad51

F

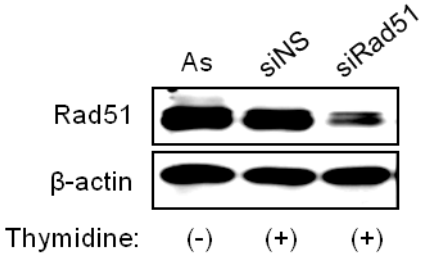
As
siNS
siRad51
Rad51
β-actin
Thymidine:
(-)
(+)
(+)

Figure 1-13. Change of cell cycle status after Rad51 depletion in mESCs.

Cells were immuno-stained with indicated antibodies for cell cycle markers after siRNA transfection for 48 hr. The relative proportion of cells to express respective cell cycle markers was shown in the plot. Error bars indicate mean ± S.D.

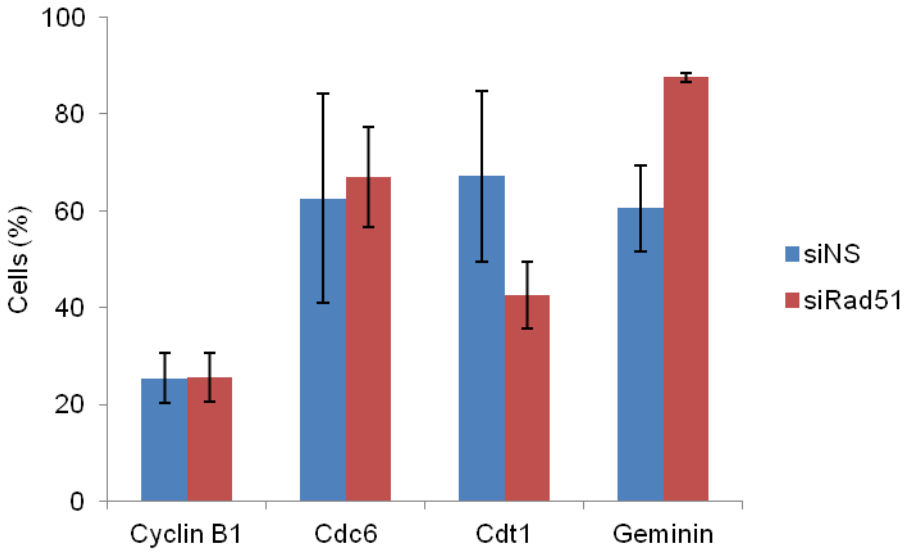
100
80
60
40
20
0
Cells (%)
Cyclin B1
Cdc6
Cdt1
Geminin
siNS
siRad51

These results suggest that Rad51 performs an essential role in normal cell cycle progression in mESCs.

I next examined whether DNA damage checkpoint activation is the main cause of G2/M accumulation among siRad51-treated mESCs. As expected, the phosphorylation of Chk1, as well as H2AX in company with the total amount of p53, was up-regulated in siRad51-treated mESCs (Fig. 1-14A). Immunofluorescence analysis confirmed that Chk1 was phosphorylated and it showed that the number of phospho-Chk1 foci increased approximately 3-fold when Rad51 expression was suppressed (Figs. 1-14B and 1-14C). This result suggests that the accumulation of Rad51 knockdown-mESCs at G2/M phase was related to the activation of DNA damage checkpoint to gain time to repair DNA damage..

Rad51 depletion does not disturb DNA replication in mESCs

As shown above, Rad51 was constitutively expressed throughout the cell cycle (Figs. 1-1A and 1-1D) in mESCs, but Rad51 foci were formed specifically at S phase (Figs. 1-4A and 1-4C). These results implied that Rad51 proteins localize on chromosomes as multiple foci during DNA synthesis. To examine whether Rad51 is required for DNA replication and S-phase progression, BrdU was incorporated into siRad51-transfected cells for 20 min,

Figure 1-14. The effect of Rad51 depletion on DNA damage checkpoint activation in mESCs.

(A) Activation of the DNA damage checkpoint by depletion of Rad51. Cells were harvested 48 hr after siRNA transfection, and markers involved in cell cycle control and DNA damage checkpoint signaling were detected by immunoblot analysis.

(B) Anti-phospho-Chk1^{Ser317} antibody was used to immunostain Rad51 knockdown-mESCs. Nuclei were visualized with DAPI staining. The scale bar indicates 10 μm.

(C) Phospho-Chk1 ^{Ser317}-positive cells (n = 200) were counted and quantified.

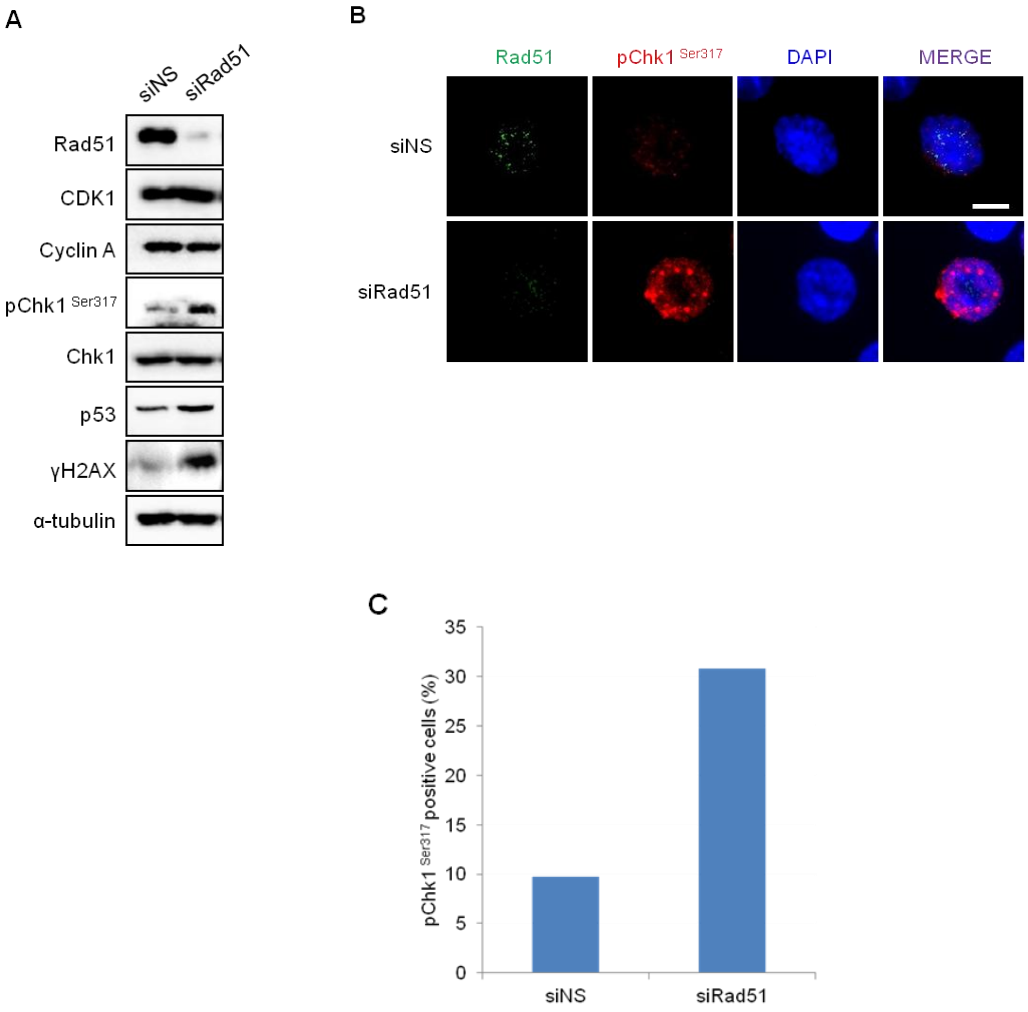
A
siNS
siRad51
Rad51
CDK1
Cyclin A
pChk1 Ser317
Chk1
p53
γH2AX
α-tubulin
B
Rad51
pChk1 Ser317
DAPI
MERGE
siNS
siRad51
C
pChk1 Ser317 positive cells (%)
35
30
25
20
15
10
5
0
siNS
siRad51

and the cells were analyzed with FACS. There was no obvious difference in the S-phase population both in control- and Rad51-siRNA mESCs (data not shown). These results show that Rad51 knockdown does not severely inhibit DNA replication.

Finally, I examined the S-phase progression of Rad51-depleted cells using a double thymidine block and release to synchronize cells at G1/S phase. Cells were treated with thymidine and siRNA as described in Fig. 1-15A. BrdU was incorporated for 20 min before harvest, and the cells were harvested at 2.5-hr intervals after release. Cell cycle index of BrdU-stained cells showed that Rad51 protein levels did not affect cell cycle progression through S phase (Fig. 1-15B). Quantification of BrdU-positive cells revealed that cell cycle progression was not significantly delayed by siRad51 (Fig. 1-15C). These findings provide a conclusion that Rad51 activity does not affect DNA replication during S phase in mESCs.

Figure 1-15. Analysis of cell cycle progression regarding DNA replication after Rad51 depletion in mESCs.

(A) Scheme used in (B). Synchronization and siRNA treatment are described in the Materials and Methods.

(B) After Rad51 knockdown, the amount of incorporated BrdU after release from a double thymidine was assessed. mESCs were treated as described. The same number of BrdU-positive cells was measured by FACS (PI: propidium iodide staining; BrdU: anti-BrdU staining).

(C) The number of BrdU-positive cells in (B) at each cell cycle phase was quantified using FlowJo software.

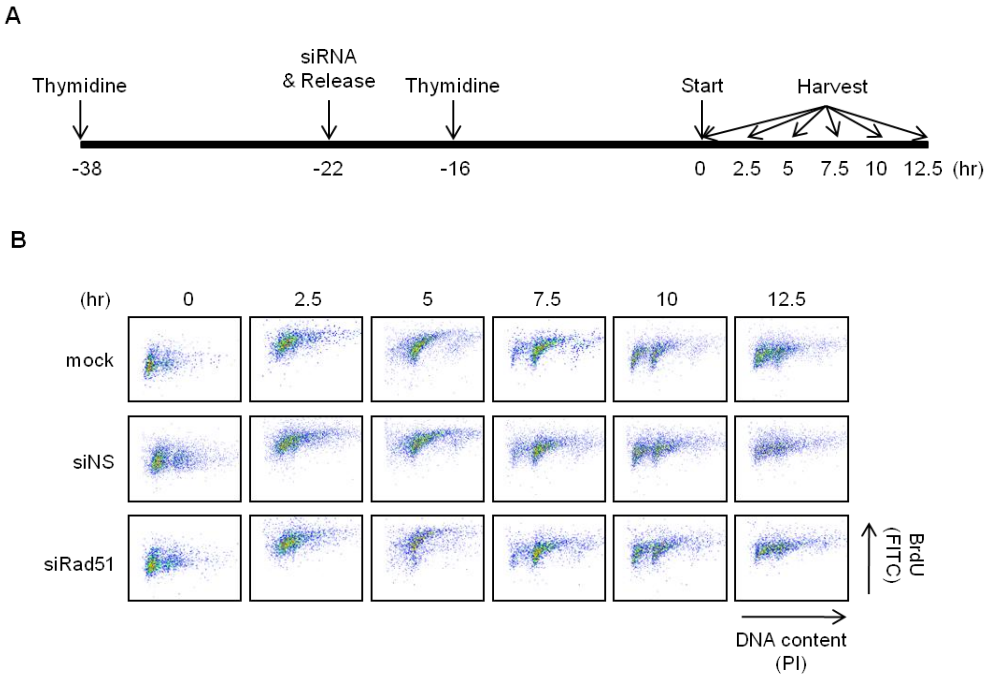
A
Thymidine
siRNA
& Release
Thymidine
Start
Harvest
-38
-22
-16
0
2.5
5
7.5
10
12.5
(hr)
B
(hr)
0
2.5
5
7.5
10
12.5
mock
siNS
siRad51
BrdU
(FITC)
DNA content
(PI)
C
mock
siNS
siRad51
BrdU positive cells (%)
100
90
80
70
60
50
40
30
20
10
0
0
2.5
5
7.5
10
12.5
Double thymidine release (hr)

Discussion

ESCs possess robust machineries to preserve their self-renewal capacity, sustain pluripotency, and maintain a stable genome. In recent studies, 50–70% of asynchronous mESCs were in S phase, compared with ~30% of asynchronous MEFs. To respond to genomic instability within short cell cycles, ESCs utilize high-fidelity regulatory repair machineries to combat DNA damage. In ESCs, HR is the main pathway for maintaining genomic integrity, repairing DSBs, and reactivating stalled DNA replication forks when sister chromatids are available. In the replication dynamics of unchallenged mammalian somatic cells, Rad51 may promote continuous replication in an HR-independent manner to protect nascent ssDNA formed at replication forks from Mre11-dependent degradation or in an HR-dependent manner to ensure replication fork progression (Daboussi et al., 2008; Hashimoto et al., 2010).

In this study, I demonstrated that Rad51 plays a novel role in the cell cycle progression of unperturbed mESCs and established a link between its activity in HR and checkpoint activation in the G2/M phase (Fig. 1-16). Our results suggested that activation of the G2/M checkpoint by depletion of Rad51 was not related to the rate of replication fork progression, even though a deficiency in Rad51 HR activity caused cells to accumulate in G2/M phase (Figs. 1-12, 1-

Figure 1-16. Multifunctional roles of Rad51 in mESCs

Rad51 plays a novel role in the cell cycle progression of unperturbed mESCs and established a link between its activity in HR and checkpoint activation in the G2/M phase.

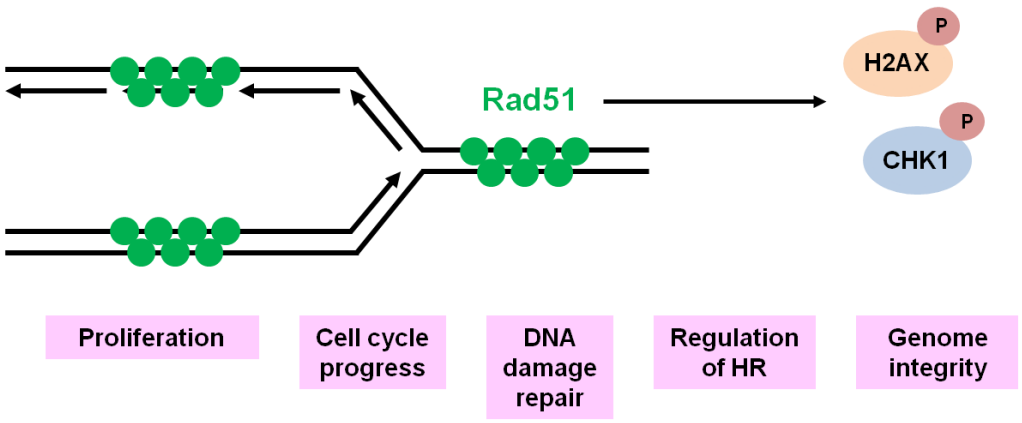
Rad51
P
H2AX
P
CHK1
Proliferation
Cell cycle progress
DNA damage repair
Regulation of HR
Genome integrity

14 and 1-15). In contrast, HR abnormalities in differentiated cell lines reduce the replication speed and increase the density of replication forks (Daboussi et al., 2008). This strongly suggests that the HR activity of Rad51 is uncoupled from replication fork progression in S phase in mESCs. It also implies that Rad51 activity in mESCs is not restricted to the restart of collapsed replication forks (Petermann et al., 2010); rather, it might extend to the repair of replication defects. Because HR activity in mESCs is not related to replication fork progression, the replication speed in mESCs is similar to that in MEFs (Vannier et al., 2013). The localization of Rad51 within 100–600 nm of ORC2 indicates that the majority of Rad51 foci are formed near the replication origin. This further supports that Rad51 foci formation is not restricted to the regions of replication origin, and thus Rad51 may play a role at postreplication stages. ORC2, the main component of the pre-RC, mainly functions during the assembly of the ORC to recruit proteins needed for replication initiation. Therefore, our results also suggest that genomic DNA in the region of the replication origin is prone to DSBs in mESCs.

A critical question is what underlies the differences in the mechanisms of Rad51 activity during the replication of unperturbed DNA in mESCs and differentiated cells. One possibility is that the high rate of proliferation in mESCs increases the risk of accumulating harmful DSBs during the replication

of genomic DNA, thus necessitating the HR function of Rad51. It has reported that the high level of DNA damage checkpoint proteins reflects that mESCs can rapidly respond to DNA damages (DSBs or stalled replication forks) in a way that does not affect the proliferation and stemness of mESCs (Tichy et al., 2012). Recent reports showed that expression of a dominant-negative Rad51 mutant in mESCs increased the level of spontaneous chromatid breaks, which further supports that DNA DSBs occur during S phase in mESCs (Kim et al., 2012). I also speculate that the unique cell cycle pattern of mESCs underlies the constant expression of high levels of Rad51 throughout the cell cycle (Fig. 1-1). Given that it takes ~12 h for mESCs to complete one round of cell cycle (Nagy et al., 2003), expeditious HR activity to repair DSBs that occur spontaneously during replication is essential. When the serum concentration was gradually decreased from 10% to 1%, Rad51 protein levels and the proliferation rate of mESCs decreased in proportion to the serum concentration, which indicates that Rad51 expression is positively related to the proliferation rate of mESCs (Fig. 1-2). The molecular mechanism by which mESCs maintain high levels of Rad51 is another important question for investigation. The results of quantitative RT-PCR analysis suggest that constant transcription of Rad51 attributes to the high level of Rad51 in mESCs (data not shown). The Rad51 promoter is positively regulated by a STAT5-dependent pathway and

negatively regulated by p53 (Slupianek et al., 2001; Pauklin et al., 2005) . It will be important to determine whether mESCs have a characteristic mechanism for the constitutive activation of Rad51 transcription.

Although Rad51 was expressed throughout the cell cycle, the number of Rad51 foci oscillated depending on the cell cycle phase, and Rad51 appeared to dissociate from chromosomes during mitosis (Figs. 1-4 and 1-7). This pattern of Rad51 localization at mitosis was previously described, regardless of cell types or species (Cappelli et al., 2011). In mitosis, Rad51 protein has strongly shown to localize in cytoplasm distinct from chromosomes, as diffuse, in human primary fibroblasts and MEFs (Cappelli et al., 2011). I also observed Rad51 signals in the nucleus immediately after cytokinesis (data not shown). These results suggest that the association of Rad51 with chromosomes is strictly regulated during the cell cycle to prevent unexpected HR activity during mitosis.

Of note, the self-renewal and differentiation capacities of mESCs were not significantly affected by Rad51 expression (data now shown). However, I do not rule out the possibility that genomic DNA related to self-renewal or pluripotency of mESCs sustains DNA DSBs during replication. Our study provides insights into the mechanism by which mESCs respond to replication stress (collapsed replication forks, endogenous DNA damage, etc.) to maintain genome stability. Human ESCs (hESCs) also express higher levels of Rad51

than differentiated somatic cells (data not shown). Whether the function of Rad51 in cell cycle progression is conserved between mESCs and hESCs remains to be determined.

CHAPTER 2

Rec8 phosphorylation mediates crossover-designated recombination and regulatory surveillance in meiosis

Abstract

Rec8 cohesin, a meiosis-specific α-kleisin subunit, is a key component of the meiotic cohesion complex that regulates sister chromatid cohesion and recombination between homologous chromosomes. Physical analysis of recombination in yeast strains expressing phosphorylation-defective Rec8 implies that Rec8 phosphorylation is required for timely and efficient progression of recombination at the double-strand break (DSB) to single-end invasion (SEI) transition and at the late stages of crossover (CO)-designated recombination that is also modulated by Zip1 and Zip3. Furthermore, Rec8 phosphorylation in aberrant pre-meiotic DNA replication continues to function during post-DSB stage in the formation of CO recombinants. Eliminating of Mek1 kinase activity relieves the delay caused by Rec8 phosphorylation-defective checkpoint activation at almost every stage of meiotic recombination progression. I discuss a general logic in the relationship between Rec8 phosphorylation and chromosome organization that is involved in recombination progression and regulatory surveillance during meiosis.

Introduction

Meiosis involves a complex progression of chromosomal events that results in the physical connection of homologous chromosomes. This connection ensures that maternal and paternal homologous chromosomes segregate to opposite poles at the first meiotic division (Kleckner et al., 2004). In budding yeast, the meiosis-specific components, Rec8 cohesin and Red1/Hop1/Mek1 (RMH) complex, bind at chromosome axes (as defined by chromatin immunoprecipitation analysis) and are observed along chromosome axes (as shown cytologically) (Zierhut et al., 2004; Storlazzi et al., 2008; Kim et al., 2010). General structural components of the chromosome also localize to chromosome axes including topoisomerase II, the cohesin-associated protein Pds5, and condensins (Klein et al., 1992; Klein et al., 1999; Yu et al., 2003). Rec8 cohesin, a meiosis-specific α-kleisin subunit, occurs abundantly in conjoined sister axes and also in paired homologous chromosomes in the presence or absence of sister chromatids (Brar et al., 2006; Kim et al., 2010; Lin et al., 2011). During meiosis, separase-mediated cleavage of Rec8 on chromosome arms triggers resolution of exchanged axes and homologs segregation (Buonomo et al., 2000; Hornig et al., 2004). However, Shugoshin (Sgo1) protects centromeric-Rec8 against cleavage by recruiting protein

phosphatase 2A (PP2A), which locally maintains Rec8 in a dephosphorylated status and thereby maintains sister-chromatid connections until meiosis II (Kitajima et al., 2006; Riedel et al., 2006).

Meiotic recombination appears to be initiated through programmed DNA double-strand breaks (DSBs), which are catalyzed by topoisomerase-like protein Spo11 after meiotic DNA replication (Keeney et al., 2001; Neale et al., 2005; Fig. 2-1). DSB ends subsequently undergo extensive nucleolytic resection and expose a 3'-single stranded overhang of approximately 500 nucleotides that is required for homology searching (Hunter et al., 2006; Garcia et al., 2011; Cannavo et al., 2013). The "first" DSB end exchanges with a homolog chromatid by a process mediated by the RecA homologs, Dmc1 and Rad51, and forms a nascent D-loop that is polymerized to single-end invasion (SEI) (Hong et al., 2013; Lao et al., 2013). The "second" DSB end engages with the same SEI duplex strand and produces a double-Holliday junction (dHJ). The interhomolog-dHJs (IH-dHJs) are resolved into crossover (CO) products; otherwise, the repair occurring in the absence of flanked DNA exchange gives rise to non-crossover (NCO) products (Börner et al., 2004; Fig. 2-1). I previously determined that Rec8 is required for timely and efficient DSB-JM (joint molecule) formation and for the progression of COs, but not NCOs, through the maintenance of homolog bias downstream of the Zip3 step

Figure 2-1. Relative timing of recombinational events and chromosomal stages during meiotic prophase I. Meiotic recombination is initiated by the programmed double-strand breaks (DSBs) that are catalyzed by topoisomerase-like protein Spo11. DSBs are then processed and stabilized into single-end invasions (SEIs) following the formation of double-Holliday junctions (dHJs), which are eventually resolved to crossovers (COs) by elaborately regulated processes.

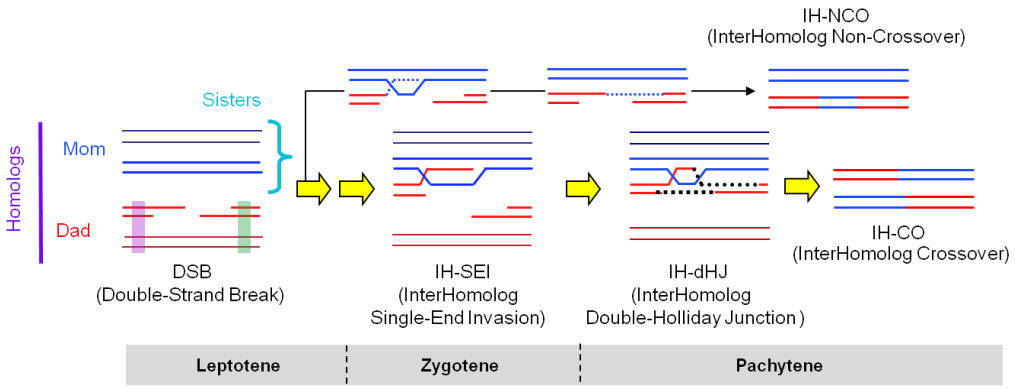
IH-NCO
(InterHomolog Non-Crossover)
Sisters
Homologs
Mom
Dad
IH-CO
(InterHomolog Crossover)
DSB
(Double-Strand Break)
IH-SEI
(InterHomolog
Single-End Invasion)
IH-dHJ
(InterHomolog
Double-Holliday Junction)
Leptotene
Zygotene
Pachytene

(Kim et al., 2010). Moreover, RMH-activated Dmc1/Rad51 locally counteracts Rec8-mediated sister channeling in the absence or presence of sister chromatids (Hong et al., 2013).

Rec8 phosphorylation is essential for the step-wise loss of cohesins and timely meiotic progression (Brar et al., 2006). Many sites important for Rec8 cleavage are phosphorylated by Cdc5, a polo-like kinase, in yeast (Brar et al., 2009; Attner et al., 2013). Moreover, the phosphorylation of Rec8 by Dbf4-dependent Cdc7 kinase (DDK) and Hrr25 mediates cohesin cleavage at meiosis I (Katis et al., 2010). These observations raise the possibility that Rec8's role in meiotic recombination is closely related to its phosphorylation status. However, it remains unclear whether Rec8 phosphorylation affects merely the establishment of cohesion between sister chromatids or plays specific roles in homologous recombination processes including DSB initiation, homolog partner choice, and CO/NCO differentiation through a ZMM (Zip1/2/3/4, Msh4/5, Mer3) pathway in meiotic prophase I. To address these key questions, I performed a DNA physical analysis of meiotic recombination by using phosphorylation-defective Rec8 cohesin mutants, in which the Rec8 phosphorylation sites were mutated to alanines. Furthermore, Rec8 can also function in global surveillance pathway during meiosis (Kim et al., 2010). Here, I show that inactivating Mek1 kinase relieves the delay of

meiotic progression caused by the absence either Rec8 cohesin or phosphorylatable Rec8. The results presented below have multiple general implications for the regulatory role of Rec8 phosphorylation in meiotic chromosomes and provide further insights into the relationship of Rec8 phosphorylation with regulatory surveillance in the progression of meiotic recombination.

Materials and Methods

Yeast stains

All yeast strains were homozygous for *nuc1::hygroB,* and heterozygotes at the *HIS4LEU2* locus for the *Bam*HI/*Ngo*MIV. Details regarding strain constructions are listed in Table 2-1. Deletion mutant strains have been constructed by polymerase chain reaction (PCR)-based one-step gene disruption and confirmed by yeast colony PCR as described (Wach et al., 1994; Longtine et al., 1998; Goldstein and McCusker, 1999). Two phosphorylation-defective mutants of *rec8* (*rec8-6A* and *rec8-29A*) have been previously described (Brar et al., 2006; Brar et al., 2009; Katis et al., 2010). To produce mutant strains encoding *mek1as*, I individually mated each strain (WT, *rec8-6A*, *rec8-29A*, and *rec8⊿*) with a *mek1as* haploid strain, and appropriated strains were selected genetically. WT, *rec8-6A* and *rec8-29A* mutants with *pMCD1-CDC6* background were generated by mating *pMCD1-CDC6* strain with WT, *rec8-6A* and *rec8-29A* strains.

Meiotic time courses

Synchronous meiosis was performed as previously described (Kim et al., 2010; Hong et al., 2013). In detail, cells were first patched onto YPG plates

(1% yeast extract, 2% Bacto-peptone, 2% Bacto-agar, and 3% glycerol) and grown for overnight, and then single colonies were picked onto YPD plates (1% yeast extract, 2% Bacto-peptone, 2% Bacto-agar, and 2% glucose) after 2 days of growth. For supplemented pre-sporulation (SPS) cultures to synchronize cells at the G1 phase, a 1/500 dilution of the culture was used with SPS medium (0.5% yeast extract, 1% Bacto-peptone, 0.67% yeast nitrogen base without amino acids, 1% potassium acetate, 0.05 M potassium biphthalate, pH to 5.5) and grown at 30^{o}C for 18hr. Meiosis was initiated by transferring cells to SPM medium (sporulation medium, 1% potassium acetate, 0.02% raffinose, and 0.01% antifoam) pre-warmed to 30^{o}C. For analysis of Mek1-dependent meiotic recombination in *rec8-6A*, *rec8-29A* and *rec8⊿* mutants, a single culture was synchronized and divided into four identical sporulation cultures. Then, to inhibit Mek1 kinase activity in *mek1as* strain, a fresh 1 μM 1-NA-PP1 was added to three identical cultures at 3 hr, 5 hr, and 7 hr, respectively.

Meiotic progression analysis

Meiotic division was monitored by fluorescence microscopy after 4′,6-diamidino-2-phenylindole (DAPI) staining (Padmore et al., 1991). Briefly, cells in meiotic culture were harvested at the time points and cells were fixed

in 0.1 M sorbitol plus 40% ethanol and stained with DAPI. The total numbers of meiosis I and meiosis II populations were calculated from DAPI nuclei staining (n=200).

DNA physical analysis

Genomic DNA preparation and recombination physical analysis were performed as described previously (Kim et al., 2010; Hong et al., 2013). For physical analysis of meiotic recombination, cells were sporulated in SPM and harvested at various time points. Genomic DNA was cross-linked with psoralen and 365nm ultraviolet light. DNA from each time point was extracted using a guanidine and phenol extraction method. Genomic DNA (2 μg) was digested with 80 units *Xho*I and dissolved in DNA loading buffer after precipitation with sodium acetate and ethanol. Electrophoresis of 1D gel (0.6% Seakem LE agarose in Tris-borate-ethylenediaminetetra acetic acid [TBE]) was performed in TBE buffer at 2V/cM for 24 hr. For two-dimensional (2D) gel analysis, 2.5 μg of *Xho*I-digested DNA was loaded onto 0.4% Seakem gold agarose gel (lacking ethidium bromide) and whole genomic DNA was separated. Gels were stained with 0.5 μg/mL ethidium bromide in TBE, and slices of each DNA lane were cut to cover the DNA of interest. The gel slices containing the DNA lane were placed onto the 2D-gel tray to the direction of

electrophoresis. DNA was positioned so that the higher molecular weights were to the left side. 2D-gel (0.8 % Seakem LE agarose gel in TBE containing 0.5 μg/ml ethidium bromide) was poured onto the gel slices. 2D electrophoresis was performed in pre-chilled TBE containing 0.5 μg/mL ethidium bromide at 6V/cm for 6 hr at 4^{o}C. For CO and NCO assays, 2 μg of DNA was digested with *Xho*I and *Ngo*MIV and analyzed on 1D gel electrophoresis as above. Gels were subjected to Southern blot analysis with "Probe A" after transfer onto positively charged nylon membranes (Bio-Rad). Probes were radiolabeled with ^{32}P-dCTP using a Random Priming kit (Agilent Technologies). Hybridizing DNA signals were visualized and quantified using a phosphoimager with Quantity One software (Bio-Rad).

Immunoblotting

Yeast cell lysates were prepared as described previously (Kushnirov, 2000) with some modifications. Briefly, yeast cells were washed in distilled water and finally resuspended in 0.3M NaOH. After 5 min incubation at room temperature, samples were centrifuged at 5,000 rpm for 1 min. Discarding the supernatant, 1x protein loading buffer was added to each pellet, mixed well followed by boiling for 5 min. Equal amounts of cell lysates were analyzed by SDS-PAGE and blotting was performed as standard procedures (Sambrook et

al., 1997). Dephosphorylation of Rec8 was assessed by phosphatase treatment. Yeast cell extracts from 6 hr-samples after sporulation were incubated in a dephosphorylation buffer (50mM HEPES pH 7.5, 100mM NaCl, 0.01% NP40, 2mM MnCl2, 2mM DTT) for 3 hr at 30 ^{o}C with or without lambda phosphatase (New England Biolabs) while agitating gently. WT and mutant Rec8 proteins were detected by HA antibody (F-7 from SantaCruz, Cat# sc-7392, diluted at 1:1,000). Pgk1 antibody was detected Pgk1 protein for a loading control (22C5D8 from Invitrogen, Cat# 459250, diluted at 1:5,000).

Chromosome spreading and immunofluorescence

Fixation of yeast cell and chromosomes spreading for immunofluorescence assay were performed as described previously (Bishop, 1994; Kim et al., 2010). Briefly, cells were harvested and spheroplasted to remove the cell walls. After centrifugation, the pellets were resuspended and incubated in ZK buffer (25mM Tris-Cl, pH 7.5, 0.8M KCl) with DTT (final concentration to 50mM) for 2 min at room temperature with gentle mixing. 100T zymolyase (USBiological) was added to reaction samples with optimal concentration, then incubated for 30 min. Pellets were obtained by centrifugation and washed once, then resuspended in cold MES buffer (0.1M MES, pH 6.5, 1M sorbitol, 1mM EDTA, 0.5mM $MgCl_2$). Fixation and lysis were conducted by 3%

paraformaldehyde with 3.4% sucrose and 1% lipsol, respectively, followed by placing samples onto a clean slide. After drying, slides were dipped in 0.2% photoflo (Kodak Ltd.) for 30 sec and transferred to TBS buffer (25mM Tris-Cl, pH 8, 136mM NaCl, 3mM KCl) followed by blocking TBS buffer plus 1% BSA (Bovine Serum Albumin). Mouse monoclonal HA antibody for detecting Rec8 protein, was diluted at 1:1,000. Rabbit polyclonal Zip1 antibody (Y-100 from SantaCruz, Cat# sc-33733) was diluted at 1:500. The secondary antibody specific for HA and Zip1 antibody was Goat anti-mouse IgG conjugated with Alexa-fluor-488 (Jackson ImmnoResearch, Cat# 115-545-003, diluted at 1:500) and Goat anti-rabbit IgG conjugated with Cy3 (Jackson ImmunoResearch, Cat# 1111-165-003). The contrast and brightness of images were adjusted using Adobe Photoshop software. The intensities of chromosomal array of WT and mutant Rec8 strains were measured and quantified using ImageJ software from NIH.

Spore viability test

Diploid single colonies from WT and each mutant strain were inoculated in SPM media (1% potassium acetate, 0.02% raffinose) and grown overnight at 30^{o}C, and then >80 tetrads were dissected for each strains. The plates were incubated at 30^{o}C for 2 days.

Results

Characterization of Rec8 phosphorylation

Amon and colleagues have shown that the Rec8 phospho-mutants (Fig. 2-2) normally support sister chromatid cohesion, but exhibit prophase delay (Brar et al., 2009; Fig. 2-3C). Further, absence of recombination abolished the delay in the meiotic cell cycle progression of the Rec8 phospho-mutants (Brar et al., 2006). These findings suggested that Rec8 phosphorylation is important for meiotic recombination. In WT, Rec8 proteins were highly expressed and clearly seen in the shifted-signal of phosphorylated form at pachytene of prophase I. However, Rec8 phosphorylation was defective in *rec8-29A* cells (Fig. 2-3A) and phosphorylated signals of Rec8 could be abolished by phosphatase (Fig. 2-3B). Furthermore, staining intensity of Rec8 phospho-mutants at the pachytene chromosome was decreased according to the phosphorylation status of Rec8 (Figs 2-3D and 2-3E).

DNA physical analysis system used for studying meiotic recombination

The physical events of meiotic recombination were monitored at the *HIS4LEU2* hotspot of chromosome III to analyze the nature of meiotic recombination (Schwacha and Kleckner, 1997; Hunter et al., 2001; Oh et al.,

Figure 2-2. Phospho-mutation sites of Rec8 mutants. Mutation of phosphorylation sites of *rec8-6A* in (A) and *rec8-29A* in (B). Phosphorylation sites were identified by mass-spectrometry (Katis et al., 2010).

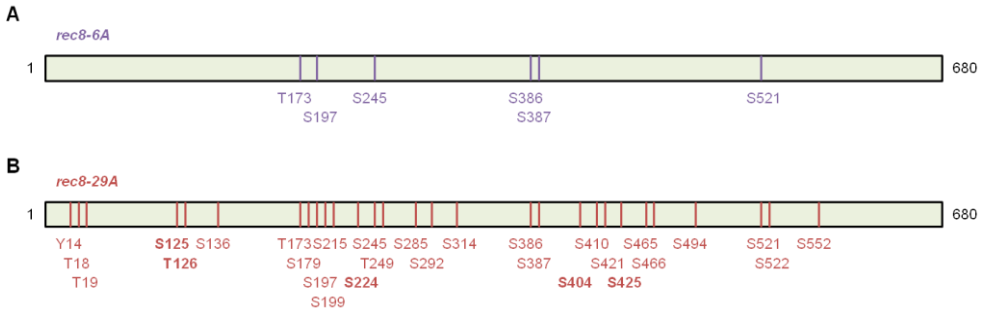
A
rec8-6A
1
680
T173
S197
S245
S386
S387
S521
B
rec8-29A
1
680
Y14
T18
T19
S125
T126
S136
T173
S179
S197
S199
S215
S224
S245
T249
S285
S292
S314
S386
S387
S404
S410
S421
S425
S465
S466
S494
S521
S522
S552

Figure 2-3. Analysis of Rec8 phosphorylation.

(A) Analysis Rec8 phosphorylation in WT and Rec8-phospho mutant cells. Meiosis was induced to express meiosis-specific Rec8 protein. Anti-HA antibody was used to detect Rec8-3HA proteins in indicated strains at various time points. Pgk1 served as loading controls.

(B) Dephosphorylation assay of Rec8. Yeast cell extracts from WT, *rec8-6A*, and *rec8-29A* at 6-hr samples after sporulation were incubated in the absence or presence of with λ-phosphatase for 3 hr at 30 ^{o}C. Mouse monoclonal HA antibody was used to detect 3HA-tagged WT and phospho-mutant Rec8 proteins. Mouse monoclonal Pgk1 antibody was used as a loading control.

(C) Meiotic division curves of in WT, *rec8-6A*, *rec8-29A* and *rec8Δ* strains. MI±MII is the percentage of cells that have completed the first and second meiotic divisions as determined by DAPI staining.

(D) Representative images showing chromosomal array of WT and Rec8 phospho-mutants at pachytene chromosome. Linear arrays of Rec8-3HA in various strains were immunostained and visualized by anti-HA antibody.

(E) Quantification of staining intensity in (D). Intensities of chromosomal Rec8 were measured by ImageJ software (NIH). Error bars indicate mean± standard deviation (SD).

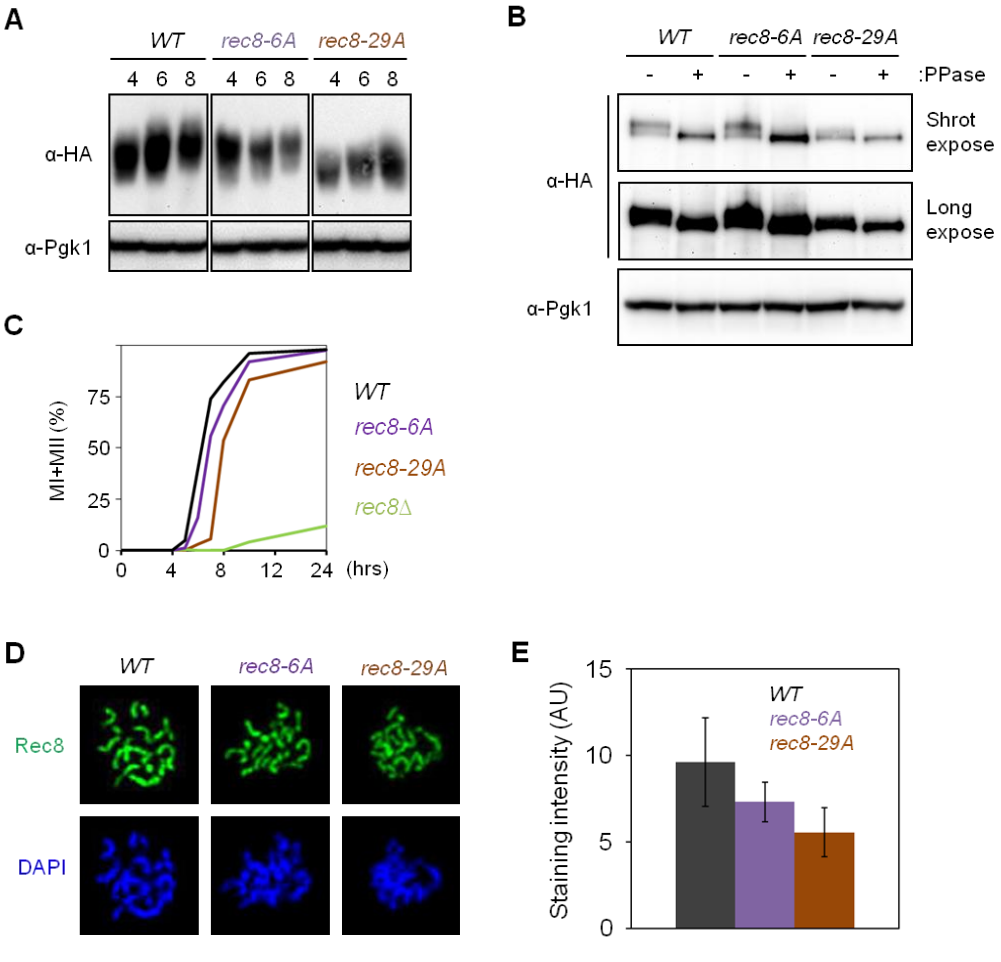
A
WT
rec8-6A
rec8-29A
4 6 8 4 6 8 4 6 8
α-HA
α-Pgk1
B
WT
rec8-6A
rec8-29A
- + - + - + :PPase
α-HA
Shrot expose
Long expose
α-Pgk1
C
MI+MII (%)
75
50
25
0
0 4 8 12 24 (hrs)
WT
rec8-6A
rec8-29A
rec8Δ
D
WT
rec8-6A
rec8-29A
Rec8
DAPI
E
Staining intensity (AU)
15
10
5
0
WT
rec8-6A
rec8-29A

Figure 2-4. System used for DNA physical analysis of meiotic recombination

(A) Physical map of the *HIS4LEU2* hotspot showing diagnostic restriction sites and the position of Probe A. DNA species digested with *Xho*I or *Xho*I + *Ngo*MIV are shown and each recombinant DNA species was detected by means of gel electrophoresis and Southern analysis performed using "Probe A". *N*, *NFS1*; *R*, *RRP7*; *S*, *STE50* (Hunter and Kleckner, 2001).

(B) One-dimensional (1D) gel analysis showing double-strand breaks (DSBs) and crossover (CO) species of wild-type (WT). Mom, mom species; Dad, dad species; JMs, joint molecules.

(C) Two-dimensional (2D) gel analysis displaying parental and JM species of WT. Different kinds of the structure of meiotic intermediates between homologous chromosomes or sister chromatids are depicted. SEIs, single end invasions; dHJ, double-Holliday Junction (Mom species: red lines, dad species: blue lines).

(D) Interhomolg-crossover (IH-CO) and interhomolog-noncrossover (IH-NCO) fragments digested with *Xho*I + *Ngo*MIV represent each set of recombinants in the WT strain during meiosis.

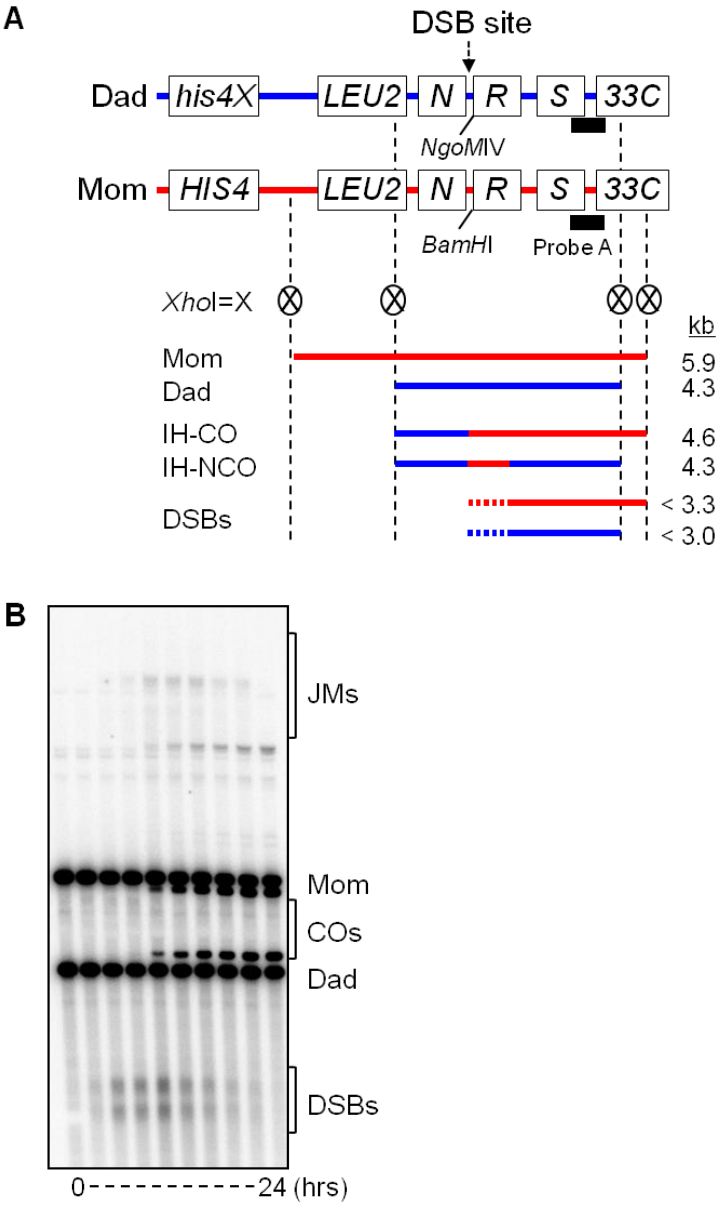
A
DSB site
Dad
his4X
LEU2
N
R
S
33C
NgoMIV
Mom
HIS4
LEU2
N
R
S
33C
BamHI
Probe A
XhoI=X
kb
Mom
Dad
5.9
4.3
IH-CO
IH-NCO
4.6
4.3
DSBs
< 3.3
< 3.0
B
JMs
Mom
COs
Dad
DSBs
0----------24 (hrs)

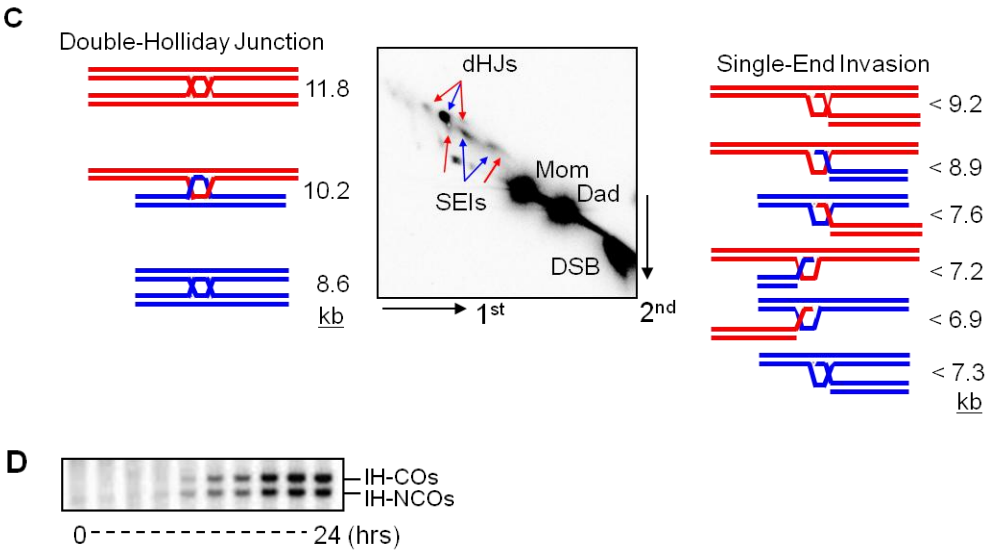
C
Double-Holliday Junction
11.8
10.2
8.6
kb
dHJs
SEIs
Mom
Dad
DSB
1st
2nd
Single-End Invasion
< 9.2
< 8.9
< 7.6
< 7.2
< 6.9
< 7.3
kb
D
IH-COs
IH-NCOs
0
24 (hrs)

2007; Kim et al., 2010; Hong et al., 2013; Sasanuma et al., 2013; Fig. 2-4). Spo11-induced meiotic DSBs occur at two parental "Mom" and "Dad" sites in the *HIS4LEU2* locus during meiosis (Fig. 2-4A). Cell cultures were induced to initiate synchronous meiosis in the SPM medium. All cell samples from the meiotic time course were treated with psoralen and exposed to UV light (365 nm) to generate intra-strand cross-links for stabilizing recombination intermediates such as JMs (Figs. 2-4B and 2-4C). Meiotic genomic DNA samples were carefully prepared using an optimized guanidine-phenol extraction method and diagnostic Mom and Dad fragments of parental chromosomes, DSBs, and recombinant chromosomes (COs) were distinguished based on *Xho*I restriction site polymorphisms (Figs. 2-4A and 2-4B). Each enzyme-digested DNA sample from the time course was subjected to one-dimensional (1D) gel electrophoresis to analyze DSBs and COs (Fig. 2-4B). To analyze the processing of meiotic DNA intermediates, I used two-dimensional (2D) gel electrophoresis, which has been applied to monitor JMs processing during meiotic recombination. *Xho*I restriction-fragment polymorphisms between parental diploid cells were integrated into the yeast genome. Thus, various species of SEIs and dHJs exhibited distinct migration mobility, which was indicated by the distinguishable shapes and sizes detected in 2D-gel analysis (Fig. 2-4C). After digesting genomic DNA with *Xho*I and

*Ngo*MIV, COs and NCOs were detected at 4.6 and 4.3 kb, respectively, in 1D-gel analysis (Fig. 2-4D). The radiolabeled "Probe A" sequences were used for Southern hybridization, and the hybridized DNA signals were quantified using phosphoimager software (Fig. 2-4).

Rec8 phosphorylation is dispensable for timely and efficient DSB formation

Once Spo11-mediated DSBs occur, they are rapidly processed through the removal of the terminally-attached Spo11 protein and then further resected at the 5´strand termini to generate 3´single-stranded DNA (ssDNA) tails (Neale et al., 2005; Garcia et al., 2011). Rec8 has been implicated in regulating meiotic DSB turnover, but whether Rec8 phosphorylation affects the regulation of DSB turnover is unclear (Kugou et al., 2009; Kim et al., 2010). To examine the role of Rec8 phosphorylation in DSB formation, I analyzed meiotic DSBs in wild-type (WT) and *rec8Δ* and in two *Rec8* alleles, *rec8-6A* and *rec8-29A*, in which several phosphorylation residues were mutated to alanines (Brar et al., 2009; Fig. 2-2). In WT strain, DSBs appear at 2.5 hr after induction of meiosis, peak at 3.5 hr, and are processed by approximately 8 hr (Fig. 2-5). The DSB turnover in *rec8Δ* mutant cells is severely delayed when compared with that in WT cells (Kim et al., 2010; Fig. 2-5). Moreover, the

Figure 2-5. Analysis of DSBs and COs in phospho-deficient Rec8 mutants.

(**A**) Results of 1D-gel analysis showing DSBs and COs arisen from WT, phospho-deficient Rec8 mutants and *rec8Δ* from meiotic time courses.

(**B**) Quantification of DSB and CO events in WT and indicated single mutants. The levels of DSBs and COs were quantified at the *HIS4LEU2* hotspot and analyzed as described elsewhere (Kim et al., 2010). Red arrows indicate the levels and timing of DSB formation at 2.5 hr.

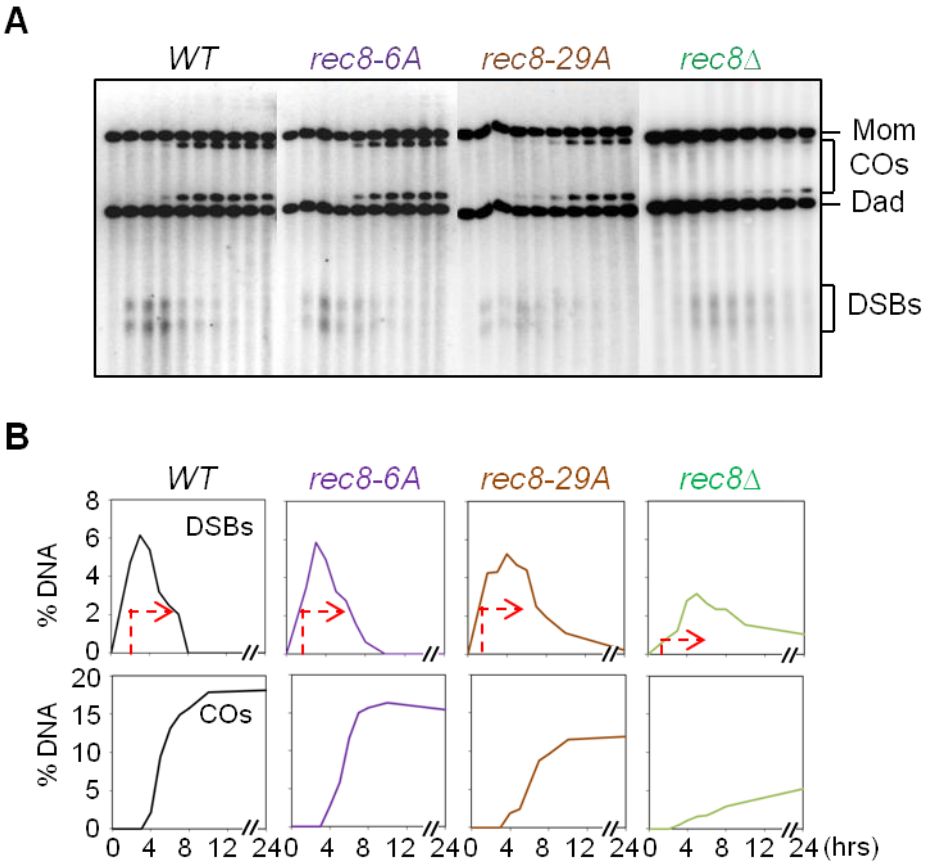
A
WT
rec8-6A
rec8-29A
rec8Δ
Mom
COs
Dad
DSBs
B
WT
rec8-6A
rec8-29A
rec8Δ
DSBs
% DNA
8
6
4
2
0
COs
% DNA
20
15
10
5
0
0 4 8 12 24 0 4 8 12 24 0 4 8 12 24 0 4 8 12 24 (hrs)

Figure 2-6. 2D-gel showing DSB resection of Rec8-phospho mutants. Images and illustrations showing DSB resection of various Rec8 mutants are depicted. Nuclease resects the single-stranded DNA in 5'-3' direction. Notably, hyper-resection phenotype of DSBs is only observed in *rec8Δ* strain.

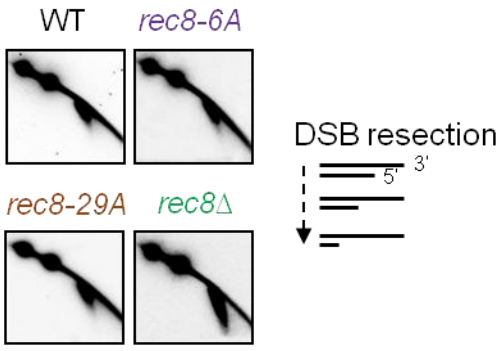
WT
rec8-6A
rec8-29A
rec8Δ
DSB resection
5'
3'

DSB level in the *rec8Δ* mutant is diminished by approximately 60% compared with that in the WT strain (Fig. 2-5). Ohta and colleagues have shown that the slowing of DSB kinetics and the occurrence of low levels of DSBs are the result of the impaired Spo11 binding to chromosomes that is related to Rec8 deletion (Kugou et al., 2009). I further observed that the timing and the level of DSB formation in *rec8-6A* and *rec8-29A* cells are highly similar to that in WT cells, except that the numbers of DSBs exhibit slower turnover (Fig. 2-5); thus, a delay in prophase I in Rec8 phosphorylation-defective alleles may not affect initial DSB occurrence (Figs. 2-3B and 2-5). In WT cells, DSBs are resected with a downward spike of length, with ≥90% being resected by ≥500 nucleotides, as determined by the extent of 5' terminal resection (Kim et al., 2010; Zakharyevich et al., 2010; Fig. 2-6). Absence of Rec8 confers a modest increase in DSB hyper-resection, which is detected as slightly elongated signals as compared with those of the WT (Fig. 2-6). However, all Rec8 phosphorylation-defective strains exhibit the same phenotypes as the WT with respect to DSB resection. Collectively, these results indicate that *rec8-6A* and *rec8-29A* strains form normal DSBs and sister-chromatid cohesion, but that the defect in the post-DSB stage of homologous recombination depends on the status of Rec8 phosphorylation.

Rec8 phosphorylation is critical for timely progression of the DSB into SEI

Contrary to the preferential use in mitosis of sister chromatids as the templates for DSB repair, meiosis preferentially uses homologous chromosomes as the templates for DSB repair. JMs, SEIs, and dHJs from homologs or sister chromatids that can be distinguished based on their molecular weight and structure (Hunter and Kleckner, 2001; Kim et al., 2010; Hong et al., 2013; Figs. 2-4A and 2-4C). In WT cells, SEIs and dHJs occur coordinately and peak at 4 hr with an IH:IS ratio of 5:1 (Fig. 2-7). These strong homolog bias and efficient JM turnover are diminished in *rec8Δ* and Rec8 phosphorylation-defective cells. In the absence of Rec8, homolog bias is established and then lost in maintenance of homolog bias at the SEI-to-dHJ transition, which resulted in a 1:1 IH:IS dHJ ratio (Kim et al., 2010; Fig. 2-7). Consistent with inefficient CO production (Fig. 2-5), the timing of JMs (SEIs and dHJs) formation is delayed by approximately by 1.5 hr and 4 hr in the *rec8-6A* and *rec8-29A* strains, respectively (Fig. 2-7B). The levels of dHJs are elevated in the *rec8-6A* and *rec8-29A* strains likely because of an increased lifespan of these species, rather than an increase in the number of recombination events. In *rec8-6A* cells, the IH:IS dHJ ratio is 5:1, but the JM process is delayed slightly compared with that in WT (Fig. 2-7B). The *rec8-*

Figure 2-7. Analysis of meiotic recombination intermediates in Rec8 phosphorylation-defective strains

(A) Results of 2D-gel analysis of JMs (SEIs and dHJs): representative images showing the maximal levels of JMs in WT and indicated single mutants at various time points. The times exhibiting the maximal levels of JMs formation are different in every indicated strains. Square bracket and trident denote SEIs and dHJs, respectively.

(B) Quantification analysis for the levels of DSBs, SEIs, interhomolog-dHJs (IH-dHJs) and intersister-dHJs (IS-dHJs) shown in (A). Lines in different colors show the levels of meiotic intermediates of indicated strains in corresponding colors. Circles in each graph denote the harvest times of corresponding strains. IH-dHJs and IS-dHJs are colored in blue and red, respectively. Error bars represent the error range in each independent experiment.

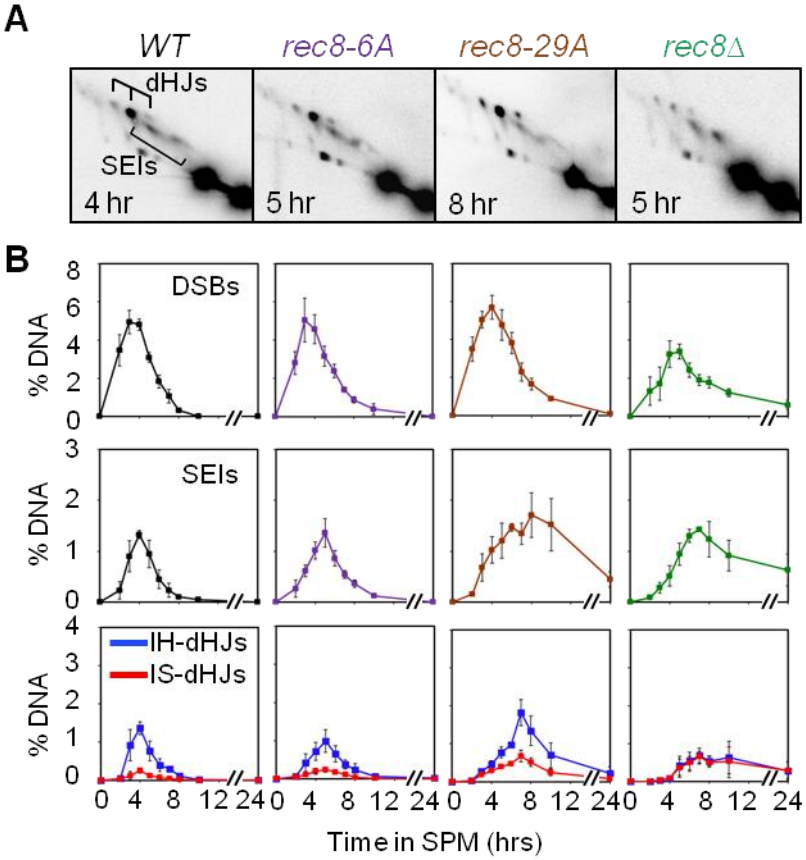
A
WT
rec8-6A
rec8-29A
rec8Δ
dHJs
SEIs
4 hr
5 hr
8 hr
5 hr
B
DSBs
SEIs
IH-dHJs
IS-dHJs
% DNA
Time in SPM (hrs)

Figure 2-8. Analysis of COs and NCOs outcome in phospho-deficient mutants of Rec8

(A) Images of interhomolog-crossovers (IH-COs) and interhomolog-noncrossovers (IH-NCOs) in WT and indicated single mutants during meiosis.

(B) Quantification of the level of IH-COs and IH-NCOs shown in (A). IH-COs and IH-NCOs are depicted in black and grey colors, respectively. Error bars represent the error range in each independent experiment.

(C) Quantitative analysis of relative ratio of IH-COs to IH-NCOs in each indicated strain. Error bars indicate mean± standard deviation (SD).

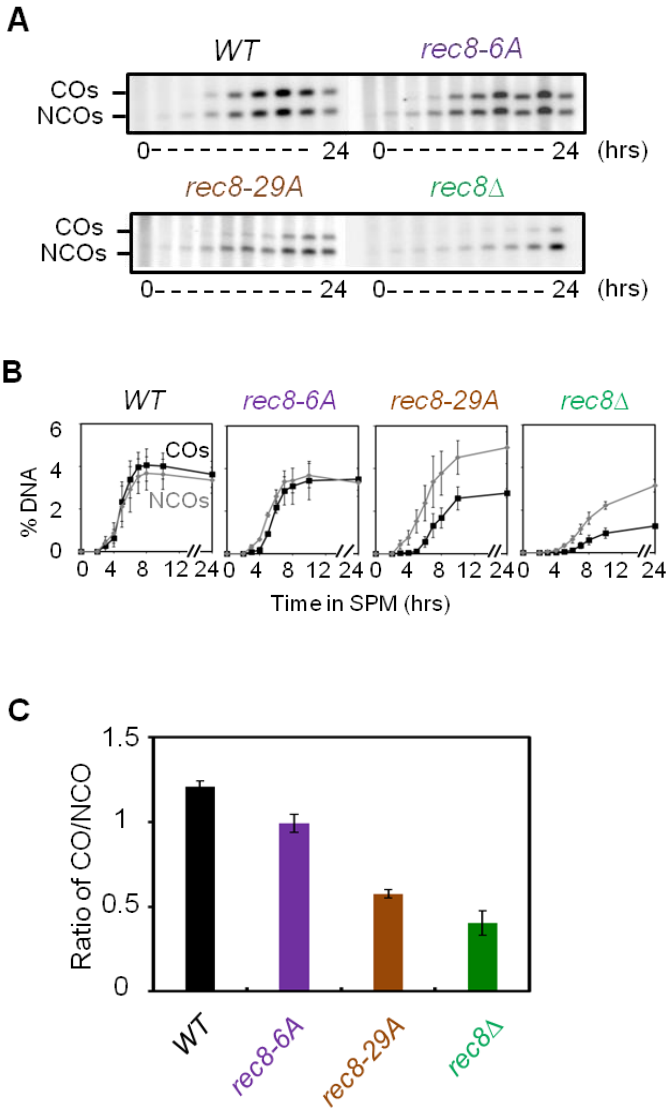
A
WT
rec8-6A
COs
NCOs
0 24 0 24 (hrs)
rec8-29A
rec8Δ
COs
NCOs
0 24 0 24 (hrs)
B
WT
rec8-6A
rec8-29A
rec8Δ
% DNA
COs
NCOs
0 4 8 12 24 0 4 8 12 24 0 4 8 12 24 0 4 8 12 24
Time in SPM (hrs)
C
Ratio of CO/NCO
1.5
1
0.5
0
WT
rec8-6A
rec8-29A
rec8Δ

29A mutant cells exhibit a 3:1 IH:IS dHJ ratio, which slightly reduced the homolog bias, and the turnover is delayed considerably. Furthermore, a substantial number of JMs in the *rec8-29A* mutant resolves to CO products (approximately 60% of the WT level; Fig. 2-5). These phenotypes suggest that the phosphorylation of Rec8 is an indispensable process in the establishment and/or maintenance of homolog bias. These two possibilities are distinguished by results showing a reduction in COs, but not NCOs, according to the Rec8 phosphorylation status (Fig. 2-8). Thus, our findings help to explain that Rec8 phosphorylation functions as a coordinating signal in the maintenance of homolog bias.

Rec8 phosphorylation mediates efficient progression of CO-designated DSBs

To identify the post-DSB CO-specific defect in the Rec8 phosphorylation-defective strains, I performed 1D-gel analysis on the WT and mutant strains to determine the timing and the levels of CO and NCO. In WT cells, both COs and NCOs occur at substantially higher level (COs, ~5.5%; NCOs, ~5.1%) than in the mutant cells at the same timing, but the turnover of NCOs occurred slightly earlier than that of Cos (Fig. 2-8). The *rec8Δ* strain is severely defective in the formation of COs, whereas the NCOs form at substantial

levels in this strain (Figs. 2-8A and 2-8B). The Rec8 phosphorylation-defective alleles exhibit a delay in the progression of CO and NCO formation depending on the phosphorylation sites being eliminated (Fig. 2-8). Furthermore, I determined that at this stage, the requirement of Rec8 phosphorylation for recombination is specific to CO formation and that whereas NCO formation occurs at normal levels, much as shown in the absence of Rec8 (Fig. 2-8A and 2-8B); only the CO-designated pathway is impaired when the phosphorylation status of Rec8 was altered (Fig. 2-8). Thus, Rec8 phosphorylation appears to be required for the maintenance of bias, and our result further show that immediately after the establishment of homolog bias, Rec8 phosphorylation is required for the efficient progression of recombination in CO-designated DSB repair (Fig. 2-9). In the *rec8-29A* mutant, the turnover of recombinant intermediates, the appearance of CO/NCO, and meiotic division are more severely delayed than compared to those in both WT and *rec8-6A* mutant (Fig. 2-9).

Rec8 phosphorylation functions in ensuring CO-fated recombinational interaction coordinating with Zip1

Rec8 is essential for axis morphogenesis and localize to distinct domains along organized chromosomes (Klein et al., 1999; Kim et al., 2010). To further

Figure 2-9. Timing and kinetics of recombination events in each of the strains. Relative timing of the turnover for DSBs (black), SEIs (purple), dHJs (red), COs, and NCOs during meiosis were analyzed as described (Kim et al., 2010). The lifespan of each recombination event was measured by the timing of the length, beginning and end of recombinant DNA formation. CO and NCO products are marked by black and blank circles, respectively, to denote their appearance and disappearance in approximately 50% of cells.

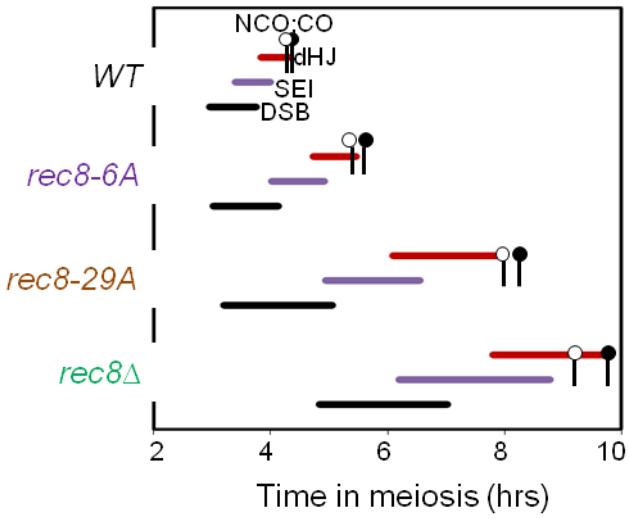
NCO:CO
dHJ
SEI
DSB
WT
rec8-6A
rec8-29A
rec8Δ
2
4
6
8
10
Time in meiosis (hrs)

characterize meiotic chromosome axis morphogenesis in Rec8-phospho mutant cells, I sorted nuclei with detectable Rec8 signals into four categories (Kim et al., 2010; Fig. 2-10A). Nuclei for four categories progressively disappear (I) and appear (II~IV) in WT and the mutant cells. Although *rec8-6A* cells exhibited no detectable defect in the pattern of Rec8 staining, *rec8-29A* cells progress category I~III at normally, but exhibited a significant delay in the progress of category IV compared to WT (Figs. 2-10C). In Rec8 phospho-mutations, Zip1 assembly became less efficient and the number of full synapsed chromosome was decreased with an elevated frequency of polycomplex formation (Figs. 2-10B and 2-10C). Thus, Rec8 phosphorylation influences SC formation in the meiotic chromosome and efficient meiotic division. These results confirmed that phosphorylation of Rec8 phospho-mutants are defective from early prophase I and the progress defect seen in *rec8-6A* and *rec8-29A* cells is partially due to defects in localization of Rec8 to the chromosome axes and in SC morphogenesis. This defect was also confirmed using spore-viability tests, which showed that impaired Rec8 phosphorylation resulted in a reduction in viable spores (Fig. 2-10D).

Mek1 activation and Rec8 phosphorylation are dispensable for recombinational progression

Figure 2-10. Chromosome morphogenesis in Rec8-phospho mutants.

(A) Immunofluoresence images for Rec8-3HA of WT cells after chromosome spreads. Category I, no staining signals; Category II, modest numbers of foci; Category III: larger numbers of foci with a clear tendency for linear arrays; Category IV: strongly staining lines. Anti-HA antibody was used to immunostain Rec8-3HA after chromosome spreads.

(B) Representative images of Zip1 formation at the pachytene chromosomes in WT and various Rec8-phospho mutants. Mouse monoclonal anti-HA antibody and rabbit polyclonal anti-Zip1 antibody were individually used to visualize Rec8-3HA and Zip1 proteins. Images were acquired from Image Pro-Express software (Olympus Co., Ltd) and adjusted with Adobe Photoshop software. White arrowhead in Zip1 image of *rec8-29A* mutant denotes a Zip1-polycomplex, which implies inefficient formation of synapsed chromosomes.

(C) Quantification of appearance and disappearance for Rec8-3HA and Zip1 staining category in (A) and (B) over time in meiosis. Over 200 nuclei were analyzed for each time point. Meiotic division (MI+MII) was described as dotted lines in azure. The percentage of full array of Zip1 and the percentages of Zip1-polycomplex (Zip1-PC) staining were shown in purple lines and in blue lines with circles, respectively (black lines, category I; green lines, category II; red lines, category III; orange lines, category IV).

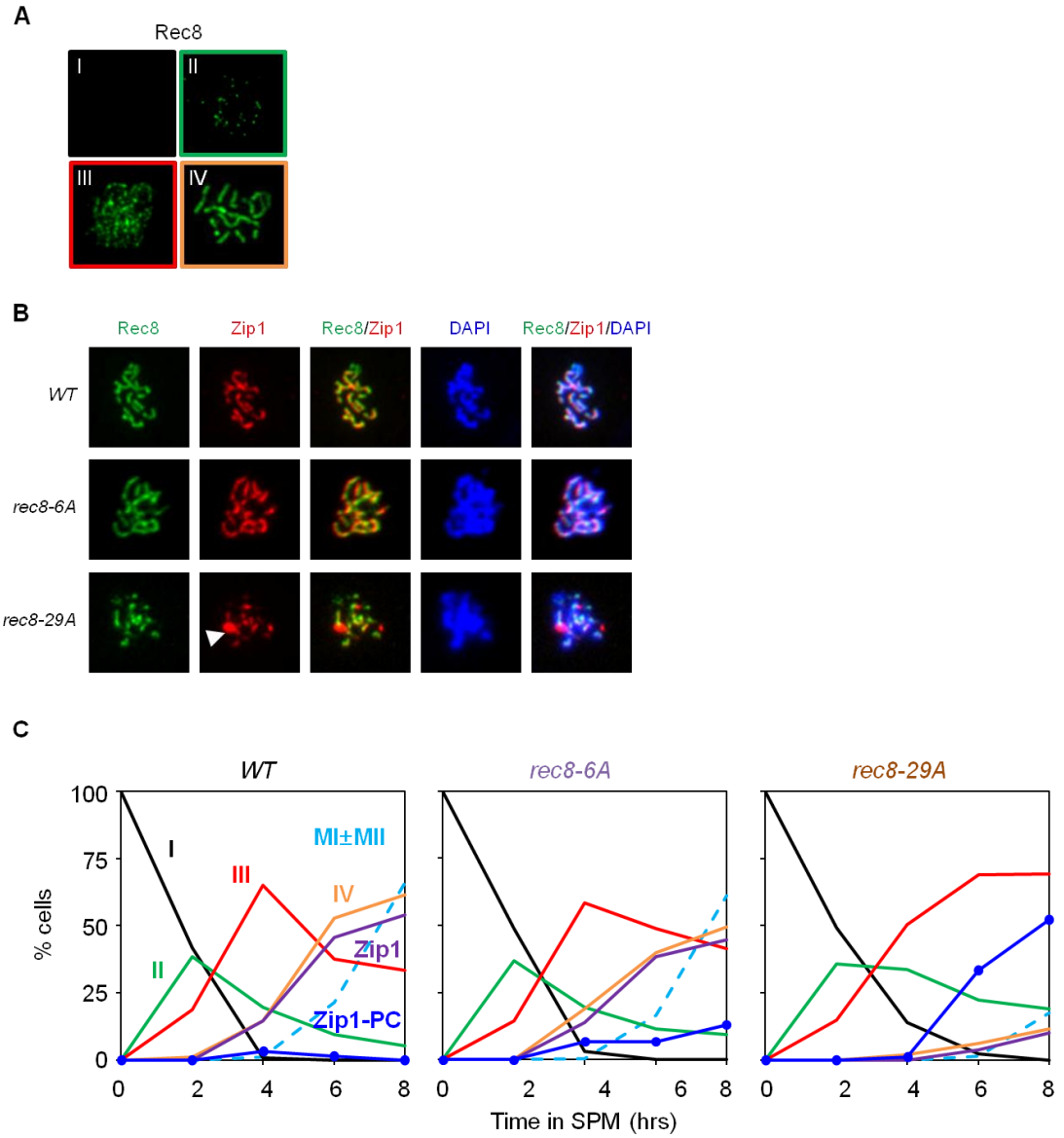
A
Rec8
I
II
III
IV
B
Rec8
Zip1
Rec8/Zip1
DAPI
Rec8/Zip1/DAPI
WT
rec8-6A
rec8-29A
C
WT
rec8-6A
rec8-29A
% cells
100
75
50
25
0
I
II
III
IV
MI±MII
Zip1
Zip1-PC
0
2
4
6
8
Time in SPM (hrs)

(D) Viable spores were counted at least >80 tetrads after tetrad dissection of the indicated mutants incubated in SPM media for overnight at 30^{o}C. Numbers indicate each spore of tetrads normally grown on YPD media for 48 hr and converted into a percentage (sv: spore viability).

D

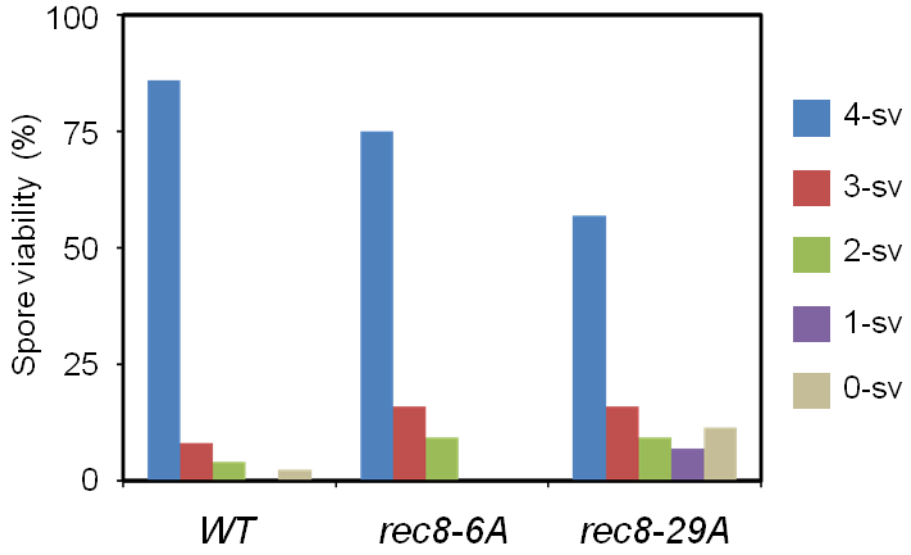
100
75
50
25
0
Spore viability (%)
WT
rec8-6A
rec8-29A
4-sv
3-sv
2-sv
1-sv
0-sv

Mek1 is required for ensuring IH bias in which a DSB engages a homolog partner rather than the sister chromatid and for signaling in checkpoint activation (Niu et al., 2007; Kim et al., 2010; Wu et al., 2010). The *mek1as* strain encodes a mutant Mek1 kinase protein in which ATP-binding affinity can be inhibited by using 1-NA-PP1 (Wan et al., 2004). Thus, Mek1 kinase activity can be abolished in the presence of this chemical inhibitor (Niu et al., 2005; Kim et al., 2010; Terentyev et al., 2010; Hong et al., 2013). Hereafter, *mek1as(+IN)* and *mek1as(-IN)* signify the *mek1as* strains in the presence and absence of 1-NA-PP1, respectively. Meiotic recombination in *mek1as(-IN)* presents the same pattern as in WT (Kim et al., 2010). Adding the inhibitor at the initial meiotic DNA replication stage results in a rapid progression of meiotic recombination, and meiotic recombination tends to exhibit sister bias; consequently, COs and NCOs cannot be readily detected through gel analysis. As noted in the preceding subsection, all recombinant intermediates are significantly delayed in *rec8Δ* (Figs. 2-5, 2-7 and 2-8); however Mek1 kinase inactivation relieves all of these timing delays (Kim et al., 2010; Figs. 2-11 and 2-14). The question remained as to whether Mek1-mediated checkpoint inactivation relieves the delays in timing by promoting DSB process to COs/NCOs in all Rec8 phosphorylation-defective strains. This correspondence was observed by inactivating Mek1 kinase at various DSB timings in the

rec8Δ mek1as, *rec8-29A mek1as*, and *rec8-6A mek1as* strains (Figs. 2-12, 2-13 and 2-14). In the *rec8Δ mek1as(-IN)* mutant, the timing of DSB is delayed in the absence of inhibitor as compared with that in the *mek1as(-IN)* strain (Fig. 2-14). In RMH- condition, the *rec8Δ* strain displays a faster pattern of DSB turnover as well as JM formation (Kim et al., 2010). These results are obtained regardless of whether the inhibitor was added at 3 hr, 5 hr, or 7 hr (Fig. 2-11 and 2-14). All recombination intermediates, DSBs and JMs, in the *rec8Δ mek1as* strain are immediately processed in the absence of Mek1 kinase activity (Fig. 2-14B). Thus, in *rec8Δ mek1as(+IN)*, the dramatic delays in progression detected in *rec8Δ* are no longer observed; DSBs, SEIs and dHJs progressed efficiently and both COs and NCOs appear (Fig. 2-14A and 2-14B). Moreover, the amount of CO and NCO products increase rapidly depending on the time at which the inhibitor is added (Fig. 2-14C and 2-14D). In the absence of both Rec8 and Mek1 kinase activity, partner choice is almost identical to that in the absence of Rec8 alone (the IH:IS dHJ ratio is ~1:1). With regard to the formation of meiotic recombination intermediates, both *rec8-29A mek1as* and *rec8-6A mek1as* alleles also exhibit rapid turnover in DSB, SEI and dHJ formation as soon as Mek1 kinase is inactivated, as shown in the *rec8Δ* mutant (Figs. 2-12, 2-13 and 2-14). No discernable differences appear among the mutant alleles until SEI formation and the ratio of COs and NCOs increase at a

Figure 2-11. Mek1-mediated checkpoint inactivation. Schematic representation of experimental procedures. A single meiotic culture was synchronized at G1 phase in SPS medium and divided into four identical cultures. Then, to inactivate Mek1-dependent checkpoint, a fresh 1-NA-PP1 was added to three identical meiotic cultures at 3 hr, 5 hr, and 7 hr after induction of meiosis, respectively.

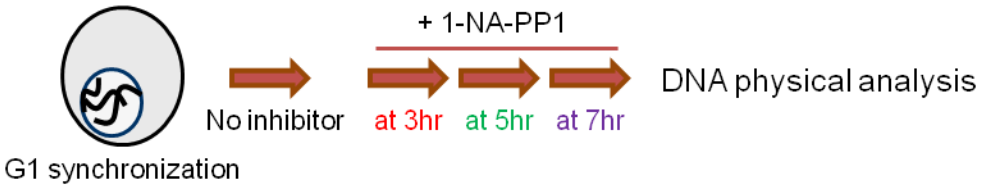
+ 1-NA-PP1
No inhibitor
at 3hr
at 5hr
at 7hr
DNA physical analysis
G1 synchronization

Figure 2-12. DNA physical analysis of *rec8-6A mek1as* strain.

(A) Representative images of 2D-gel of *rec8-6A mek1as* strain in the absence or presence of 1-NA-PP1 at the indicated time points. Square brackets and arrowheads denote JMs and DSBs, respectively. The time points in the images means the time points after induction of meiosis (IN: 1-NA-PP1, inhibitor of Mek1 kinase)

(B) Quantification of recombination intermediates in the *rec8-6A mek1as* strain shown in (A). Black lines represent the turnover of DSBs and JMs of *rec8-6A mek1as* strain without inhibitor. Red, green, purple lines represent the turnover of DSBs and JMs of *rec8-6A mek1as* strain with inhibitor at 3 hr, 5 hr, and 7 hr, respectively.

(C) Analysis of CO and NCO formation in the *rec8-6A mek1as* strain in the absence or presence of 1-NA-PP1 at the indicated time points.

(D) Corresponding quantification data in (C). The levels of COs and NCOs were shown in black and grey lines, respectively.

(E) Total 2D-gel images show joint molecule formation of *rec8-6A mek1as* strain in the absence or presence of Mek1 kinase inhibitor during meiosis.

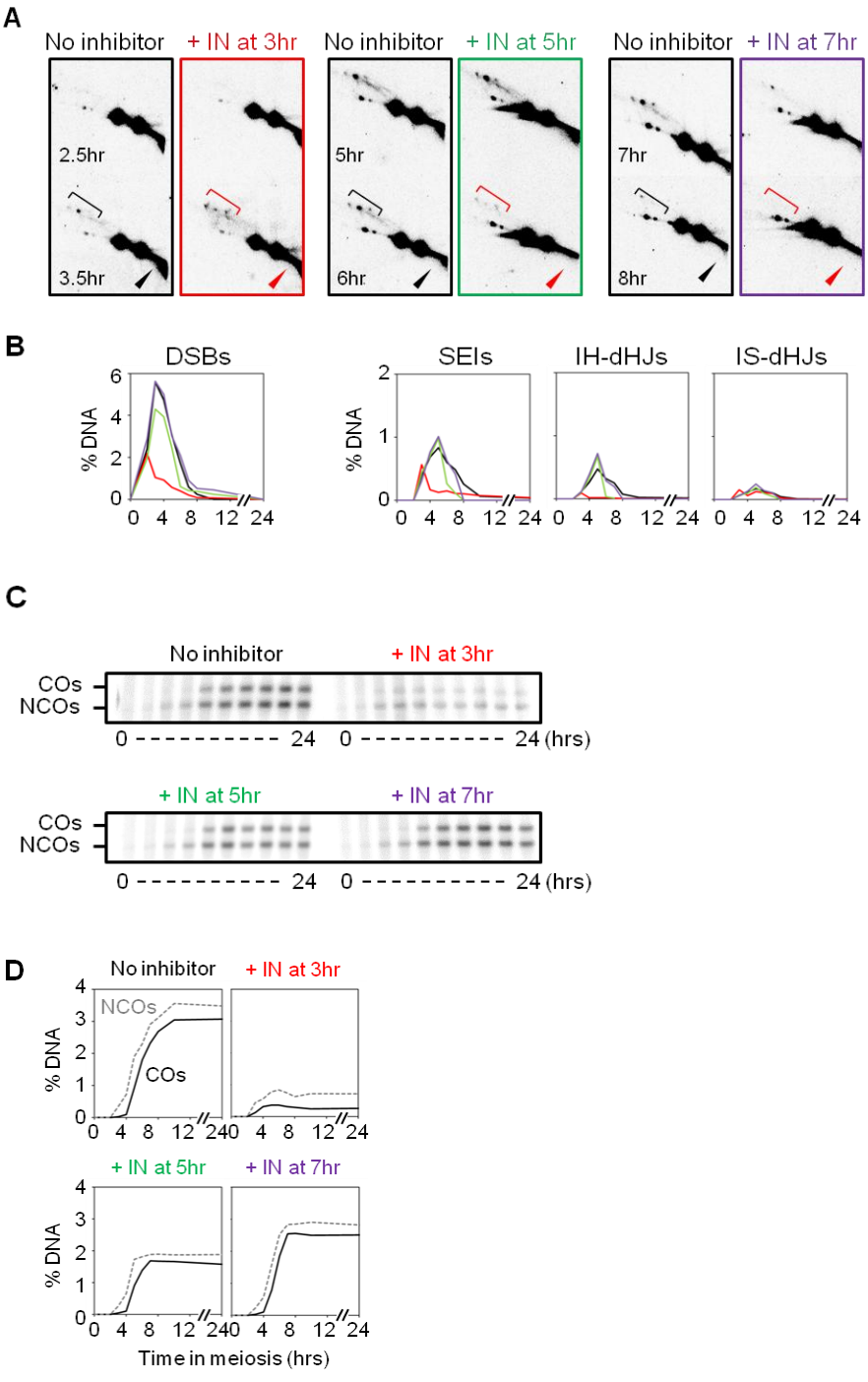
A
No inhibitor
+ IN at 3hr
No inhibitor
+ IN at 5hr
No inhibitor
+ IN at 7hr
2.5hr
3.5hr
5hr
6hr
7hr
8hr
B
DSBs
SEIs
IH-dHJs
IS-dHJs
% DNA
0 4 8 12 24
C
No inhibitor
+ IN at 3hr
COs
NCOs
0 ---------- 24 0 ---------- 24 (hrs)
+ IN at 5hr
+ IN at 7hr
D
NCOs
COs
% DNA
Time in meiosis (hrs)

E

rec8-6A mek1as

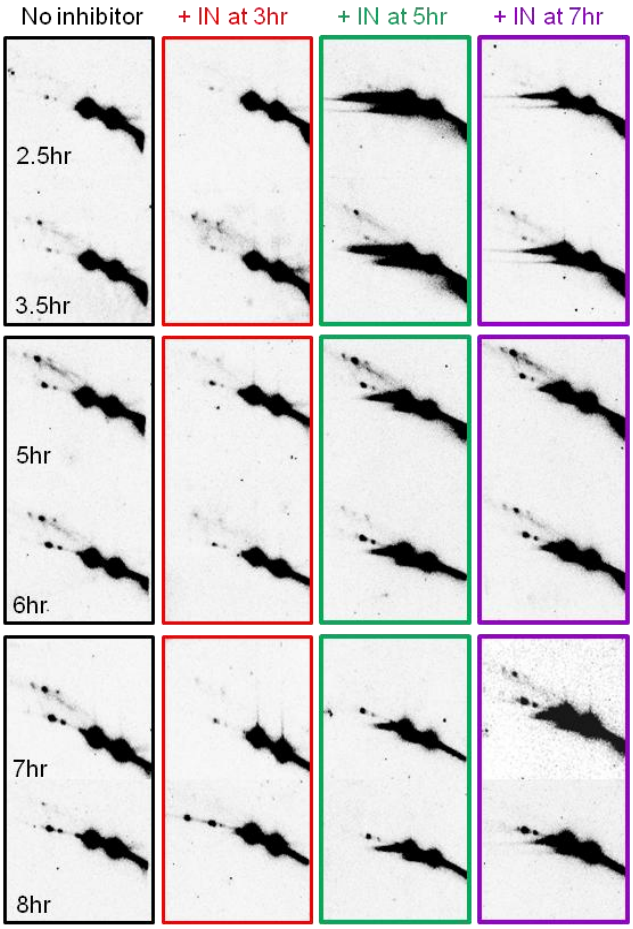

Figure 2-13. DNA physical analysis of *rec8-29A mek1as* strain.

(A) Representative images of 2D-gel of *rec8-29A mek1as* strain in the absence or presence of 1-NA-PP1 at the indicated time points. Square brackets and arrowheads denote JMs and DSBs, respectively. The time points in the images means the time points after induction of meiosis (IN: 1-NA-PP1, inhibitor of Mek1 kinase)

(B) Quantification of recombination intermediates in the *rec8-29A mek1as* strain shown in (A). Black lines represent the turnover of DSBs and JMs of *rec8-29A mek1as* strain without inhibitor. Red, green, purple lines represent the turnover of DSBs and JMs of *rec8-29A mek1as* strain with inhibitor at 3 hr, 5 hr, and 7 hr, respectively.

(C) Analysis of CO and NCO formation in the *rec8-29A mek1as* strain in the absence or presence of 1-NA-PP1 at the indicated time points.

(D) Corresponding quantification data in (C). The levels of COs and NCOs were shown in black and grey lines, respectively.

(E) Total 2D-gel images show joint molecule formation of *rec8-29A mek1as* strain in the absence or presence of Mek1 kinase inhibitor during meiosis.

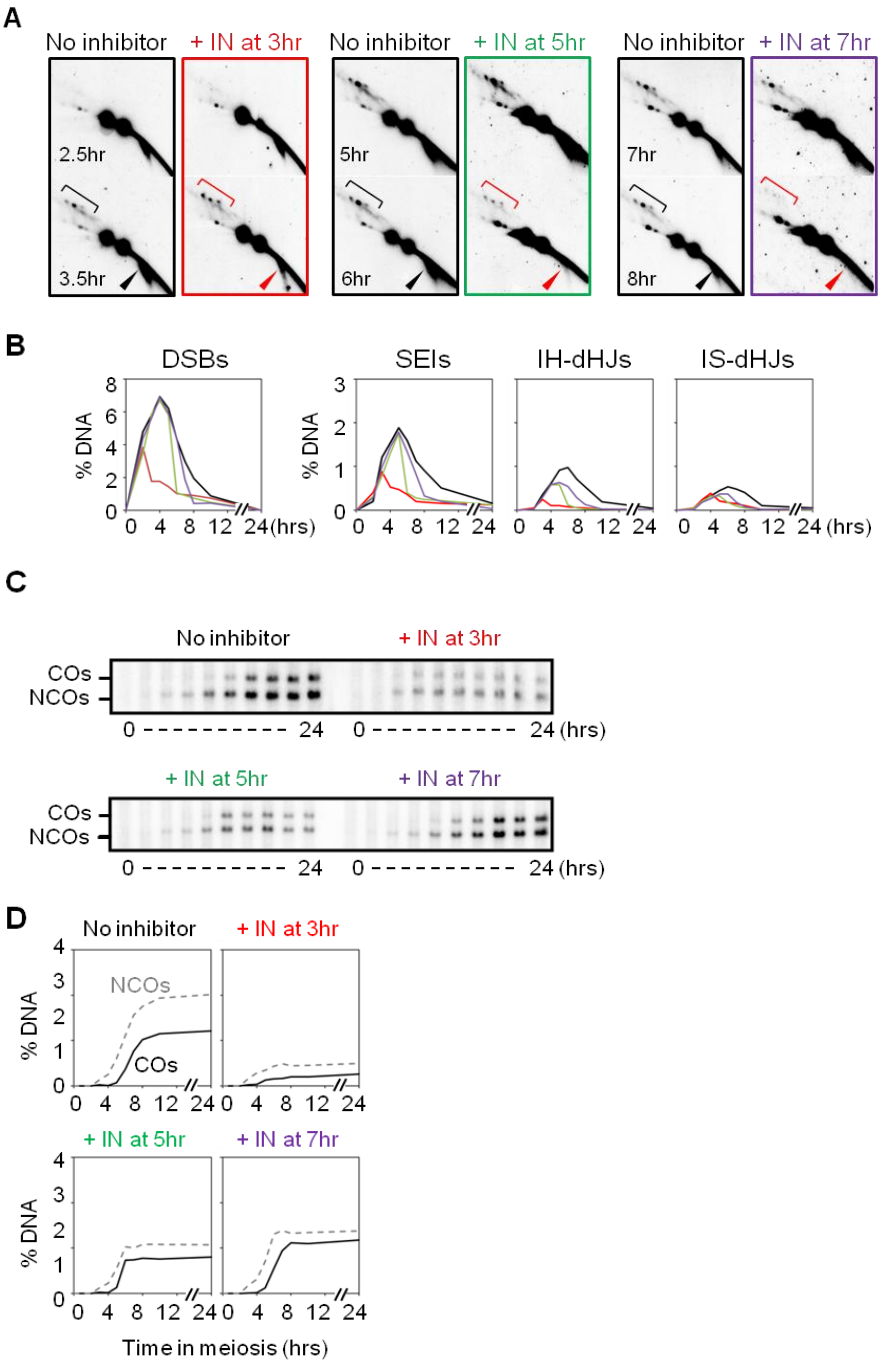
A
No inhibitor
+ IN at 3hr
No inhibitor
+ IN at 5hr
No inhibitor
+ IN at 7hr
2.5hr
3.5hr
5hr
6hr
7hr
8hr
B
DSBs
SEIs
IH-dHJs
IS-dHJs
% DNA
0 4 8 12 24 (hrs)
C
No inhibitor
+ IN at 3hr
+ IN at 5hr
+ IN at 7hr
COs
NCOs
0 ---------- 24
D
NCOs
COs
% DNA
Time in meiosis (hrs)

E

rec8-29A mek1as

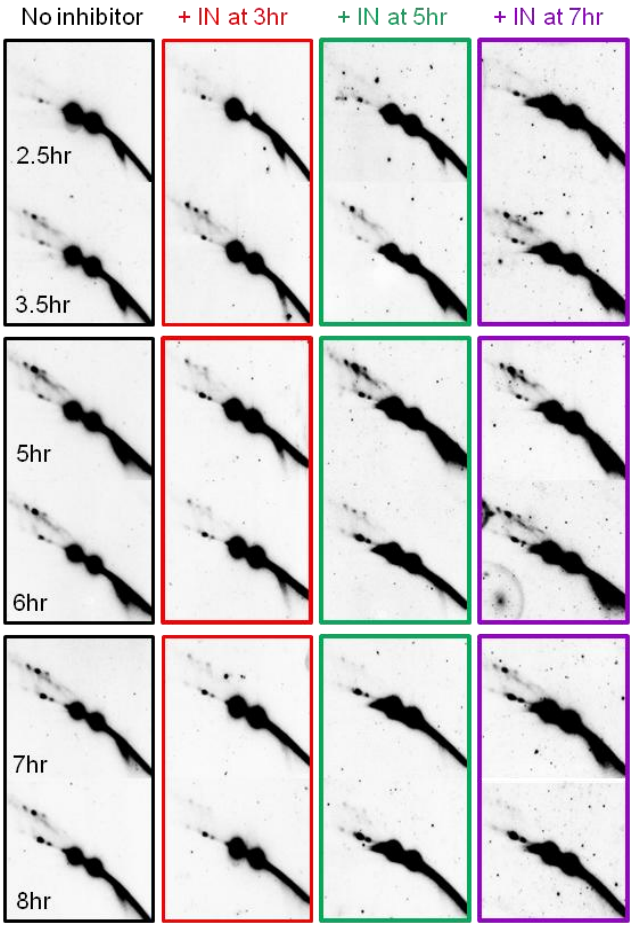

Figure 2-14. DNA physical analysis of *rec8Δ mek1as* strain.

(A) Representative images of 2D-gel of *rec8Δ mek1as* strain in the absence or presence of 1-NA-PP1 at the indicated time points. Square brackets and arrowheads denote JMs and DSBs, respectively. The time points in the images means the time points after induction of meiosis (IN: 1-NA-PP1, inhibitor of Mek1 kinase)

(B) Quantification of recombination intermediates in the *rec8Δ mek1as* strain shown in (A). Black lines represent the turnover of DSBs and JMs of *rec8Δ mek1as* strain without inhibitor. Red, green, purple lines represent the turnover of DSBs and JMs of *rec8Δ mek1as* strain with inhibitor at 3 hr, 5 hr, and 7 hr, respectively.

(C) Analysis of CO and NCO formation in the *rec8Δ mek1as* strain in the absence or presence of 1-NA-PP1 at the indicated time points.

(D) Corresponding quantification data in (C). The levels of COs and NCOs were shown in black and grey lines, respectively.

(E) Total 2D-gel images show joint molecule formation of *rec8Δ mek1as* strain in the absence or presence of Mek1 kinase inhibitor during meiosis.

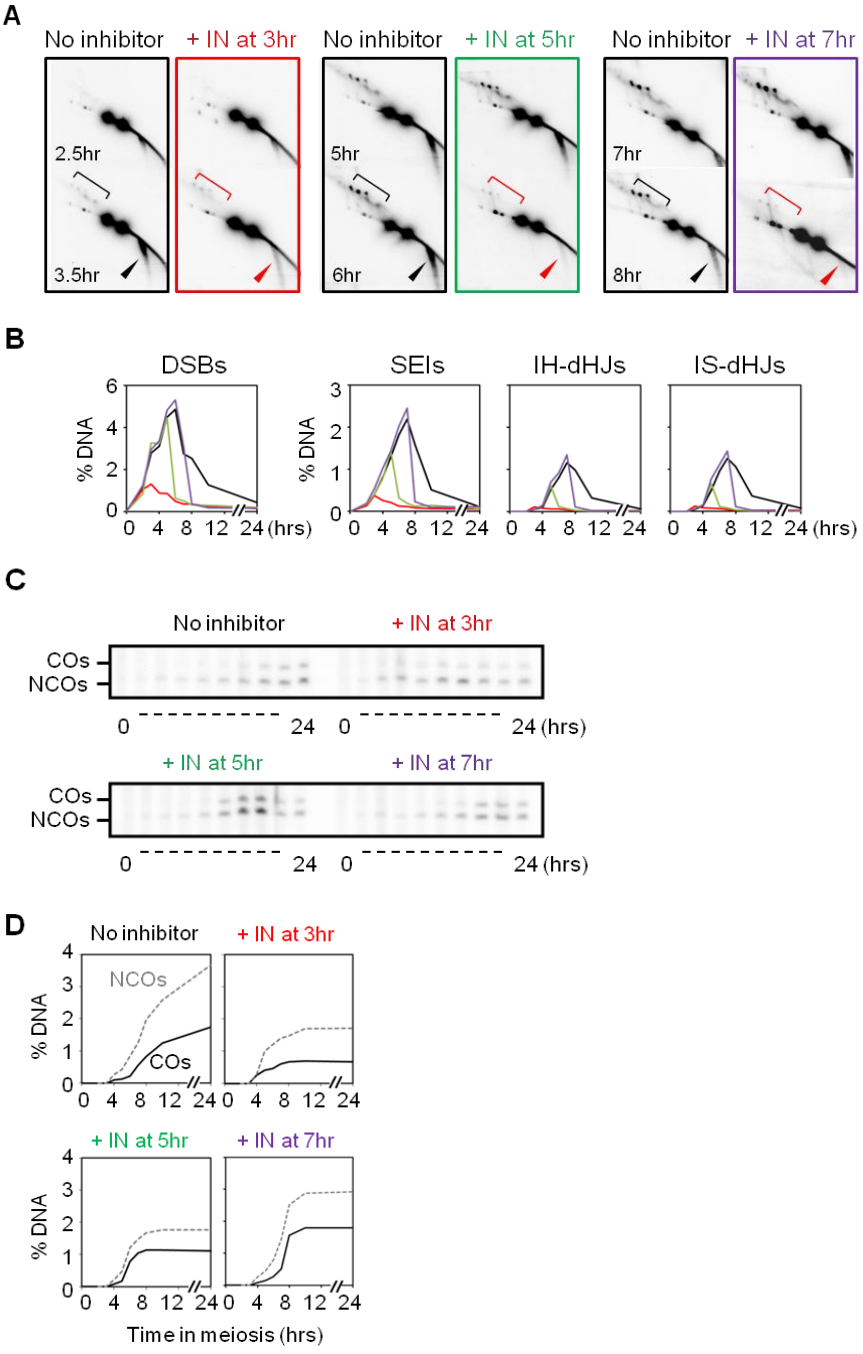
A
No inhibitor
+ IN at 3hr
No inhibitor
+ IN at 5hr
No inhibitor
+ IN at 7hr
2.5hr
3.5hr
5hr
6hr
7hr
8hr
B
DSBs
SEIs
IH-dHJs
IS-dHJs
% DNA
0 4 8 12 24 (hrs)
C
No inhibitor
+ IN at 3hr
+ IN at 5hr
+ IN at 7hr
COs
NCOs
0 24 0 24 (hrs)
D
No inhibitor
+ IN at 3hr
+ IN at 5hr
+ IN at 7hr
NCOs
COs
% DNA
0 4 8 12 24
Time in meiosis (hrs)

E

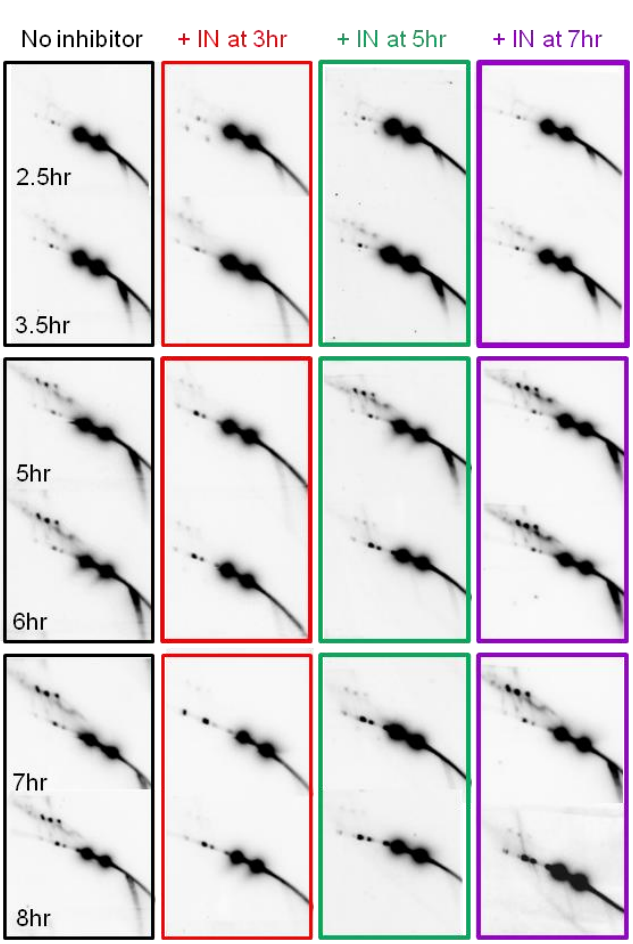
rec8Δ mek1as
No inhibitor
+ IN at 3hr
+ IN at 5hr
+ IN at 7hr
2.5hr
3.5hr
5hr
6hr
7hr
8hr

similar rate (Figs. 2-12 and 2-13).

The aforementioned results are obtained from analyses performed at 33 ^{o}C, at which CO/NCO differentiation is most tightly controlled (Börner et al., 2004). I also analyzed the strains at 23 ^{o}C (data not shown). Temperature sensitivity was demonstrated by means of physical analysis of DNA, and it confirmed in this study that even at low temperature, checkpoint inactivation relieves the delay caused by the absence of Rec8 (data not shown). These results suggest that in conjunction with the Rec8-phosphorylation status, Mek1 is a master regulator of meiotic progression.

Rec8 phosphorylation is responsible for recombinational progression in the absence of sister chromatids

I have previously reported that Rec8 is essential for Dmc1-mediated recombination in the absence of sister chromatids (Hong et al., 2013). As described in the preceding subsection, Rec8 phosphorylation is found to be indispensable during post-DSB CO-designated recombination after DNA replication. Therefore, I sought to determine whether Rec8 phosphorylation can support meiotic recombination in the absence of sister chromatids. I used a Cdc6 meiotic null strain in which the mitosis-specific MCD1 promoter is replaced (Hochwagen et al., 2005; Hong et al., 2013); thus, in these Cdc6-

depleted cells, sister chromatids cannot be formed during meiosis. In a *pMCD1-CDC6* background, physical analysis reveals that recombination exhibits substantial levels of DSBs, SEIs, dHJs, and COs in the mutant cells, but the turnovers are delayed by approximately 1.5 hr compared with the timing in WT (Fig. 2-15). The turnovers of DSBs and COs are markedly delayed in the Rec8 phosphorylation-defective strains with the *pMCD1-CDC6* background (Figs. 2-15A and 2-15B). Furthermore, in *rec8-6A* and *rec8-29A*, a subset of JMs remains even at 24 hr and the CO levels gradually decrease depending on the status of Rec8 phosphorylation (Fig. 2-15C and 2-15D). IH-COs and IH-NCOs are also decreased in Rec8-phospho mutants without sister chromatids (Figs. 2-15E and 2-15F). Taken all together, these results suggest that even in the absence of sister chromatids. Rec8 phosphorylation stimulates the transition from DSB to JM formation and concomitant CO formation.

Figure 2-15. Analysis of meiotic recombination intermediates in the absence of sister chromatid.

(A) Results of 1D-gel analysis showing DSBs and COs during meiotic time courses in the absence of sister chromatids. All strains are *pMCD1-CDC6* strains.

(B) Quantification data of DSBs and COs shown in (A). Black lines represent the levels of DSBs and COs of *pMCD1-CDC6* single mutant. Purple lines represent the levels of DSBs and COs of *rec8-6A pMCD1-CDC6* double mutant. Brown lines represent the levels of DSBs and COs of *rec8-29A pMCD1-CDC6* double mutant.

(C) Representative 2D-gel images of JMs in indicated mutants of *pMCD1-CDC6*. The signals of IH-dHJs were observed in all mutants. The time points means the maximal peak time of JMs formation after sporulation

(D) Quantification of SEIs and dHJs shown in (C). Black, purple, and brown lines represent *Rec8, rec8-6A*, and *rec8-29A* of *pMCD-CDC6* mutants, respectively.

(E) IH-COs and IH-NCOs formation in indicated mutants of *pMCD-CDC6*.

(F) Quantification of IH-COs and IH-NCOs levels shown in (E). The levels of IH-COs and IH-NCOs in indicated mutants of *pMCD-CDC6* were shown in black and grey lines, respectively.

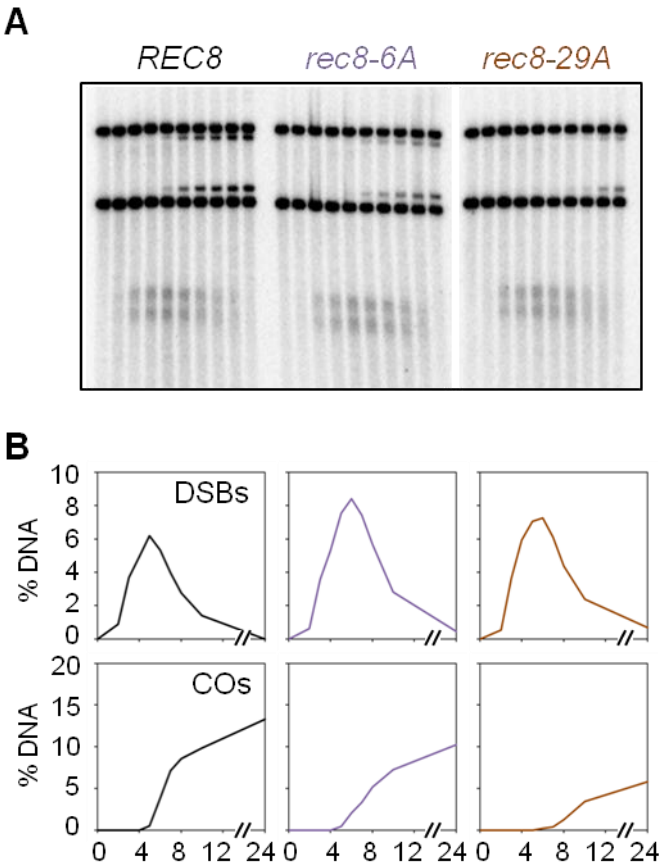
A
REC8
rec8-6A
rec8-29A
B
DSBs
COs
% DNA
% DNA
0
2
4
6
8
10
0
5
10
15
20
0 4 8 12 24
0 4 8 12 24
0 4 8 12 24

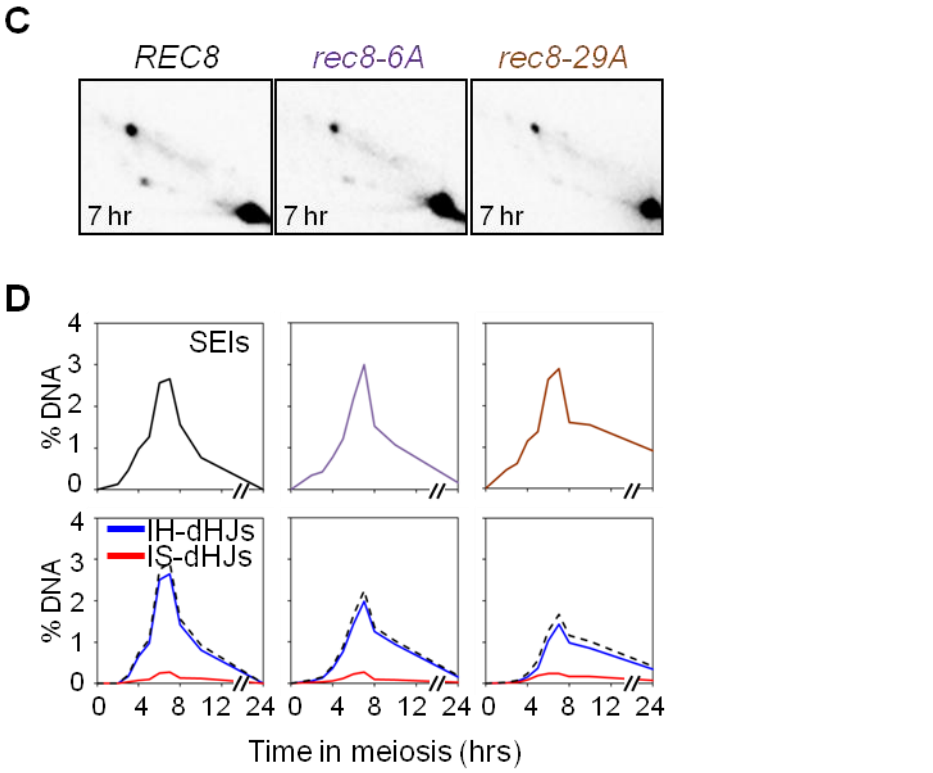
C
REC8
rec8-6A
rec8-29A
7 hr
7 hr
7 hr
D
SEIs
% DNA
IH-dHJs
IS-dHJs
% DNA
0 4 8 12 24 0 4 8 12 24 0 4 8 12 24
Time in meiosis (hrs)
E
REC8
rec8-6A
rec8-29A
IH-COs
IH-NCOs
0 24 0 24 0 24 (hrs)
F
REC8
rec8-6A
rec8-29A
IH-COs
IH-NCOs
% DNA
0 4 8 12 24 0 4 8 12 24 0 4 8 12 24

Discussion

The results of this study suggest that Rec8 phosphorylation is required for the progression of recombination and that Rec8 phosphorylation critically regulates CO/NCO differentiation and the maintenance of homolog bias during an early stage of recombination, prior to the onset of stable strand exchange. These findings have additional implications for regulatory surveillance and crossover control.

The localization of Spo11 on DNA is depends on the presence of Rec8 binding sites. Thus, Spo11 binding to DNA is strongly impaired following Rec8 deletion, and consequently, DSB formation is diminished (Kugou et al., 2009). Similarly, yeast strains lacking Rec8 phosphorylation may also exhibit defects in Spo11 binding at DSB sites; however, normal timing and levels of DSB formation were unexpectedly observed in the DNA physical analysis. The step immediately after DSB formation was just impaired and this resulted in inefficient DSB repair, and therefore an overall delay in meiosis was observed in the *rec8-29A* strain. This result raises the possibilities that Rec8 phosphorylation may play a role as a molecular scaffold during meiotic recombination or that this phenotype develops because of functional defects caused by the structural change in non-phosphorylatable Rec8 proteins.

Previous results have suggested that Rec8 acts positively to ensure maintenance of homolog bias independently of sister chromatid cohesion (Brar et al., 2009; Kim et al., 2010), and I extended those findings through DNA physical analysis to discriminate between COs and NCOs. The CO and NCO products, which are the final outcomes of meiotic recombination, are formed separately and appeared depending on Rec8 phosphorylation. Delayed and low-level CO formation, but not WT levels of NCO formation, is observed in *rec8-29A* strain despite the presence of high levels of IH-dHJs and a reduction in the IH:IS dHJ ratio. However, the high dHJ level might originates from the accumulation of JMs after the delay in pachytene exit. The *rec8-29A* phenotype exhibits a reduction in homolog bias with a 3:1 IH:IS dHJ ratio. Thus, considerable amounts of DSBs could be also resolved into IS-COs because of the defect in the maintenance of homolog bias (Fig. 2-16). The kinetics of SEI and dHJ formation is also abnormal in Rec8 phosphorylation-defective strains that show DSB-turnover defects, indicating that the leptotene exit in meiosis I is aberrant because non-phosphorylatable Rec8 protein is present. Rec8 locates adjacent to chromosome arms starts to degrade in pachytene, and centromeric Rec8 disappears at anaphase II (Watanabe et al., 1998). This outcome might occur because separase (*Esp1* in budding yeast), a cysteine protease that mediates responsible for anaphase entry by degrading

Figure 2-16. Rec8 phosphorylation-dependent modulation of meiotic recombination.

In WT meiosis, DSBs occur during leptotene; DSBs designated to become COs are converted to SEIs during zygotene, then to dHJs at mid-pachytene and finally to IH-COs at late pachytene or pachytene exit. The remainders of nascent D-loop molecules are processed to the IH-NCO fate via the SDSA pathway. Absence of Zip1 or Zip3 leads to defects in the progression of CO-fated interactions and also abrogates SC formation, thus triggering a regulatory checkpoint that delays or blocks progression of meiosis beyond the pachytene stage. The presented results show that Rec8 phosphorylation is required after DSB formation, specifically for CO-designated recombination. Many sites important for Rec8 cleavage are phosphorylated by Cdc5, a polo-like kinase in yeast. However, Cdc5 interact with Rec8 from mid- or late- prophase I, and is required for the execution of meiosis I events and the resolution of dHJs. In two additional kinases, Hrr25 and DDK, mediate Rec8 phosphorylation from early prophase I and contribute to Rec8 cleavage (Katis et al., 2010). Rec8 phospho-mutant cells (*Rec8 P-*), CO-fated DSBs do not efficiently progress to SEIs/dHJs and the few dHJs that form exhibit maintenance of homolog bias. Regardless of Rec8's phosphorylation state, in *Mek1-* cells, all recombination intermediates disappear rapidly, implying progression to other fates.

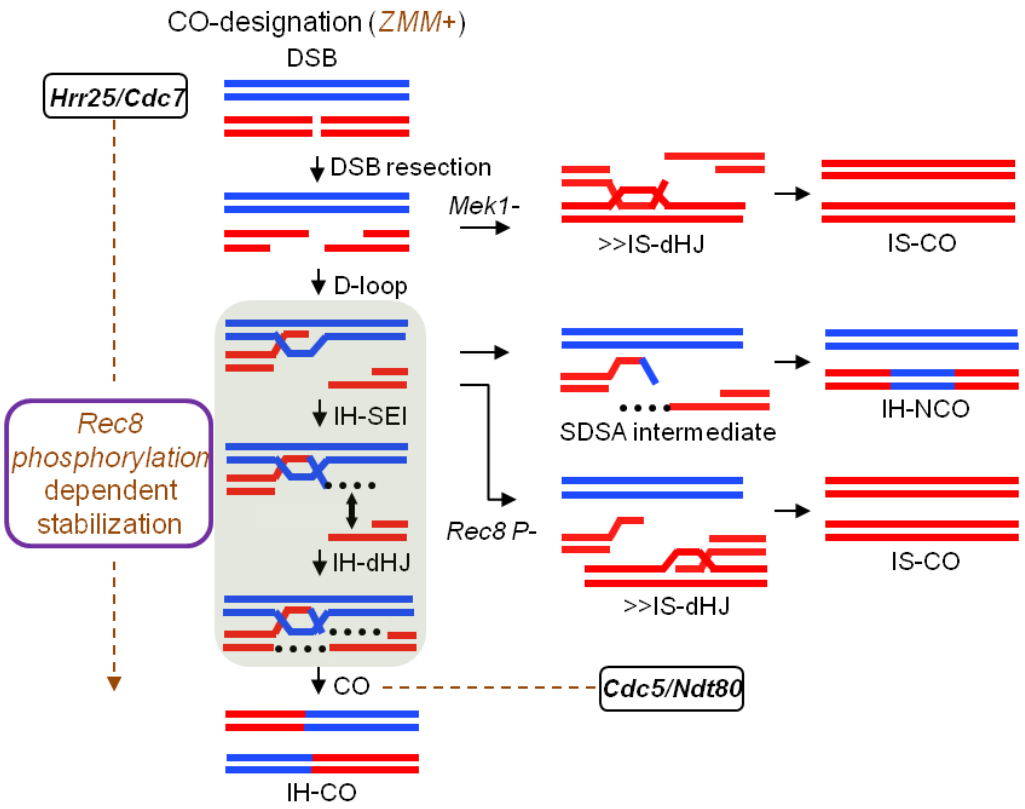
CO-designation (ZMM+)
DSB
Hrr25/Cdc7
DSB resection
Mek1-
>>IS-dHJ
IS-CO
D-loop
IH-SEI
SDSA intermediate
IH-NCO
Rec8 phosphorylation dependent stabilization
Rec8 P-
IH-dHJ
>>IS-dHJ
IS-CO
CO
Cdc5/Ndt80
IH-CO

cohesin, cannot recognize and cleave the meiotic cohesin, Rec8, i.e. the non-cleavable form of Rec8, *rec8-24A*, is resistant to separase (Katis et al., 2010). Conversely, meiotic defects resulting from the presence of mutant Rec8 might be involved in unknown mechanisms. All meiotic delays in *rec8-29A* and *rec8-6A* strains are definitely eliminated just as in the strains with Rec8 deletion on Mek1 kinase inactivation. Mek1 kinase activity is required specifically for the establishment of ends-apart homolog partner interaction by enabling the eviction of the first DSB end from the recombinosome/axis/sister complex. The kinetics of DSB, SEI and dHJ formation is similar in RMH- (Red1-Mek1-Hop1 deleted) and WT strains, and residual COs and NCOs arise featuring the same timing but not the same level as those in the WT strain.

In *rec8-29A Mek1-* cells, the impaired lesion is promptly repaired toward sister bias, indicating that Rec8 phosphorylation affects the progression of recombination, with specific CO-designated DSBs occurring at a late stage of DSB formation, but that Mek1 fundamentally governs the switch that determines the mitotic or meiotic mode at an early stage of recombination and checkpoint activation in all meiotic stages (Fig. 2-16).

The synatonemal complex (SC) is a highly conserved proteinaceous structure that forms between homologous chromosomes. The *rec8-6A* and *rec8-29A* cells display proper sister chromatid cohesion and chromosome axis formation,

but are severely impaired in the assembly of Zip1 onto chromosomes. This inability of the mutants to assemble Zip1 onto meiotic chromosomes could be a reason for the defective progression of recombination. However, the *rec8-6A* and *rec8-29A* alleles can support homolog pairing. As described in the preceding paragraph, when Rec8 protein is depleted during meiosis, meiotic progression is severely delayed or even incomplete. Furthermore, all meiotic recombination processes from the beginning to the end are disturbed; therefore, the level of the final product is abnormal. Specifically, in the *rec8-29A* mutant, complete homologous recombination is not accomplished as in the case of the *rec8Δ* mutant, although the mutant supports sister chromatid cohesion to allow meiotic chromosome organization. And, it is possible that prophase defects in Rec8 phospho-defective mutants are due to structural changes of Rec8 protein. When amino acid residues in phosphorylation sites of *rec8-6A* mutant were changed to aspartates (*rec8-6D*) or glutamates (*rec8-6E*), Rec8 proteins in these Rec8 phospho-mimetic mutants were no longer detected by western blotting analysis (Brar et al., 2009). This means that Rec8 proteins of phospho-mimetic mutants are unstable proteins. Therefore, it is not clear whether structural changes or phosphorylation is important for the function of Rec8 in SC formation.

Our results indicate that Rec8 phosphorylation is essential for generating

mature recombinants through CO-fate DSB repair (Fig. 2-16). Thus, the delay in meiotic progression delay in *rec8-6A* and *rec8-29A* mutants could result from regulatory checkpoint activation caused by defects in SC formation, implying that Rec8 phosphorylation promotes, together with ZMM proteins, DSB-to-SEI/SC nucleation transition (Fig. 2-16).

It is previously reported that only low levels of JMs occurred in the absence of sister chromatids and Rec8 (Hong et al., 2013). Rec8 phosphorylation-defective strains show homolog bias, albeit with a reduced IH:IS dHJ ratio and also show defects in progression to the CO pathway. When incomplete replication occurs in *Cdc6*- cells, all recombination intermediates in the Rec8 phosphorylation-defective strains are efficiently formed, however, the levels of SEIs and dHJs are lower than those in WT. In Rec8 phosphorylation-defective cells, much of CO-designated DSBs are aberrant in the CO pathway as shown by the severe impairment of JM resolution and CO formation in a phosphorylation status-dependent manner. In the absence of sister chromatids, Rec8 cohesin can still load onto meiotic chromosomes, much as it does in the WT (Lin et al., 2011). Consequently, whether or not sister chromatids are present, Rec8 phosphorylation is essentially required for the formation of CO products.

This study has shown that controlled DSB progression and the commitment

of a DSB to utilization/maintenance of homolog partner interaction are dependent not only upon Rec8 phosphorylation but also on Mek1 kinase. In this context, the key roles of structural components in general, and the modulation of sister chromatid cohesion in particular, can be understood by the necessity to destabilize sister cohesion as required for recombination, and ultimately for crossing over, to occur between one chromatid of each homolog, rather than between sisters, while sister cohesion is concomitantly maintained globally along the chromosomes.

Table 2-1. Yeast strains used in this study

Strain number	Relevant genotypes
KKY10	*MATa/MAT HIS4::LEU2-(BamHI)/his4x::LEU2-(NgoMIV)--URA3*
KKY1756	*MATa/MAT HIS4::LEU2-(BamHI)/his4x::LEU2-(NgoMIV)--URA3, Rec8-3HA::URA3*
KKY179	*MATa/MAT HIS4::LEU2-(BamHI)/his4x::LEU2-(NgoMIV)--URA3, rec8Δ::KanMX4::rec8-6A-3HA::LEU2*
KKY173	*MATa/MAT HIS4::LEU2-(BamHI)/his4x::LEU2-(NgoMIV)--URA3, rec8Δ::KanMX4::rec8-29A-3HA::LEU2*
KKY11	*MATa/MAT HIS4::LEU2-(BamHI)/his4x::LEU2-(NgoMIV)--URA3, rec8Δ::KanMX4*
KKY197	*MATa/MAT HIS4::LEU2-(BamHI)/his4x::LEU2-(NgoMIV)--URA3, mek1::LEU2::mek1-as::URA3*
KKY194	*MATa/MAT HIS4::LEU2-(BamHI)/his4x::LEU2-(NgoMIV)--URA3, rec8Δ::KanMX4, mek1::LEU2::mek1-as::URA3*
KKY856	*MATa/MAT HIS4::LEU2-(BamHI)/his4x::LEU2-(NgoMIV)--URA3, rec8Δ::KanMX4::rec8-6A-3HA::LEU2, mek1::LEU2::mek1-as::URA3*
KKY857	*MATa/MAT HIS4::LEU2-(BamHI)/his4x::LEU2-(NgoMIV)--URA3, rec8Δ::KanMX4::rec8-29A-3HA::LEU2, mek1::LEU2::mek1-as::URA3*
KKY132	*MATa/MAT HIS4::LEU2 (BamHI; ori)/his4x::LEU2-(NgoMIV+ori)--URA3, cdc6::kanMX6::pMCD1::3HA-CDC6*
KKY919	*MATa/MAT HIS4::LEU2-(BamHI)/his4x::LEU2-(NgoMIV)-URA3, rec8Δ::KanMX4::rec8-6A-3HA::LEU2, cdc6::kanMX6::pMCD1::3HA-CDC6*
KKY917	*MATa/MAT HIS4::LEU2-(BamHI)/his4x::LEU2-(NgoMIV)-URA3, rec8Δ::KanMX4::rec8-29A-3HA::LEU2, cdc6::kanMX6::pMCD1::3HA-CDC6*

All strains are isogenic derivatives of SK1 background homozygous for the mutation *ho::hisG, leu2::hisG, ura3 (PstI-SmaI), nuc1::HygroB.*

REFERENCES

Adams BR, Golding SE, Rao RR and Valerie K. (2010) Dynamic dependence on ATR and ATM for double-strand break repair in human embryonic stem cells and neural descendants. *PLoS One* **5**:e10001.

Andrews PW. (2002) From teratocarcinomas to embryonic stem cells. *Philos Trans R Soc Lond B Biol Sci* **357**, 405-417.

Attner MA, Miller MP, Ee LS, Elkin, SK and Amon A. (2013) Polo kinase Cdc5 is a central regulator of meiosis I. *Proc Natl Aca. Sci U S A* **110**, 14278-14283.

Badie S, Escandell JM, Bouwman P, Carlos AR, Thanasoula M, Gallardo MM, Suram A, Jaco I, Benitez J, Herbig U, Blasco MA, Jonkers J and Tarsounas M. (2010) BRCA2 acts as a RAD51 loader to facilitate telomere replication and capping. *Nat Struct Mol Biol* **17**, 1461-1469.

Baker DE, Harrison NJ, Maltby E, Smith K, Moore HD, Shaw PJ, Heath PR, Holden H and Andrews PW. (2007) Adaptation to culture of human embryonic stem cells and oncogenesis in vivo. *Nat Biotechnol* **25**, 207-215.

Bell SP and A Dutta. (2002) DNA replication in eukaryotic cells. *Annu Rev Biochem* **71**, 333-374.

Blow JJ and PJ Gillespie. (2008) Replication licensing and cancer-a fatal entanglement? *Nat Rev Cancer* **8,** 799-806.

Börner GV, Kleckner N and Hunter N. (2004) Crossover/noncrossover

differentiation, synaptonemal complex formation, and regulatory surveillance at the leptotene/zygotene transition of meiosis. *Cell* **117**, 29-45.

Branzei D and Foiani M. (2010) Maintaining genome stability at the replication fork. *Nat Rev Mol Cell Biol* **11**, 208-219.

Brar GA, Kiburz BM, Zhang Y, Kim JE, White F and Amon A. (2006) Rec8 phosphorylation and recombination promote the step-wise loss of cohesins in meiosis. *Nature* **441**, 532-536.

Brar GA, Hochwagen A, Ee LS and Amon A. (2009) The multiple roles of cohesin in meiotic chromosome morphogenesis and pairing. *Mol Biol Cell* **20**, 1030-1047.

Bugler B, Schmitt E, Aressy B and Ducommun B. (2010) Unscheduled expression of CDC25B in S-phase leads to replicative stress and DNA damage. *Mol Cancer* **9**, 29.

Buisson R, Dion-Cote AM, Coulombe Y, Launay H, Cai H, Stasiak AZ, Stasiak A, Xia B and Masson JY. (2010) Cooperation of breast cancer proteins PALB2 and piccolo BRCA2 in stimulating homologous recombination. *Nat Struct Mol Biol* **17**, 1247-1254.

Buonomo SB, Clyn, RK, Fuchs J, Loidl J, Uhlmann F and Nasmyth K. (2000) Disjunction of homologous chromosomes in meiosis I depends on proteolytic cleavage of the meiotic cohesin Rec8 by separin. *Cell* **103**, 387-398.

Burhans WC and Weinberger M. (2007) DNA replication stress, genome instability and aging. *Nucleic Acids Res* **35**, 7545-7556.

Cannavo E, Cejka P and Kowalczykowski SC. (2013) Relationship of DNA degradation by Saccharomyces cerevisiae exonuclease 1 and its stimulation by RPA and Mre11-Rad50-Xrs2 to DNA end resection. *Proc Natl Acad Sci U S A* **110**, 1661-1668.

Cappelli E, Townsend S, Griffin C and Thacker J. (2011) Homologous recombination proteins are associated with centrosomes and are required for mitotic stability. *Exp Cell Res* **317**, 1203-1213.

Carr AM, Paek AL and Weinert T. (2011) DNA replication: failures and inverted fusions. *Semin Cell Dev Biol* **22**, 866-874.

Chi P, Komen SV, Sehorn MG, Sigurdsson S and Sung P. (2006) Roles of ATP binding and ATP hydrolysis in human Rad51 recombinase function. *DNA Repair (Amst)* **5**, 381-391.

Daboussi F, Courbet S, Benhamou S, Kannouche P, Zdzienicka MZ, Debatisse M and Lopez BS. (2008) A homologous recombination defect affects replication-fork progression in mammalian cells. *J Cell Sci* **121**, 162-166.

Dresser ME, Hunter N and Bishop DK (2013) Meiotic crossover control by concerted action of Rad51-Dmc1 in homolog template bias and robust homeostatic regulation. *PloS Genet* **12**, e1003978.

Dupre A, Boyer-Chatenet L, Sattler RM, Modi AP, Lee JH, Nicolette ML, Kopelovich L, Jasin M, Baer R, Paull TT and Gautier J. (2008) A forward chemical genetic screen reveals an inhibitor of the Mre11-Rad50-Nbs1 complex. *Nat Chem Biol* **4**, 119-125.

Garcia V, Phelps SE, Gray S and Neale MJ. (2011) Bidirectional resection of DNA double-strand breaks by Mre11 and Exo1. *Nature* **479**, 241-244.

Goldstein AL and McCusker JH. (1999) Three new dominant drug resistance cassettes for gene disruption in Saccharomyces cerevisiae. *Yeast* **15**, 1541-1553.

Hashimoto Y, Chaudhuri AR, Lopes M and Costanzo V. (2010) Rad51 protects nascent DNA from Mre11-dependent degradation and promotes continuous DNA synthesis. *Nat Struct Mol Biol* **17**, 1305-1311.

Hochwagen A, Tham WH, Brar GA and Amon A. (2005) The FK506 binding protein Fpr3 counteracts protein phosphatase 1 to maintain meiotic recombination checkpoint activity. *Cell* **122**, 861-873.

Holloman WK. (2011) Unraveling the mechanism of BRCA2 in homologous recombination. *Nat Struct Mol Biol* **18**, 748-754.

Hong S, Sung Y, Yu M, Lee M, Kleckner N and Kim KP (2013) The logic and mechanism of homologous recombination partner choice. *Mol Cell* **51**, 440-453.

Hornig NC and Uhlmann F. (2004) Preferential cleavage of chromatin-bound cohesion after targeted phosphorylation by Polo-like kinase. *EMBO J* **23**, 3144-3153.

Hunter N and Kleckner N (2001) The single-end invasion: an asymmetric intermediate at the double-strand break to double-holliday junction transition of meiotic recombination. *Cell* **106**, 59-70.

Hunter N. (2006) Meiotic recombination. *Topics in Current Genetics, Molecular Genetics of Recombination* 381-442.

Katis VL, Lipp JJ, Imre R, Bogdanova A, Okaz E, Habermann B, Mechtler K, Nasmyth K and Zachariae W. (2010) Rec8 phosphorylation by casein kinase 1 and Cdc7-Dbf4 kinase regulates cohesin cleavage by separase during meiosis. *Dev Cell* **18**, 397-409.

Keeney S. (2001) Mechanism and control of meiotic recombination initiation. *Curr Top Dev Biol* **52**, 1-53.

Kim KP, Weiner BM, Zhang L, Jordan A, Dekker J and Kleckner N. (2010) Sister cohesion and structural axis components mediate homolog bias of meiotic recombination. *Cell* **143**, 924-937.

Kim TM, Ko JH, Hu L, Kim SA, Bishop AJ, Vijg J, Montagna C and Hasty P. (2012) RAD51 mutants cause replication defects and chromosomal instability. *Mol Cell Biol* **32**, 3663-3680.

Kitajima TS, Sakuno T, Ishiguro K, Iemura S, Natsume T, Kawashima SA and Watanabe Y. (2006) Shugoshin collaborates with protein phosphatase 2A to protect cohesin. *Nature* **441**, 46-52.

Kleckner N, Zickler D, Jones GH, Dekker J, Padmore R, Henle J and Hutchinson J. (2004) A mechanical basis for chromosome function. *Proc Natl Acad Sci U S A* **101**, 12592-12597.

Klein F, Laroche T, Cardenas ME, Hofmann JF, Schweizer D and Gasser SM. (1992) Localization of RAP1 and topoisomerase II in nuclei and meiotic chromosomes of yeast. *J Cell Biol* **117**, 935-948.

Klein F, Mahr P, Galova M, Buonomo S, Michaelis C, Nairz K and Nasmyth K. (1999) A central role for cohesins in sister chromatid cohesion, formation of axial elements, and recombination during yeast meiosis. *Cell* **98**, 91-103.

Koberna K, Ligasova A, Malinsky J, Pliss A, Siegel AJ, Cvackova Z, Fidlerova H, Masata M, Fialova M, Raska I and Berezney R. (2005) Electron microscopy of DNA replication in 3-D: evidence for similar-sized replication foci throughout S-phase. *J Cell Biochem* **94**, 126-138.

Krejci L, Altmannova V, Spirek M and Zhao X. (2012) Homologous recombination and its regulation. *Nucleic Acids Res* **40**, 5795-5818.

Kugou K, Fukuda T, Yamada S, Ito M, Sasanuma H, Mori S, Katou Y, Itoh T, Matsumoto K, Shibata T, Shirahige K and Ohta K. (2009) Rec8 guides canonical Spo11 distribution along yeast meiotic chromosomes. *Mol Biol Cell* **20**, 3064-3076.

Kushnirov VV. (2000). Rapid and reliable protein extraction from yeast. *Yeast* **16**, 857-860.

Lao JP, Cloud V, Huang CC, Grubb J, Thacker D, Lee CY, Dresser ME, Hunter N and Bishop DK. (2013) Meiotic crossover control by concerted action of Rad51-Dmc1 in homolog template bias and robust homeostatic regulation. *PloS Genet*. **12**, e1003978.

Leonhardt H, Page AW, Weier HU and Bestor TH. (1992) A targeting sequence directs DNA methyltransferase to sites of DNA replication in mammalian nuclei. *Cell* **71**, 865-873.

Leonhardt H, Rahn HP, Weinzierl P, Sporbert A, Cremer T, Zink D and Cardoso MC. (2000) Dynamics of DNA replication factories in living cells. *J Cell Biol* **149**, 271-280.

Lim DS and Hasty P. (1996) A mutation in mouse rad51 results in an early embryonic lethal that is suppressed by a mutation in p53. *Mol Cell Biol* **16**, 7133-7143.

Lin W, Wang M, Jin H and Yu HG. (2011) Cohesin plays a dual role in gene regulation and sister-chromatid cohesion during meiosis in Sacchromyces cerevisiae. *Genetics* **187**, 1041-1051.

Liu J, Doty T, Gibson B and Heyer WD. (2010) Human BRCA2 protein promotes RAD51 filament formation on RPA-covered single-stranded DNA. *Nat Struct Mol Biol* **17**, 1260-1262.

Longtine MS, Mckenzie A, Demarini DJ, Shah NG, Wach A, Brachat A, Philippssen P and Pringle JR. (1998) Additional modules for versatile and economical PCR-based gene deletion and modification in Saccharomyces cerevisiae. *Yeast* **14**, 953-961.

Maitra A, Arking DE, Shivapurkar N, Ikeda M, Stastny V, Kassauei K, Sui G, Cutler DJ, Liu Y, Brimble SN, Noaksson K, Hyllner J, Schulz TC, Zeng X, Freed WJ, Crook J, Abraham S, Colman A, Sartipy P, Matsui S, Carpenter M, Gazdar AF, Rao M and Chakravarti A. (2005) Genomic alterations in cultured human embryonic stem cells. *Nat Genet* **37**, 1099-1103.

Tsuzuki T, Fujii Y, Sakumi K, Tominaga Y, Nakao K, Sekiguchi M, Matsushiro A, Yoshimura Y and MoritaT. (1996) Targeted disruption of the

Rad51 gene leads to lethality in embryonic mice. *Proc Natl Acad Sci U S A* **93**, 6236-6240.

Murti KG, He DC, Brinkley BR, Scott R and Lee SH. (1996) Dynamics of human replication protein A subunit distribution and partitioning in the cell cycle. *Exp Cell Res* **223**, 279-289.

Nagy A, Gertsenstein M, Vintersten K and Behringer R. (2003) Manipulating the Mouse Embryo: A Laboratory Manual (Third Edition). *Cold Spring Harbor Laboratory Press*.

Neale MJ, Pan J and Keeney S. (2005) Endonucleolytic processing of covalent protein-linked double-strand breaks. *Nature* **436**. 1053-1057.

Niu H, Wan L, Baumgartner B, Schaefer D, Loidl J and Hollingsworth NM. (2005) Partner choice during meiosis is regulated by Hop1-promoted dimerization of Mek1. *Mol Biol Cell* **16**, 5804-5818.

Niu H, Li X, Job E, Park C, Moazed D, Gygi SP and Hollingsworth NM. (2007) Mek1 kinase is regulated to suppress double-strand break repair between sister chromatids during budding yeast meiosis. *Mol Cell Biol* **27**, 5456-5467.

Oh SD, Lao JP, Hwang PY, Taylor AF, Smith GR and Hunter N. (2007) BLM ortholog, Sgs1, prevents aberrant crossing-over by suppressing formation of multichromatid joint molecules. *Cell* **130**, 259-272.

Paques F and Haber JE. (1999) Multiple pathways of recombination induced by double-strand breaks in Saccharomyces cerevisiae. *Microbiol Mol Biol Rev* **63**, 349-404.

Pauklin S, Kristjuhan A, Maimets T and Jaks V. (2005) ARF and ATM/ATR cooperate in p53-mediated apoptosis upon oncogenic stress. *Biochem Biophys Res Commun* **334**, 386-394.

Paull TT, Rogakou EP, Yamazaki V, Kirchgessner CU, Gellert M and Bonner WM. (2000) A critical role for histone H2AX in recruitment of repair factors to nuclear foci after DNA damage. *Curr Biol* **10**, 886-895.

Petermann E, Orta ML, Issaeva N, Schultz N and Helleday T. (2010) Hydroxyurea-stalled replication forks become progressively inactivated and require two different RAD51-mediated pathways for restart and repair. *Mol Cell* **37**, 492-502.

Riedel CG, Katis VL, Katou Y, Mori S, Itoh T, Helmhart W, Gálová M, Petronczki M, Gregan J, Cetin B, Mudrak I, Ogris E, Mechtler K, Pelletier L, Buchholz F, Shirahige K and Nasmyth K. (2006) Protein phosphatase 2A protects centromeric sister chromatid cohesion during meiosis I. *Nature* **441**, 53-61.

Rossant J. (2001) Stem cells from the Mammalian blastocyst. *Stem Cells* **19**, 477-482.

San-Filippo J, Sung P and Klein H. (2008). Mechanism of eukaryotic homologous recombination. *Annu Rev Biochem* **77**, 229-257.

Sasanuma H, Tawaramoto MS, Lao JP, Hosaka H, Sanda E, Suzuki M, Yamashita E, Hunter N, Shinohara M, Nakagawa A and Shinohara A. (2013) A new protein complex promoting the assembly of Rad51 filaments. *Nat Commun* **4**, 1676.

Savatier P, Lapillonne H, Jirmanova L, Vitelli L and Samarut J. (2002) Analysis of the cell cycle in mouse embryonic stem cells. *Methods Mol Biol* **185**, 27-33.

Scaife RM. (2004) G2 cell cycle arrest, down-regulation of cyclin B, and induction of mitotic catastrophe by the flavoprotein inhibitor diphenyleneiodonium. *Mol Cancer Ther* **3**, 1229-1237.

Scholzen T and Gerdes J. (2000) The Ki-67 protein: from the known and the unknown. *J Cell Physiol* **182**, 311-322.

Schwab RAV and W Niedzwiedz. (2011) Visualization of DNA replication in the vertebrate model system DT40 using the DNA fiber technique. Journal of visualized experiments: *JoVE* **56**, 3255.

Schwacha A and Kleckner N. (1997) Interhomolog bias during meiotic recombination: meiotic functions promote a highly differentiated interhomolog-only pathway. *Cell* **90**, 1123-1135.

Serrano L, Liang L, Chang Y, Deng L, Maulion C, Nguyen S and Tischfield JA. (2011) Homologous recombination conserves DNA sequence integrity throughout the cell cycle in embryonic stem cells. *Stem Cells Dev* **20**, 363-374.

Sieber OM, Heinimann K and Tomlinson IP. (2003) Genomic instability--the engine of tumorigenesis? *Nat Rev Cancer* **3**, 701-708.

Sioftanos GA, Ismail LF, Shanley S, Worku M and Short SC. (2010) BRCA1 and BRCA2 heterozygosity in embryonic stem cells reduces

radiation-induced Rad51 focus formation but is not associated with radiosensitivity. *Int J Radiat Biol* **86**, 1095-1105.

Slupianek A, Schmutte C, Tombline G, Nieborowska-Skorska M, Hoser G, Nowicki MO, Pierce AJ, Fishel R and Skorski T. (2001) BCR/ABL regulates mammalian RecA homologs, resulting in drug resistance. *Mol Cell* **8**, 795-806.

Sonoda E, Sasaki MS, Buerstedde JM, Bezzubova O, Shinohara A, Ogawa H, Takata M, Yamaguchi-Iwai Y and Takeda S. (1998) Rad51-deficient vertebrate cells accumulate chromosomal breaks prior to cell death. *EMBO J* **17**, 598-608.

Storlazzi A, Tesse S, Ruprich-Robert G, Gargano S, Poggeler S, Kleckner N and Zickler D (2008) Coupling meiotic chromosome axis integrity to recombination. *Genes Dev* **22**, 796-809.

Terentyev Y, Johnson R, Neale MJ, Khisroon M, Bishop-Bailey A and Goldman AS. (2010) Evidence that MEK1 positively promotes interhomologue double-strand break repair. *Nucleic Acids Res* **38**, 4349-4360.

Tichy ED. (2011) Mechanisms maintaining genomic integrity in embryonic stem cells and induced pluripotent stem cells. *Exp Biol Med (Maywood)* **236**, 987-996.

Tichy ED, Pillai R, Deng L, Liang L, Tischfield J, Schwemberger SJ, Babcock GF and Stambrook PJ. (2010) Mouse embryonic stem cells, but not somatic cells, predominantly use homologous recombination to repair double-strand DNA breaks. *Stem Cells Dev* **19**, 1699-1711.

Tichy ED, Pillai R, Deng L, Tischfield JA, Hexley P, Babcock GF and Stambrook PJ. (2012) The abundance of Rad51 protein in mouse embryonic stem cells is regulated at multiple levels. *Stem Cell Res* **9**, 124-134.

Tsuzuki T, Fujii Y, Sakumi K, Tominaga Y, Nakao K, Sekiguchi M, Matsushiro A, Yoshimura Y and Morita T. (1996). Targeted disruption of the Rad51 gene leads to lethality in embryonic mice. *Proc Natl Acad Sci U S A* **93**, 6236-6240.

Vannier JB, Sandhu S, Petalcorin MI, Wu X, Nabi Z, Ding H and Boulton SJ. (2013) RTEL1 is a replisome-associated helicase that promotes telomere and genome-wide replication. *Science* **342**, 239-242.

Wach A, Brachat A, Pohlmann R and Philippsen P. (1994) New heterologous modules for classical or PCR-based gene disruptions in Saccharomyces cerevisiae. *Yeast* **10**, 1793-1808.

Wan L, de los Santos T, Zhang C, Shokat K and Hollingsworth NM. (2004) Mek1 kinase activity functions downstream of RED1 in the regulation of meiotic double strand break repair in budding yeast. *Mol Biol Cell* **15**, 11-23.

Watanabe Y and Nurse P. (1999) Cohesin Rec8 is required for reductional chromosome segregation at meiosis. *Nature* **400**, 481-484.

West SC. (2003) Molecular views of recombination proteins and their control. *Nat Rev Mol Cell Biol* **4**, 435-445.

Wold MS. (1997) Replication protein A: a heterotrimeric, single-stranded DNA-binding protein required for eukaryotic DNA metabolism. *Annu Rev Biochem* **66**, 61-92.

Wu HY, Ho HC and Burgess SM. (2010) Mek1 kinase governs outcomes of meiotic recombination and the checkpoint response. *Curr Biol* **20**, 1707-1716.

Yata K, Lloyd J, Maslen S, Bleuyard JY, Skehel M, Smerdon SJ and Esashi F. (2012) Plk1 and CK2 act in concert to regulate Rad51 during DNA double strand break repair. *Mol Cell* **45**, 371-383.

Yu HG and Koshland DE. (2003) Meiotic condensin is required for proper chromosome compaction, SC assembly, and resolution of recombination-dependent chromosome linkages. *J Cell Biol* **163**, 937-947.

Zakharyevich K, Ma Y, Tang S, Hwang PY, Boiteux S and Hunter N. (2010) Temporally and biochemically distinct activities of Exo1 during meiosis: double-strand break resection and resolution of double Holliday junctions. *Mol Cell* **40**, 1001-1015.

Zierhut C, Berlinger M, Rupp C, Shinohara A and Klein F. (2004) Mnd1 is required for meiotic interhomolog repair. *Curr Biol* **14**, 752-762.

국 문 초 록

배아줄기세포는 배반포기의 내세포집단에서 유래하는 세포로, 세포본연의 다분화능을 유지하면서 무한적으로 자가분열 및 성장하는 능력을 가지고 있다. 줄기세포는 자가세포재생 및 정확한 DNA 복제를 위하여, 분화된 체세포와는 차별화된 강력한 분자기전을 발전시켜 왔다. 하지만, 이에 대한 연구는 현재까지 많이 이루어져 있지 않다. 따라서, 유전자손상에 따른 돌연변이발생을 억제시키는 기작이 배아줄기세포의 유전체 안정성 유지는 물론, 세포증식 및 형질유전에 필수적이다.

상동염색체 재조합은 DNA 복제스트레스에 맞서서 유전체 안정성을 유지하는 필수적인 생물학적 과정이다. 진핵세포의 상동염색체 재조합 과정에서, Rad51 은 상동서열을 찾아서 DNA 가닥을 교환하는 데 중요한 기능을 하는 단백질이다. 본 연구에서는 Rad51 이 G2/M 기로의 전이조절을 통하여 세포주기 진행을 조절하고, 배아줄기세포에서의 높은 S 기의 비율이 Rad51 단백질과 관련이 있음에 초점을 맞추고 있다. 배아줄기세포는 분화된 체세포와 달리 현저히 많은 양의 S 기 세포를 유지하고 있다. 체세포들이 세포주기-의존적으로 Rad51 단백질을 발현하는 반면, 배아줄기세포에서는 각 세포주기에 관계없이 체세포에 비해 매우 높은 양을 항상 발현하고

있다. 세포주기-비의존적인 Rad51 단백질의 발현과는 달리, Rad51 foci 는 S 기 동안 그 형성이 증가하고, 하나의 모세포가 두 개의 딸 세포로 분열을 하는 유사분열 기에는 그 형성이 거의 관찰되지 않는다. 이런 Rad51 foci 형성은 DNA 이중가닥손상의 신호단백질인 γH2AX foci 형성패턴과 일치하는 현상을 보여준다. 또한, Rad51 은 유사분열 기에는 염색체로부터 완전히 떨어지는 것을 관찰하였다. 실험적으로 Rad51 단백질의 발현양을 억제시키면 세포수의 증가가 현저히 감소되고, G2/M 기의 세포들이 증가함은 물론, 유전자손상 신호전달과정이 활성화되는 것을 Chk1 단백질의 인산화로 관찰하였다. 결론적으로, Rad51 에 의한 상동염색체 재조합 기능이 배아줄기세포 특이적인 빠르고 빈번한 유전체 복제과정으로 인해, 자연적으로 발생하는 유전자 이중가닥손상을 수선하여 유전체 안정성에 기여함을 제시한다.

감수분열은 염색체교차를 위하여 상동염색체간의 물리적인 연결을 발생시키는 아주 정교한 생물학적 과정이다. 감수분열동안, cohesin 단백질결합체는 복제된 염색분체를 연결시키는 기능을 통하여, DNA 이중가닥손상 수선과 정확한 상동염색체 분리를 위한 필수적인 역할을 수행한다. Rec8 은 감수분열동안만 발현되어, 염색분체응축 및 상동염색체간의 재조합과정을 조절하는 단백질이다. 본 연구에서는, 효모에서의 물리적인 DNA 재조합연구를 통해, Rec8 단백질인산화가

DNA 이중가닥손상의 발생부터 dHJ 형성에 중요한 역할을 함을 밝히고 있다. 이에 따라, Rec8 단백질인산화과정이 DNA 이중가닥손상에서 시작되어 염색체교차로 진행되는 유전자 재조합과정에 필수적이라는 단서를 제시하고 있다. 더욱이, Mek1 인산화효소는 Rec8 단백질비인산화에 따른 감수분열동안 발생하는 재조합결함들을 완화시키는 상위조절자로서의 역할을 하고 있음을 알 수 있다. 본 연구에서는 염색분체응축 단백질인 Rec8 과 Mek1 인산화효소의 상관관계연구를 통하여 감수분열동안 재조합과정의 일반적인 논리에 대해 밝히고 있다.

중심어: 배아줄기세포, 상동염색체 재조합, Rad51, 세포주기, DNA 복제, 유전체 안정성, 감수분열 유전자재조합, Rec8, Mek1, Cdc6, 단백질인산화, 교차

학번: 2007-22846